Eindhoven University of Technology

MASTER

Development of a photovoltaic- and electrical storage system for investigation of demand side management strategies in office buildings

de Bont, K.F.M.

Award date:
2016

Link to publication

Author
K.F.M. de Bont

Student ID:
0831181

Master Thesis

Date
March 2016

Development of a Photovoltaic- and Electrical Storage System for Investigation of Demand Side Management Strategies in Office Buildings

Where innovation starts

DEVELOPMENT OF A PHOTOVOLTAIC- AND ELECTRICAL STORAGE SYSTEM FOR INVESTIGATION OF DEMAND SIDE MANAGEMENT STRATEGIES IN OFFICE BUILDINGS

Master thesis

March 2016

University

University of Technology Eindhoven
Faculty of the Built Environment
Building Physics and Services

Student

K.F.M. (Kevin) de Bont (0831181)
kevindebont@outlook.com
M4 – Graduation project (7SS37)

Supervisors

Prof. ir. W. Zeiler	1st faculty supervisor
Ir. G. Boxem	2nd faculty supervisor
K.O. Aduda MSc.	3rd faculty supervisor, PhD candidate
Ir. J.A.J. van der Velden	Company supervisor Kropman Installatietechniek B.V

Preface

This report is the result of the final project of my master Building Physics & Services, at Eindhoven University of Technology. It is accomplished in collaboration with Building Services Company Kropman B.V, and realized as part of the promotional study entitled: 'Smart-Grid Building Energy Management System. Graduation projects tend to have an unpredictable behaviour; during my research I encountered a subject change after finishing my M3 research (preliminary research), due to uncertainty of specific practical project continuation. Now this report in front of you is my final graduation project about the interesting topic on the practical development of a Photovoltaic-generation and Battery Energy Storage System for facilitating demand side management strategies in office buildings. During this research, I got the opportunity to present some preliminary results during a KIEN 'Technodag' at the yearly energy fair in Den Bosch and to publish some of my work in the TVVL-magazine. These were interesting chances to promote this research- and myself in the professional field.

With this, I would like to express my gratitude to the people whom assisted me during the realization of this research. First the chair of the committee, prof. ir. W.(Wim) Zeiler for his supervision, great project involvement and valuable lessons on the building services discipline. Also, I would like to thank ir. G.(Gert) Boxem, for his supervision, advice on reporting and critical questions throughout the process. Furthermore, I would like to thank Kennedy O. Aduda MSc. for his kind assistance and setting up the research requirements in order to gain maximum benefit for the promotional study. As said before, this research is accomplished in collaboration with Kropman B.V. and with this; I would like to thank my company supervisor ir. J.A.J. (Joep) van der Velden for his assistance during my project, especially at the design phase where we had to develop a facility for the challenging design task. I also would like to thank my colleagues at the Kropman Breda office, without their assistance, practical knowledge and commitment to build the facility in their office, it was never there within my graduation time. Their continuous support to participate in this project is from great importance during my final project.

As last, I would like to thank my family, friends and especially my girlfriend for their personal assistance and patience during the project.

Kevin de Bont

March 2016

Abstract

The increasing awareness of climate change, often related to worldwide carbon emissions, increases the presence of renewable distributed energy resources connected to the grid. The electrical infrastructure changes from a centralized to a decentralized system. The consumption technologies, as Electric- Vehicles and Heat Pumps, and production technologies as wind & solar-energy, patterns are more volatile and distributed compared to conventional energy production and consumption technologies. A new mechanism is required to remain the grid effective, robust and reliable in the near future. In this study, research was done on active participation of office buildings in the electrical grid as demand side resource to the next generation Smart-Grid by developing a photovoltaic- and electrical storage system for a Dutch office building. In this study a Photovoltaic (PV)-generation and Battery Electrical Storage System (BESS) was designed, developed, built and commissioned in order to test Smart-Grid facilitating demand side management (DSM) scenarios. Dimensioning of the PV-facility was done by linking it to the summer operations of the electrical chiller. The capacity of the BESS is dimensioned in order to provide short-term power flexibility for smart-grid support (0....60min), optimize self-consumption of on-site produced PV-energy and in conjunction with comfort-based loads clipping. These comfort-based loads include clipping the summer operations of the chiller and then especially the second stage behaviour and clipping the morning peak demand of the electrical steam humidifier. The work was completed as part of the promotional studies: the Development of a Micro-Grid strategy for process control on Room-level and Smart Grid – Building Energy Management System: the art of optimizing the connection between comfort demand and energy supply.

Content

1 Introduction

1.1 Background

Building accounts for approximately 40% of the total energy consumption and about 36% of the Carbon Dioxide (CO_2) emissions in Europe [1]. CO_2 emissions are often related to the climate change and global warming. In the Netherlands, the built environment accounts for the highest consumption of energy at 35%, industry and traffic sector 28% and 24% respectively [2]. As at 2014, only 17%, of this energy demand was attributed to electrical energy, of this about 10% was derived from renewable energy as wind, solar and biomass [2], for more information and graphs see Appendix A. To effectively manage energy consumption and limit carbon emissions in the building sector the European Union (EU) established the Energy Performance of Building Directive (EPBD) [3]. The EPBD improvement of the energy performance of buildings within the Union, taking into account outdoor climatic and local conditions, as well as indoor climate requirements and cost-effectiveness [3]. Further preconditions in EPDB requiring member states to formulate individual strategy to reach agreed targets released in 2010. Additional pre-conditions also required that all new buildings after 31 December 2020 should have a high-energy performance rating and be built with on-site or nearby electrical renewable energy sources (RES-E) to reach a nearly zero energy footprint. This means that in the near future, renewables as solar power will increase significantly to meet required targets. In connection with this the Dutch government is committed to ensure that renewable energy sources with contribute to 14% overall energy production by 2020 and 16% by 2023[4]. The Dutch government policy is part of the EU 2050 roadmap [5], in this Roadmap the EU committed to reducing greenhouse gas emission to $80-95\%$ below 1990 levels by 2050. In the future, fluctuations in wind and Photovoltaic-panels (PV) production will demand significantly greater 'flexibility' [6] from the power system, technical solutions to provide sufficient flexibility readily exist today [7]. Flexibility [6] in the Smart-grid context is: *'The ability to deviate from an initial intended energy demand or supply. This deviation can either imply a change in time, amount of energy, amount of power, location or a combination of these'.*

The electric demand profile is changing; relative new users (as Distributed Generators-RES-E, Heat Pumps and Electric Vehicles, EVs: up to a million [8] in 2025) are connected to the grid and are increasing their share quickly. The infrastructure changes from a centralized to a decentralized system. The consumption and production, patterns of those technologies are more volatile and distributed compared to conventional energy production and consumption technologies. 'Since these technologies are becoming more main stream it is expected that the effectiveness, reliability, and robustness of the energy grid could be highly susceptible to compromise [6]. The grid would require significant upgrades [9] (as switches, cable and transformer replacements) to absorb this changing behaviour and to match the supply with the available demand, to avoid grid instability, black-outs and undesired high voltage fluctuations while the infrastructure don't operate at full capacity in the majority of the time. This is unacceptable due to associated high costs. Therefore, research on active participation of buildings in the electrical grid is required to service (balance) the grid from the demand-side. In the context of this project the 'smart grid' refers to as an upgradable electricity distribution network that enables intelligent power control and multi-directional communication between sources, loads and components to facilitate cooperative and economical use of energy [10], see appendix B. Demand-side participants, that actively approach their building processes (consume) and have an on-site production facility (produce), are called Prosumers [11]. Who physically may have a combination of: energy sources, loads, storage; and an electric grid. Currently, in the building sector, electrical energy storage is rarely applied, cases are found at island-situations, households for optimizing the self-consumption of on-site produces solar-energy, and for grid-support (grid-level) activities on large-scale (MW) [12]. In this study, the focus is on a new case, by adding a Photovoltaic (PV) -generation and Battery Energy Storage System (BESS) to investigate participation future office Demand Side Management strategies (DSM).

1.2 Problem definition

This study focusses on interactive informational and power exchange between the building and the power network. The Master project is within the framework of PhD research project entitled 'Smart-Grid Building

Energy Management System'[13]. The PhD research aims at developing a building control framework for sustainable energy exchange between office buildings and future power systems network (here referred to as smart grids) [14]–[17]. Here, the focus is on design, development, implementation and commissioning of PV generation plant and battery energy storage system (BESS) at a case study office building located in Breda.

Use of demand side located BESS in the manner envisioned (provision of grid support activities) is innovative; BESS are normally applied for maximizing self-consumption of local produced renewable energy and as a back-up service. Integration of BESSs for DSM in the building sector is currently not an attractive business case due to battery costs and lack of price incentives of the utility. However, this will rapidly change in the near future. BESSs could become economically feasible due to large scale production of batteries (Tesla) and large R&D efforts cost undertaken as described in [18], [19], [20].

PV-facility investment costs have already decreased significantly last few years [18], [21]–[25]. The levelized cost of energy (LCOE) had already reached grid parity for Dutch households by the end of 2010. For Dutch commercial buildings, the grid parity was cost was halved in 2010, then equaled in 2014. From 2010 to 2014 the average LCOE price halved [26] and reached grid-parity for Dutch commercial buildings which have a yearly consumption above 50.000 kWh (lowest tax-rate). This decrease will to continue up to LCOE of 4-6 eurocent per kWh in 2025 and ultimately reach 2-4 eurocent per kWh in 2050 [26]. This will result to a higher renewable energy generation share, and even lower energy costs than for fossil powered plants. The mentioned growth will affect the effectiveness of the grid on all levels (building, neighbourhood, city and central-level) [6].

Designing a hybrid facility incorporates two or more electricity supply options, in this case by a PV-generation facility and a BESS. Due to the lack of optimum designing and sizing hybrid systems, systems may be oversized or not properly planned or designed, resulting in undesirably high installation costs [27]. Software tools (full list: [27]) are available for the design, analysis, optimization and economic planning. Most researches ends at the modelling phase, but in this study, the construction- and commissioning phase is also included.

1.3   Aim of the research

'To develop a Photovoltaic- and Electrical Storage System for investigation of Smart Grid facilitating demand side management strategies for an office building in Breda, Netherlands'

1.3.1   Research Questions

1. Which are the desirable properties of PV + BESS facility that would comply with SG-BEMS research requirements?
2. What is the best suitable PV- and BESS facility available in the market?
3. How can the selected PV- and BESS facility be adapted for installation and operation with the existing electrical infrastructure, building management system and building?
4. How to verify the performance of the PV- and BESS facility for fitness of purpose?
5. What is the operational performance of the developed system in relation to the SG-BEMS requirements and operational flexibility?

1.4 Methodology

A more or less typically sized and equipped office building, Kropman Breda, was selected as case study building to test the approach in a real setting. If the approach has an added value here than that would mean a large opportunity for application, as the large part of Dutch offices is comparable. The building will be transformed from a traditional operation role as 'consumer' (left fig. 1.4.1) to a role as 'prosumer [11]' by adding a local generation (Photovoltaic (PV) - and battery electrical energy storage (BEES) facility (right fig. 1.4.2.). The building can become energy positive, during sunny weekends, but also throughout the week by parallel operations of PV + BESS. In blue highlighted: the focus areas: development of a PV generation- and electrical energy storage facility.
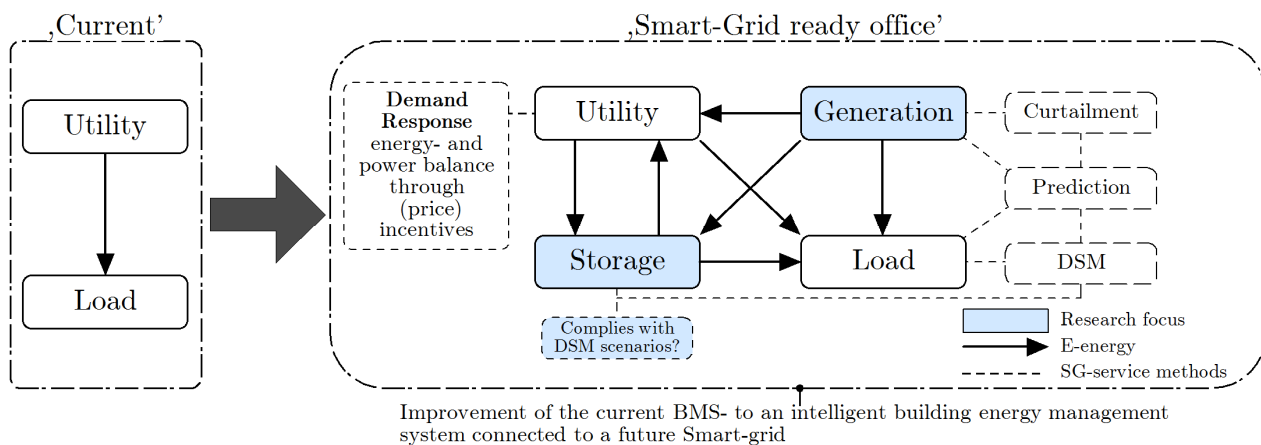

Fig. 1.4.1: Adding a non-utility generation and electrical storage facility, modified from [28]

To specify the properties of the PV + BESS facility a list of requirements is made to comply with the SG-BEMS promotional project, building characteristics, electrical infrastructure and facility management or host company dependent constraints. Based on the listed requirements a market review is done and conceptual design variants are assessed with the Kesselring-S methodology [29]. The Kesselring-S methodology is an easy understandable design assessment method [30], evaluated in an earlier done research M3-project.

Facility capacity determination according the research requirements is more complex and therefore a dynamic model was developed. These requirements were numerically evaluated using a self-developed Simulink model. This developed model contains three specific components namely:

1. General PV-generation model for capacity and performance study
   - partly consists with solar functions developed by Sandia National Laboratory [31]
2. Kropman Breda building loads model (with empirical data) for evaluation of; the resulting net-load (total load − PV generation) and to match with possible Smart operational scenarios.
3. Simplified battery system model (inspired by: [32]) with DSM controller, to test if a designed ESS satisfies with the set requirements and DSM (smart) operation scenarios.

After a specific facility was chosen based on the outcome of the Kesselring-S assessment matrix and developed dynamic developed model, it is procured, constructed and verified during the commissioning period. For the verification study, research-required instrumentation were selected and installed to identify the behaviour and performance of the PV + BESS.

Further sections of this research are outlined as follows:
Chapter 2 provides the facility requirements
Chapter 3 presents the design methodology and evaluation framework
Chapter 4 presents the selection of a specified PV + BESS facility
Chapter 5 specifies in details the final design and procurement of the PV + BESS whereas
Chapter 6 reports on installed systems verification study.
Chapter 7 reports on the operational flexibility for future SG-integration
Chapter 8 discussion and conclusion

2 Facility design requirements

This chapter outlines the design requirements for PV+BESS facility. Prominent in shaping the requirements is the need to identify and leverage building side flexibility; this includes consideration of building loads, on-site storage and generation. Building side flexibility is considered within the framework of Demand Side Management (DSM: 'includes everything that is done on the demand side of an energy system, ranging from exchanging old incandescent light bulbs to compact fluorescent light up to installing a sophisticated dynamic load management system' [33]). Therefore, interaction of designed facility with load pattern modification strategies is explored. These include enhancing self-consumption of generated energy (for example charging the battery with excess solar-power, charging battery during off peak and discharging it during night-time), valley filling and load shifting. The designed system must facilitate these types of dynamic energy management and which in future will be integrated in building energy management system for Smart grid supportive operation scenarios.

2.1 Research facility

This section describes design requirements for the PV- and BESS facility. Also discussed are installation requirements such as construction and safety, investments, connectivity to electrical infrastructure, instrumentation and control.

2.1.1 PV-capacity

The PV systems requirements are guided by the following:

- Capacity need to link PV generation with cooling system energy use during summer time. It is desired that the PV system should generate enough power to fulfil the average Chiller load. In earlier done research [34] there was found that the cooling machine energy use for a full active day (is 36% of the total chiller operations) is on average: 11kW during an hourly interval. During these active days the cooling machine operates for about 08:20 HH:MM (50minutes * 10hours). This implies to an electrical energy demand of 91 kWh, which should be linked, to the production of the new PV-facility.

- The coupling of PV generation with Chiller demand is based on the philosophy of maximizing the consumption of the on-site PV-produced renewable energy (self-consumption) and takes advantage of coincidental high PV yield and cooling energy need occurring during summer period. Chiller operates on a characteristic on-off modulated mode which alternates between the single stage demand of 7 kW and double stage demand of up to 19 kW (2014 till now, however, the double stage demand is always 17 kW except for outlier conditions). The result is peak capping for summertime electricity requirement; this may be advantageous in cases whereby peak demands are need to be capped for smart scenarios.

- Power and energy performance operational verification include yield profile under various conditions (kW versus time)

- Other requirements are total system lifespan, investment costs and benefits accrued from the system.

2.1.2 BESS-capacity

The following outlines key considerations guiding BESS design:

- The BESS should be capable of peak power capping, especially during start up periods of humidifier and second-stage consumption of the chiller. This aids in smart scenario whereby peaks are capped at critical periods of demand by second stage chiller operation and humidifier start up load spikes requirements. The BESS should have sufficient storage capacity to clip the intermittency of the chiller and humidifier load and PV-generation. Humidifier peaks (if absolute humidity < 7.0 g/kg) are mainly expected during winter season and occasionally during autumn- and spring season. Chiller operations are expected during summertime and occasionally during spring and autumn.

- The BESS must be able to enable participation of the building in smart grid-support activities especially in conjunction with comfort-based loads. This with specific reference to short-term power flexibility services of less than one hour (0 to 60 mins). The BESS should aid in achieving an optimized self-consumption of building produced renewable energy.

- Other requirements include consideration of total lifespan, costs and benefits for a specific system.

- Energy and power performance operational verification are with respect to the following: characteristics are identified:
  - Availability period (time)
  - Charging/discharging cycle time boundaries (time and SOC)
  - Demand reduction (kW)
  - Energy delivered (kWh)

2.2   Design requirements

2.2.1   Construction and safety related issues considered:

- Roof needs to be strong enough and cover needs to be in good condition (weight PV-panels/ballast)
  - Easy and safely accessible to facilitate inspections and maintenance.
  - Safety regulations at roof edges as advised by the Dutch ARBO should be adhered to; for example (within 2 meter), there must be safety-line and clear signage.
- Battery system should be well insulated and should be in protective cages that are finger proof and no open connections should be placed as required by the NEN 3140.
- Fire-safety and danger of explosion must be taken into account and appropriate detection sensors installed.
- Battery weight in relation to the building construction strength should be evaluated.

2.2.2   Budget

- The facility should meet the minimum research requirements as well as the maximum possible financial benefits from generation and DSM for the lowest possible investment costs.

2.2.3   Connectivity to Electrical infrastructure

- PV + BESS are ideally connected to an existing electrical group, however only a 3 x25A group is available (about 15.5 kVA). Dependent on the chosen system this group can be extended to facilitate a higher facility capacity.
- All legal requirements governing on-site electricity production were considered (Dutch Grid-Code [35] and NEN-1010[36])

2.2.4   Instrumentation

- To evaluate electrical energy balances of Building-, PV- and BESS load(s)
  - Instruments which measures: Voltage, Current and reactive-, active- and real- Power of main and total building load(s), BESS and PV-generation.
- Weather conditions for PV production analysis. According IEC 61724 [37]:
  - In-plane irradiance, ambient air temperature, wind Speed & module temperature.
- PV generation data: Array voltage, Array current, Array Power
- Battery conditions data: SOC, Current, Voltage, time, Temperature

2.2.5   Control:

- The instruments need to be connected to the in-house developed Insiteview BMS (master), where the battery management system and PV-system is configured as slave.
- The measurements and data are historically saved for performance- and smart scenario analysis. The existing logging interval settings of 1 minute for power 8 minute for temperature is sufficient for analysis.
- In the end, the facility must be capable to control with intelligent agent software. Kropman B.V. established an agent control plugin called 'Remote-control-agent' for the Insiteview BMS.
  - Measurements data can be extracted and operational set-points can be changed dynamically when a connection through the 'InsiteConnect' gateway is made.

3   Facility design concepts

In this chapter, facility designs are being detailed and assessed based on the design requirements (chapter 2). In this research available PV+BESS systems in the market are reviewed, and proposed system design variants are undertaken using the Kesselring methodology [29]. After a conceptual design is chosen, a study on facility sizing and capacity is done for the case study building using a model developed in Matlab − Simulink. The design steps are illustrated in Fig. 3.1. The experimental steps (blue blocks Fig. 3.1) are explained in details in chapter 5 and 6.
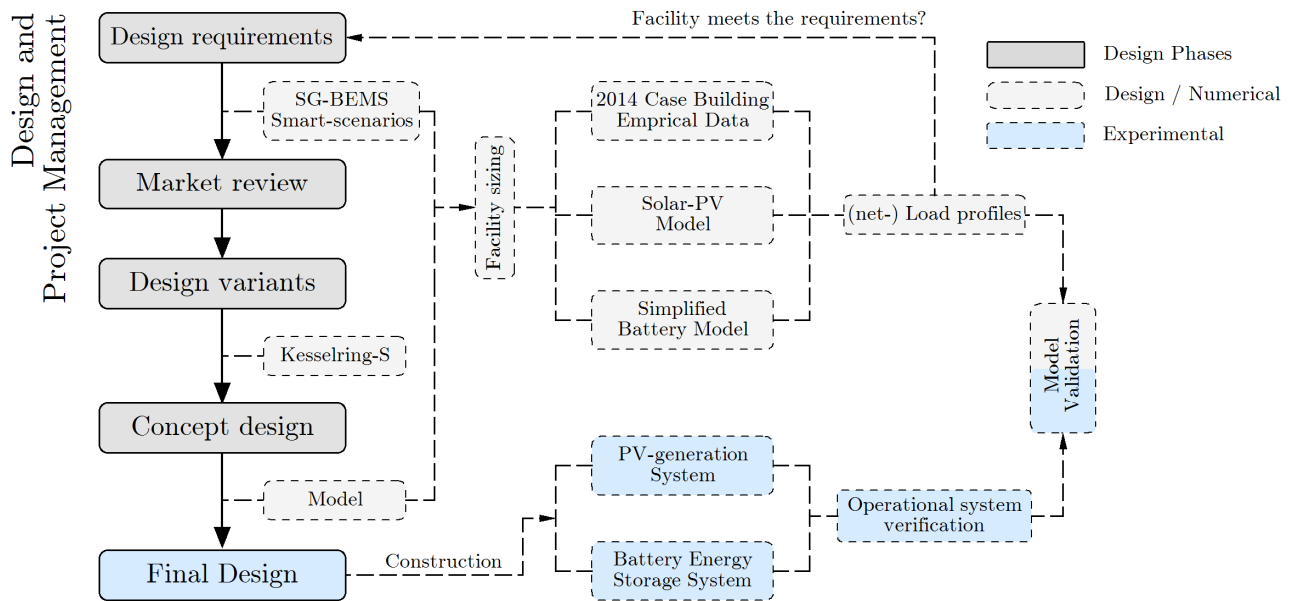

Fig. 3.1: Overview of design methodology: Design, built and commissioning

3.1   Selection PV + BESS facility

The design variants are called hybrid, since it contains two production facilities, hence PV- and BESS. For the development of this facility, we can make a distinction between three main system categories:

1. Market ready system: all-in-one hybrid system; it contains a single-phase bi-directional inverter where the batteries, PV-panels and the AC-bus are connected in one component (the bi-inverter).
2. A system variant that requires separate DC/DC charge controllers for charging battery banks and the connection of the PV-panel strings. Secondary sides of controllers usually operate at low voltage (≤48V) and are connected to a bi-directional inverter to generate a single phase AC-current (230V).
3. The third system separates both of the systems, into an independent operating PV-facility and BESS.

These configurations are shown in figure 3.1.1, page 9, and performance characteristics are provided in table 3.1.1. It is expected that the BESS is often used as demand side service (AC) to the smart-grid and partially as storage function for optimizing the self-consumption of the on-site produced RES-E − PV.

3.1.1   Hybrid system design variants

Based on three categories (3.1), five (market-ready) variants are designed. Schematic overviews of these solutions are provided in figure 3.1.1 and background information can be found in appendix C.

1. **All-in-one Hybrid** (Power-router)
   a. Single Phase nominal power $3.7 - 5$kW, for 3phase 3x (24VDC & 48VDC)
   b. System efficiency $= 93\%$

Ideal for optimizing self-consumption of on-site produced renewable energy (PV-production), since the PV-panels and battery storage are both configured at the DC-side. However, the single phase system is mainly developed for the household sector and battery types (chemistries) are limited. Connected batteries are only configurable in a 24VDC lead-acid or 48VDC li-ion. Drawback of this system is that PV-production is dominant, for power flexibility of the battery during the day.

2. **Hybrid system with charge-controllers** (from: Schneider, Outback Solar, SMA sunny Island, Selectronic)
   a. Single phase bi-directional inverter nominal power 2.3 to 6.8 kW ($\eta = 92\%$ to 95.8%, highest nominal power and efficiency for SE-XW+)
   b. Charge controllers: 2.4 to 5.0 kW ($\eta = 97.5\%$ to 98.1%)

Ideal for self-consumption of PV-power, batteries and PV-panels are configured both at the DC-side. Charge-controllers are required to connect the PV-panels and batteries after which they are connected to the single-phase bi-directional inverter(s). To operate in a 3-phase system, three bi-directional inverters are required. This system has the advantage over the first that any battery chemistry below 48VDC can be connected due to custom program possibilities.

System configurations 3, 4 and 5 operate independently: the PV-system performs at maximum efficiency/capacity, and battery system can be used for peak shaving (for example) without PV-production dominancy. Efficiency for-self consumption of PV-power is worse than system 1 and 2, since the batteries are not 'directly' charged at the DC-side. The BESS configuration is customized programmable and variant have good monitoring (PV+BESS) possibilities. Difference in system 3, 4 and 5 lies in the type of independent operating PV-system (S: 1,2,3).

3. **Separate ESS with string PV system type 1** (panel level DC/DC optimizers)
   a. String inverter PV-system with panel level optimizers (DC/DC: $\eta = 99.1\%$ and central inverter DC/AC η: 97.6%)
   b. Independent battery energy storage system (DC/AC: $\eta = 97$-98%)

PV – system solution 1 (S1): provides optimal monitoring possibilities (from individual panel to inverter level), no efficiency loss due to mismatch problem (current) between panels (see solution S2). Each panel is optimized to operate at its maximum power point (MPPT) and the energy production is monitored from panel- to inverter level. With this, panel level DC/DC optimizer, a constant voltage is provided allowing the DC strings to operate constantly at 750VDC (SolarEdge), for optimal inverter- performance, low ohmic cable losses and longest lifetime. For the SolarEdge system this implies that string lengths can vary (uneven lengths) without compromising the system efficiency. In the future individual panels are exchangeable for testing newer types without compromising on the efficiency of other connected panels.

4. **Separate ESS with string PV system type 2** (string inverter, string level maximum power tracker)
   a. String inverter system, with central Maximum Power Point Tracker (MPPT)- (SMA STP15000, η: 97.8%)
   b. Independent battery energy storage system (DC/AC: $\eta = 97$-98%)

PV – system solution 2 (S2): in practice most often applied, it requires the least components and has good conversion efficiency when there is no mismatch between the panels. However, the disadvantage of this system is during situations when mismatch occur. This can occur due local shading, uneven aging, soiling, manufacture tolerances and transportation/mounting losses (small cracks in cells for example). PV-production monitoring is only possible on inverter- and string level.

5. **Separate ESS with micro-inverter PV system (PV system type 3)**
   a. Enphase micro-inverters (η = 96.5%)
   b. Independent battery energy storage system (DC/AC: η = 97-98%)

PV – system solution 3 (S3): provides optimal monitoring possibilities on panel level, no mismatch problem, lowest conversion efficiency compared to the above. With this configuration no central inverter is required since the DC/AC conversion is achieved at panel level, hence micro-inverter. However system costs are about 3 times (appendix C) [22] higher than PV solution 2 and 3 and construction takes time.

3.1.2 Hybrid variants evaluation

Each design variant (figure 3.1.1) is evaluated and assesed with the Kesselring-S method (table 3.1.1), shown at page 9 . The design criteria were divided into functionality and realization categories. The relative scores of all design criteria and functionalities are visualized on an S-(Stärke) diagram (appendix C). The best design variants lay near the diagonal and have high scores (%) within the selection area. This selection area is practically set by a border x- and y-value of 40% and by (x+y) value of 55% [38]. Based on the design variant study and assessment table a kesseldiagram is made in figure 3.1.2.

According the Kesselring-S diagram, figure 3.1.2 established from the functional and realization scores shown in table 3.1.1, concept 3 and 5 are the good choices, where number 3 is slightly better. Concept 1 and 2 scores best on self-consumption, but for grid support activities (main-focus) they have their limitations due their dependency of PV-production. For example, when the PV-panels generate electricity only the rest capacity of the bi-directional inverter can be used to discharge the battery. The 3rd, 4th and 5th design variant have the highest potential for grid support activities in power and energy flexibility, however their functionality for efficient self-consumption is lower than the first two design variants. The energetic performance of the PV-conversion for variant 3, 4 and 5 is higher than design variant 1 and 2. For the last three variants, the functional difference is in the Photovoltaic generation part.

The investment costs for all variants, is 'high'. Three single phase inverters are relatively more expensive than one three phase inverter (for the same capacity) [22]. The advantage of the last three variants above the others is the flexibility role for research on smart operation scenarios (as linking second stage of chiller power demand and humidifier start-up period $(10 - 17kW)$ to ESS). This system variant is not restricted to one single battery technology, and operates independently from PV-production.

The design variant, 3 and 5, with high scores have the advantage that PV-cell technologies can be changed over-time (for future research on different PV-panels) due the usage of panel level micro-inverters or optimizers. This in relation to a typical string inverter where a new panel type (with own specific voltage/current curve) would normally affect the power output of other panels in a string.

Variants 3 is safest during construction phase, since the panel voltage output is kept low when there is no live communication with the inverter (for SolarEdge 1VDC). With this low standby voltage, the system will stay below the safety limit of 120 VDC [36], while other variants operate at high DC-voltage.

According the outcome of the design assessment, concept variant number 3 was chosen: two independent operating systems for PV- and BESS. Where the PV-system uses panel level optimizers and centralized inverter.
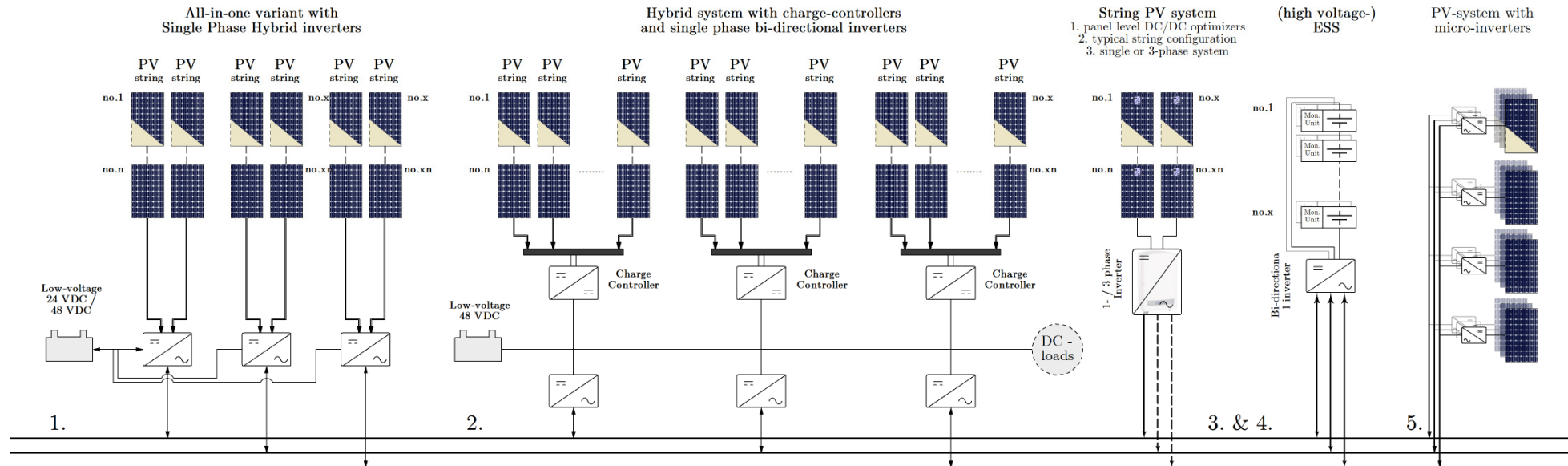
Fig. 3.1.1: System design variants

Table 3.1.1: Kesselring design assessment based on [22], [39] and appendix C.
(Market review: Power router, Schneider-XW, Outback Solar, Selectronic, SMA sunny island, SMA, SolarEdge & Enphase)

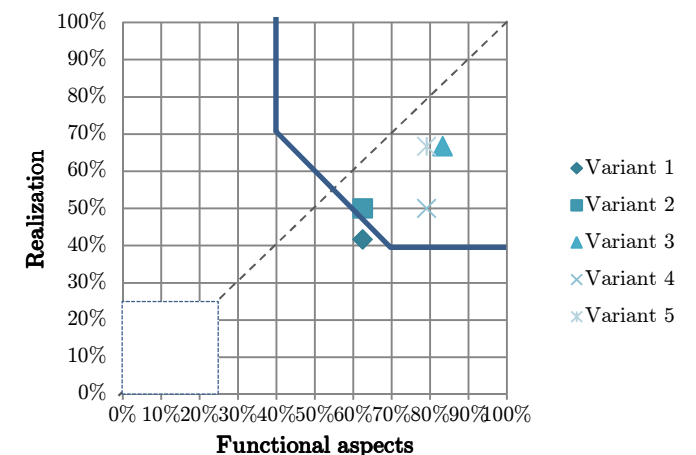|	*Total*	*Variant 1*	*Variant 2*	*Variant 3*	*Variant 4*	*Variant 5*
Energetic performance Battery part	4	3	2	2	2	2
Energetic performance PV part	4	2	2	4	3	3
Power - Grid support activity	4	1	2	4	4	4
Energy - Grid support activity	4	2	3	4	4	4
Self-consumption PV	4	4	4	2	2	2
Control	4	3	2	4	4	4
Monitoring	4	2	2	4	2	4
Sum	28	17	17	24	21	23
Functionality Score	100%	*63%*	*63%*	*83%*	*79%*	*79%*
Investment costs	4	1	1	1	1	1
Flexibility	4	2	3	4	3	4
Safety & construction	4	2	2	3	2	3
Sum	16	8	8	11	9	11
Realization Score	100%	*42%*	*50%*	*67%*	*50%*	*67%*

Fig. 3.1.2: Kesselring-diagram for PV + ESS facility

3.1.3 PV – cell technology

The next step is the PV-cell technology determination. PV-cell definition according NASA [40]:

'Photovoltaic is the direct conversion of light into electricity at the atomic level. Some materials exhibit a property known as the photoelectric effect that causes them to absorb photons of light and release electrons. When these free electrons are captured, an electric current results that can be used as electricity.'

Market available cell-technologies [41]:

- Crystalline silicon, typical poly-crystal: η = 16% with a maximum η = 23% for mono-crystal[1]
- Amorphous silicon; typical: η = 5 to 10%
- Thin Film Silicon; typical: η = 11 to 14%[2]

  [1] Sunpower, [2] Solar-Frontier

- Organic PV: maximum η = 12%
- Multi-layer cells: up to η = 45% (not commercially available)
- Electrochemical: η = 7 to 10% (not commercially available)

When a cell heats up the efficiency goes down, this is more or less a linear process. See table 3.1.2.

Table 3.1.2: The temperature effect on common PV-modules [39]:

	Monocrystalline	Polycrystalline	Thin Film
Output power derating: STC: 25°C	-0.45%/°C	-0.5%/°C	0 to -0.3[2]%/°C

PV-Panels are tested according the Standard Test Conditions (STC): Module temperature of 25°C, insolation value of 1000 W/m^2 and an Air Mass of 1.5. For a polycrystalline panel of 260 Watt peak (Wp), 1000 W/m^2 and 50°C, this result in a generation efficiency loss of 12.5%, in other words it would generate 227.5W instead of 260W. This temperature effect is less for thin film cells, these panels also operates better compared to crystalline when they are partly shaded. However, more space is required to reach the same yearly energy yield. In this case, the investment costs and market average efficiency were decisive and therefore poly-crystalline panels were the most optimal. The typical behaviour of crystalline panels is shown in the verification study, chapter 6.

3.2 Selection Battery Technology

Electrical storage systems can be categorized into 4 categories, namely electrical (as capacitors), mechanical (as pumped hydro), thermal (thermoelectric storage) and chemical (as Lead-acid, Li-ion) [19] (figure in Appendix C). For decentralized systems, the focus is on the electrochemical systems, that stores and releases power through chemical reactions. The main difference between the batteries are the materials used for the anode, cathode and electrolyte [42], each battery chemistry has its own advantage and drawbacks and therefore there is no ideal battery for each purpose [14]. Again, the Kesselring-S design methodology is used to find the best technology for the case building research facility. In appendix C the working principle of a simple chemical battery is given. There are six aspects which should be taken into account for the functionality aspects namely; efficiency, durability, reliability, response time, energy- and power density, energy- and power capacity [14]. Battery cycle life is non-linear process; it is related to the number of cycles, temperature, charge rates, voltage, State of Charge level, Depth of Discharge (DOD) or others as battery failures due to leakages etc. Each cell technology has its own optimal operation window. In general there can be said that deeper cycles reduces the maximum number of cycles, a constant temperature is preferred during storage and usage, and overvoltage can cause high pressure, explosive gas release and high temperatures. An important parameter for load levelling is energy capacity, but for systems where short-term power must be provided response time and power rates are more important. Batteries are suitable for more than one application as they are fast responding and can operate for hours, dependent on the capacity, that is making them appropriate for power management and load shifting [43]

Table 3.1.3: Comparison of chemical energy storage technologies [44], [45]

Battery Technology	Cycle efficiency [%]	Cycle number	Recyclability 1 = low 5 = high	Operating temp [°C]	Recharge time	Power investment cost [$/kW]	Energy investment cost [$/kWh]
Lead-Acid	$80 - 90\%$ [45]	2000	5	+25	8h-16h	200 - 650	50 - 300
Li-ion	$85 - 98$	±4000	4	-10 to 50	Min-h	$700 - 3000$	200 - 1800
NiMH	$60 - 66$[44] $70 - 75$[45](90^1)	$200 - 2500^1$	5	-20 to 45	$0.5h^1$ - 4h	$420 - 1200$	240 - 1200
NiCD	70 - 75	1500	4-5	-40 to 45	1h	$350 - 1000$	200 - 1000
NaNiCl	$85 - 90$	$1000 - 2500$	5	+270 to +350	6h-8h	$100 - 200$	70 - 150
NaS	85	2000 - 4500	5	+300	9h	$700 - 2000$	70 - 150
ZnAir (new)	$70 - 75$	2000 - 20000	5	+20 to +50	$3h - 4h$	$500 - 1800$	$100 - 700$

[1] Nilar battery at 60% SOC window

Each technology has its specific energy and power density range. The range for a specific technology is strongly dependent on the battery design/construction.
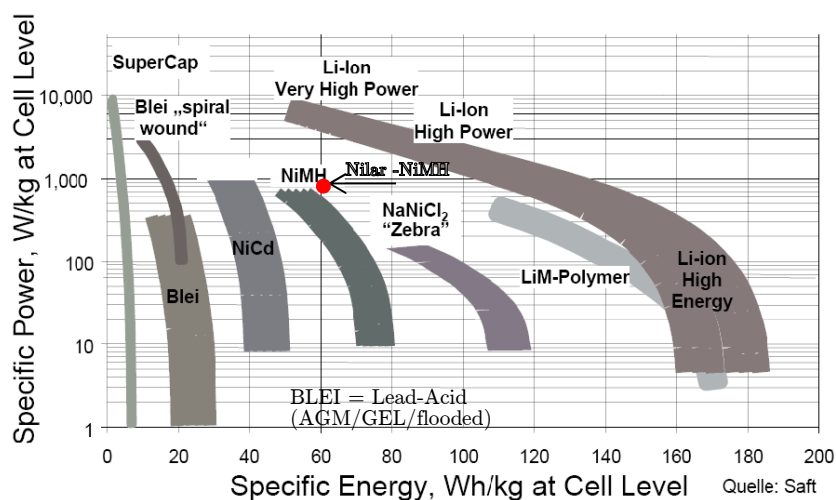

Fig. 3.1.5: Battery technology comparison [46]

According the EN-50272 batteries, as NiCD and Lead-Acid requires room ventilation. This is not the case for Li-Ion and NiMH systems according the standard. Batteries based on the following chemistries were evaluated with the Kesselring-S design selection technique: lead-acid, NiMH, li-ion and an advanced Aqueous Hybrid Ion battery technology.

Table: 3.1.4: Kesselring design assessment based on [44], [45], [46] & market offers (appendix C)

	Total	*Li-Ion*	*NiMH*	*Lead AGM*	*Lead GEL*	*Aquion-Energy*
Energy density	4	4	3	1	2	*1*
Power density	4	4	3	2	4	*1*
Cycle efficiency	4	4	3	2	1	*3*
Life cycle (cycles)	4	4	3	2	2	*3*
Charge rate / power capacity	4	3	4	2	1	*1*
Non-operation loss	4	3	2	3	2	*3*
Charge control / response	4	2	3	3	2	*3*
Sum	28	24	21	15	14	*15*
Functionality Score	**100%**	**86%**	**75%**	**54%**	**50%**	**54%**
Investment costs	4	1	1	4	4	2
Sustainability & Recycling	4	3	4	3	3	4
(fire-)Safety	4	2	3	1	1	4
Commercial business benefit	4	1	4	2	3	1
Sum	16	7	12	10	11	11
Realization Score	**100%**	44%	75%	63%	69%	69%

The li-ion battery technology offers the highest functionality score, followed by the NiMH battery technology. The mature technologies lead-AGM and lead-GEL are both sufficient for load levelling, but for high power rates, they are not. These technologies also require special ventilated rooms due the H_2 gas emission during any normal operations (even for the sealed AGM & GEL batteries). They are the cheapest solution. The functionality score on energy and power density of a NiMH battery is somewhere between the Lead-acid and Li-ion batteries. Due a business related decision this battery technology scores high on the realization, while the costs are almost equal to Li-ion based batteries which scores the highest at functionality and lowest on realization due cost and (fire-) safety issues [47]. A new, sustainable technology is also compared, the Aquion-energy battery, which is a competitive choice for the lead based systems.
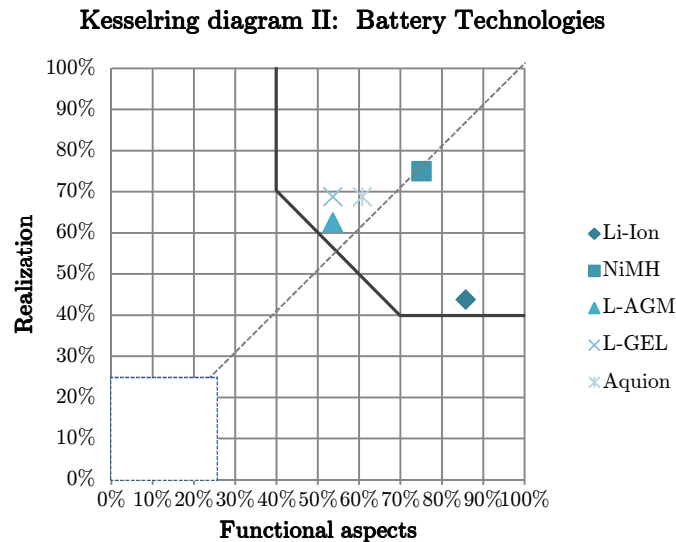

Fig. 3.1.6: Kessel diagram for Battery technology

Based on the battery technology combined with the hybrid design variants the following solution was chosen: Kesselring assessment matrix I & II: Hybrid variant 3(I). It offers an appropriate system to connect the high-voltage NiMH (*Nilar) (II) battery technology. It contains two independently operating systems: the panel optimized (SolarEdge) local generation system and a NiMH battery electrical storage system.

4 Realization of concept design at case building

The conceptual design of the PV + BESS facility is selected in chapter 3 (research question 2); the next step is a facility sizing study (research question 3) in order to meet with the earlier set research requirements. These requirements are provided in chapter 2 (research question 1). In the next section background information about the case building for the realization of the PV+BESS facility is provided.

Kropman building operation schedule (2016)

	Time Start:	Time End:
Monday	06:00	17:00
Tuesday	07:00	17:00
Wednesday	07:00	17:00
Thursday	07:00	17:00
Friday	07:00	16:45
Saturday	00:00	00:00
Sunday	00:00	00:00
Public holidays	00:00	00:00

Fig. 4.1: Front view of Kropman Breda office building

The in 1994 built Kropman office is three storeys high and has a gross floor area of about 1.400m². It contains conventional methods (Appendix C) for heating, cooling, ventilation, and humidification; this is achieved by a gas-fired boiler, compression cooling machine, AHU with two fans, heating battery, heat recovery wheel and an electrical steam humidifier respectively. The building management system (BMS) consisting of Priva and Insiteview, controls and monitors the Heating, Ventilation and Air-Conditioning (HVAC) system. All control settings can be changed within the Insiteview environment, developed by Kropman B.V. Insiteview can be used as Software Gateway to connect almost any other third-party software. In this research Insiteview will be extended with a BESS-control module (without the use of PRIVA). In the future (not in the scope of this research) it will be extended with a new intelligent control layer, operating on an agent-platform, for testing smart scenarios. For placement of the BESS there is space available in the installation room and for the PV-facility the upper part of the building is available for PV-panel installation. The roof is constructed by layers of: 200mm concrete-hollow core slab, 80mm of insulation and finished with a bituminous layer and gravel. The effective area for the construction of the panels is about 230m². The flat roof has a slight slope, from the dashed line (figure 4.2) under a gradient of 110mm.
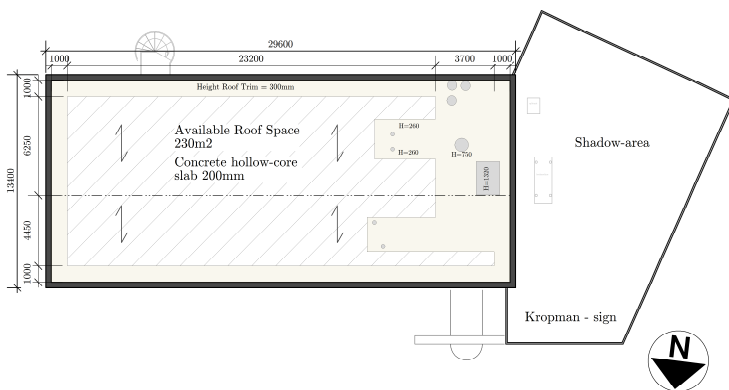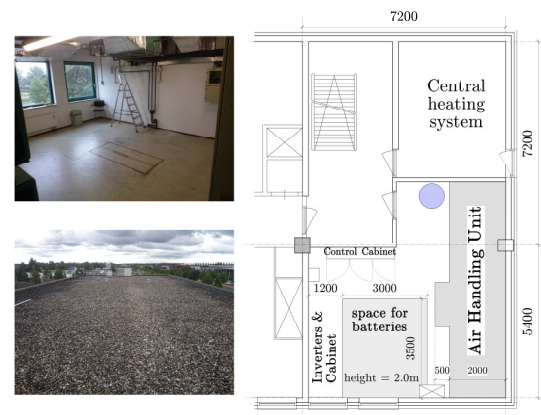

Fig: 4.2: Roof-plan Kropman Breda office

Fig. 4.3: Installation room for battery placement

The roof on the west side is one storey lower than the east side and therefore for a large fraction of the day in the shadow. For the battery system there is about 15m² of area available for battery placement and wall mounting of the required battery management- and inverter cabinets.

4.1 Dimensioning of PV+BESS system for Kropman Breda office

After a concept design was selected in chapter 3, a system must be dimensioned in order to meet the set research requirements in chapter 2 and fits to existing building construction and infrastructure. In order to

investigate if a specific facility capacity meets the research requirements a model is made. This model is divided into three: first, the photovoltaic generation model based on a detailed Solar-PV (numerical) model is shortly explained (4.1.1), continued with the electrical storage model of a simplified representative battery (control) model (numerical) (4.1.2) and closed with a DSM control model (4.1.3). These specific models were developed as blocks in Matlab − Simulink, figure 4.1.1 (see also Appendix D).

The first and second are adaptable models, characteristics (as capacity, orientation and inclination) and set points (charge, discharge time and rates) can be changed. It is possible to simulate the PV-production for any climate year which is available in the KNMI database [48]. PV-model blocks are partly retrieved from the Sandia PV performance collaborative [31]. The second model is a simplified battery model based on the typical performance characteristics of most important parts of the system (battery exothermic losses, inverter, transformer and filters, these efficiency conditions are received from NiMH battery manufacture: Nilar international AB see also chapter 5. It is the only operational flexible load in this model configuration. The model is used to verify if a chosen facility size and capacity meets the design requirements. The empirical data electricity consumption (1) of year 2014 is used, since this is the first year that the most important measurements of building loads are available.
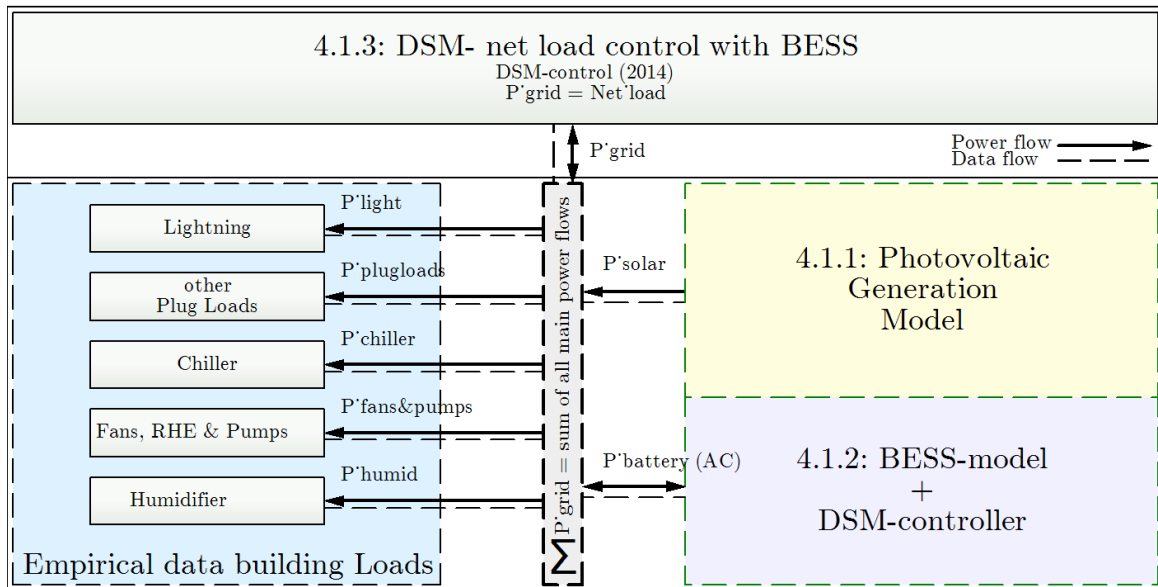

Fig. 4.1.1: Schematic overview simulation model

4.1.1 Photovoltaic-generation model

Numerical assessment of variable facility capacities and mounting possibilities is done in order to see if a specific design meets the design requirements by linking the PV-generation to the chiller power and energy demand and evaluating the impact on the yearly load.

The PV-model only require the following time series data: global horizontal irradiation (GHI), outdoor temperature in °C (T_e) and wind speed in m/s (WS) for a specific location in latitude in degrees, longitude in degrees and altitude. The altitude is used to define the typical atmospheric pressure; here a site pressure of 1013.25 hPa or one atmosphere is used (sea level). The time series data can be extracted from a nearby meteorological station of KNMI [48], in this case station Gilze-Rijen. Hourly validated data is available, but also 10minute data can be received on personal request. The best and worst insolation year only deviate 15% compared to the average, in de Bilt: 983 [kWh/m²] and Gilze-Rijen 1013 [kWh/m²] [49]. Figure 4.1.2 presents the basic model structure with corresponding literature references.

A detailed explanation and equations of all model components is provided in appendix D, a short description is provided here. The power output of the PV-facility is modelled as following: First the sun's position is calculated, this is achieved with a dynamic Sun zenith and Sun azimuth model [50], it is able to
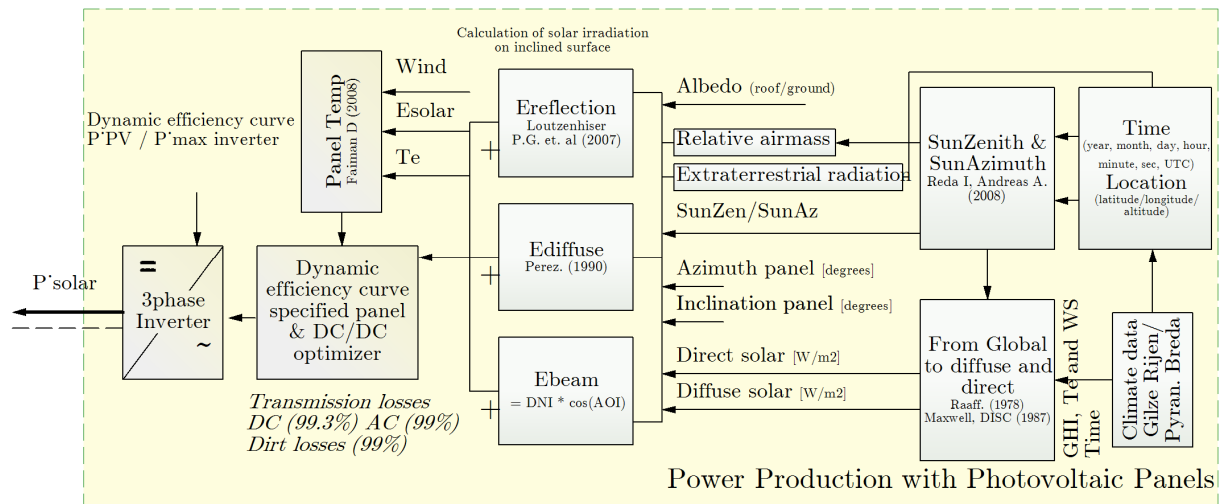
Fig. 4.1.2: Photovoltaic-generation model overview of all components and used references

calculate the angles for year -2000 to 6000 with uncertainties of ±0.0003°. Knowing the sun's position, at a given moment (time) and location, the relative air mass (AM.1 at equator AM.1.5 at northern latitudes) and extra-terrestrial irradiation (ETI) can be determined. First, the GHI is separated into a diffuse and direct radiation component. The direct normal irradiation is calculated with Direct Insolation Simulation Code (DISC) [51] it uses hourly values of the GHI, sun's zenith angle and day of year as input and empirical relations of the direct normal transmittance and global horizontal transmittance and clearness indices to determine this. In literature [52] is written that the DISC [51] is the best model (with lowest BIAS error) to determine the DNI. It has the smallest Mean Bias Error (MBE: 25 W/m²) and Root Mean Squared Error (RMSE: 85 W/m²) under all conditions. Known the DNI and GHI, the diffuse horizontal irradiance (DHI) component can be determined (eq. D.8).

From this point, the irradiance on a specific Plan of Array (POA) can be estimated. It is the sum of the diffuse, direct and reflected radiation on a specific oriented [°] and inclined [°] surface (in this case a PV-panel). The first parameter, the diffuse radiation, can be determined with the Perez et.al (1990) model [53]. It uses the array inclination and azimuth angle, DHI, DNI (without angle conversion), ETI, Sun zenith and azimuth angle the relative AM as input values. The direct irradiation on POA is calculated by the DNI times the cosines of the angle of the solar ray's incidence. As last reflections are taken into account, using the GHI, panel tilt angle and ground reflectance factor (Albedo), usually around the 0.2 for a roof surface [54].

At this point the solar energy on a specific plane is known which then must be converted to an electrical power. The efficiency of a PV-panel is strongly dependent on the cell temperature. The temperature is calculated based on simple steady state heat transfer principles using the outdoor temperature, irradiance on a POA and wind speed [55]. This method [55] has a maximum uncertainty of ± 2°C, this only result in a panel efficiency error of 1% (with a panel power efficiency coefficient of [0.5 %/°C]. Knowing the panel temperature the conversion efficiency can be determined based on manufacture STC test results (eq. D.15). The chosen system solution uses panel level DC/DC optimizers and a central DC/AC inverter. The conversion efficiency is determined based on the function of DC input power divided by the nominal optimizer power (for the optimizer) or nominal inverter power (for the central inverter) and is implemented as functions in the PV-model.

4.1.2 Electrical storage system model

To evaluate a chosen battery capacity in relation to the research requirements, about clipping the second stage of the humidifier and early morning peak of the chiller, a BESS-model is made. The electrical storage system model is modelled based on the in figure 4.1.3 shown scheme. A detailed BESS model description and derived equations is presented in the appendix D.
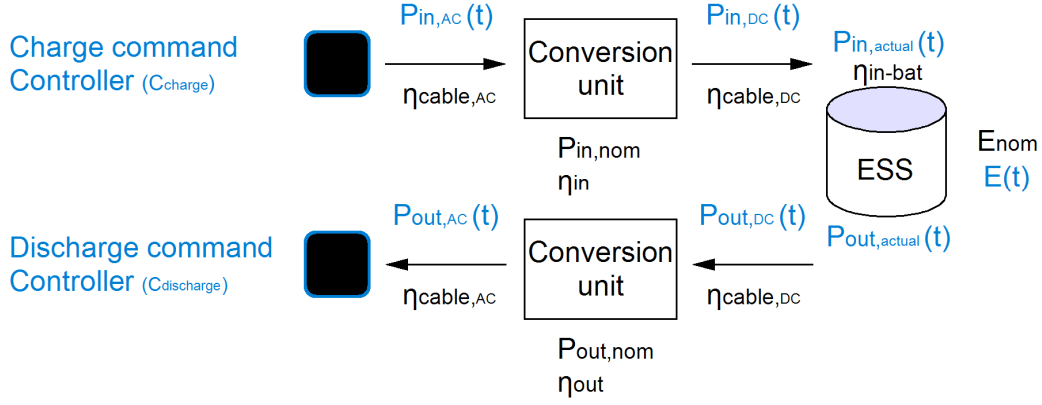
Fig. 4.1.3: Battery Electrical circuit model

The BESS is charged or discharged based on an AC power request (command) (chapter 4.1.3), when there is battery capacity available. The battery capacity at a specific moment t, E(t), is defined as the initial energy summed with the integral of actual DC_{in} power and integral of DC_{out} power for E(t-1). The minimum and maximum SOC limits are set in the net-load controller (4.1.3).

(4.1)

$$E(t) = E_{initial} + \int_{t-1}^{t} P_{in,actual}(t)dt + \int_{t-1}^{t} P_{out,actual}(t)dt \quad \text{and} \quad SOC(t) = \frac{E(t)}{E_{nom}} \ [\%]$$

The conversion efficiency is a function of the requested AC power divided by the nominal AC power of the inverter, filters and transformer. This resulting DC_{in} power is multiplied with the chemical loss of the battery due the exothermic reaction. According the battery manufacture (NiMH: Nilar) losses only occurs during charging (and non-operation loss). During the discharging process, chemical losses are negligible. The exothermic loss depends on the charge rate, but moreover to the SOC level. In the model the losses are known (chapter 5) for a 0.2C and 0.3C charge rate at 10% SOC intervals (from 20 to 100%), which is translated to an exothermic efficiency factor (η_{in-bat}). For discharging only conversion losses of the inverter, filters, transformer and cabling are taken into account. The discharge controller uses a nearest value technique (appendix D) for calculating the required DC battery output power to reach the requested AC output power. The model assumes that there are no-losses during non-operation state and no time-delay between the (dis-)charge command and actual process start. However in practice this start up time-delay is about 5 sec. (see system characteristics in chapter 5.1), which is fast enough to be neglected in a first evaluation study, due the usage of 1 minute interval empirical data

4.1.3 DSM (net-load) control model

The DSM controller aims to change the building net-load or stay in idle. It is used to numerically evaluate demand-side comfort based loads management scenarios/requirements (chapter 2). The building net load is defined as:

(4.2)

$$P_{net}(t) = P_{building}(t) + P_{PV}(t) + P_{battery}[kW]$$

Where:

P_{net}, $P_{building}$, P_{PV} = Net load, total Building load and PV production respectively [kW]

The building loads are modelled as one block in Simulink, the empirical minute data and corresponding date and time series can be requested with a start- and end time & date. The PV production is (niet beinvloedbare parameter) fixed and simulated, the building net-load (P net-load) is only adaptable by charging, and discharging (P-Battery (AC)) the battery see figure 4.1.4.
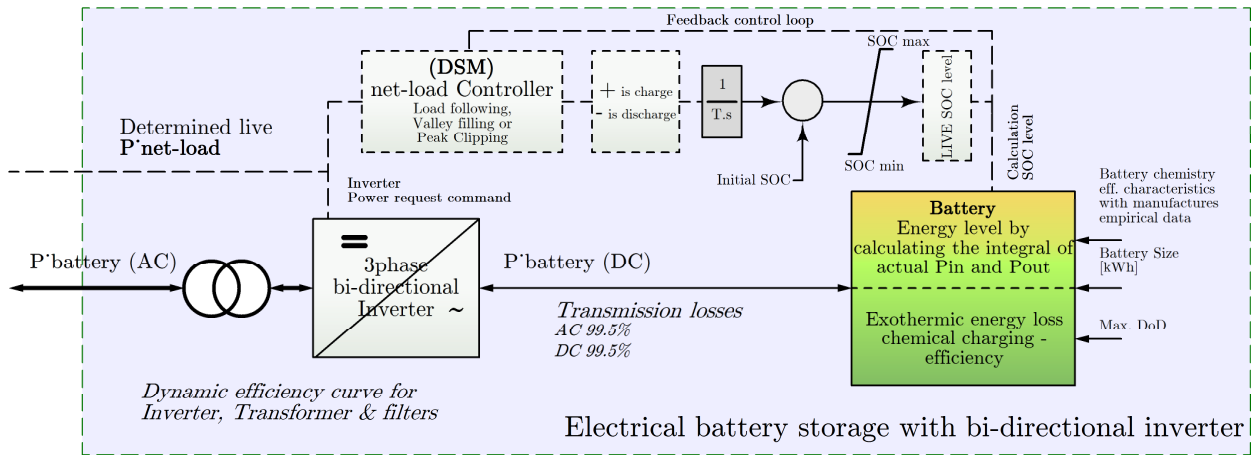
Fig. 4.1.4: Schematic overview of ESS model & DSM controller

Net-load Controller

The controller's goal is to change the net-load curve with the use of the available energy in an ESS. It is a rule based (if, else constraints) controller. First, the settings are explained, followed by a rule based structure.

Adaptable set points for all control functions (next page):

- Set min SOC level → SOC_{min}
- Set max SOC level → SOC_{max}
- Set initial SOC level → SOC_{start}

- Set min operating value (for example: >1kW threshold)
- Conditional programming applied in Simulink: 1 = true, 0 = false.

It contains four specific control functions:

1. **Charging** → valley filling
   a. Set lower limit net-load
   b. Set time start [sec]
   c. Set time end [sec]
   d. Stop when: $SOC_{live} ≥ SOC_{max}$

2. **Discharging** → peak clipping
   a. Set upper limit net-load
   b. Set time start [sec]
   c. Set time end [sec]
   d. Stop when: $SOC_{live} ≤ SOC_{min}$

3. **S**tart **F**ull **C**harge Procedure (fixed from 80% → 100%)
   a. Switch on = 1 — switch off = 0
   b. Set charge rate SOC ≤ 80%
   c. Set time start [sec]
   d. Set time end [sec]

4. Charge during negative net-load → valley filling / **load curve following** (also called **PV Charge**)
   a. Switch on = 1 — switch off = 0
   b. Set time start [sec]
   c. Set time end [sec]
   d. Set upper limit net-load

Where:
SOC = State of Charge
T_{start} = Time start BESS control strategy in seconds
T_{end} = Time end BESS control strategy in seconds
T_{live} = Time live in seconds

Table 4.1.1: charge and discharge algorithms

Step:	Discharge algorithm	Step:	Charge algorithm
A	True when: $T_{start} ≤ T_{live} ≤ T_{end}$	A	True when: $T_{start} ≤ T_{live} ≤ T_{end}$
B	True when: $P_{net} ≥ P_{upper-limit}$ & (P_{net} - $P_{upper-limit}$) ≥ $P_{min-operating-threshold}$	B	True when: $P_{net} ≤ P_{lower-limit}$ & ($P_{lower-limit}$ - P_{net}) ≥ $P_{min-operating-threshold}$
C	if B and C are true than charge command = (P_{net} − $P_{upper-limit}$)	C	if B and C are true than charge command = ($P_{lower-limit}$ - P_{net})
C.1	and (P_{net} − Charge command) to Grid	C.1	and (P_{net} − Charge command) to Grid
C.2	Else: if statement A and B are not true do nothing and distribute all to/from grid	C.2	Else: if statement A and B are not true do nothing and distribute all to/from grid
D	if Charge command is higher than inverter capacity than the difference is added to C.1.	D	if Charge command is higher than inverter capacity than the difference is added to C.1.

4.2   PV-facility capacity determination

In chapter 4.1 the models were described which are used to determine the required capacity of the PV+BESS facility. In the next paragraphs, the PV- and BESS facility capacity is determined using the described models (4.1.1, 4.1.2 and 4.1.3), first the PV-facility in chapter 4.2, than the BESS-capacity in chapter 4.3.

For the PV-facility capacity determination first the available area and maximum number of panels is determined, then the specific yield performance on possible panel arrangements is evaluated, continued with linking the PV-capacity to the research requirements (to chiller demand). In figure 4.2.1 the available area and maximum number of panels is shown, for the vertical (90°) placed panels on the façade an assumption is made that about 90% of the available area, where no windows are located, can be used to mount a PV-panel (size: 1.65m * 0.991m). For the flat-roof care is taken on the panel-distance, an increase of inclination angle result in a longer distance between the panels to avoid shade (appendix E). For example panels facing south on 15° require about 1m[1] between the panels and at 35°, 2.20m[1] [56].
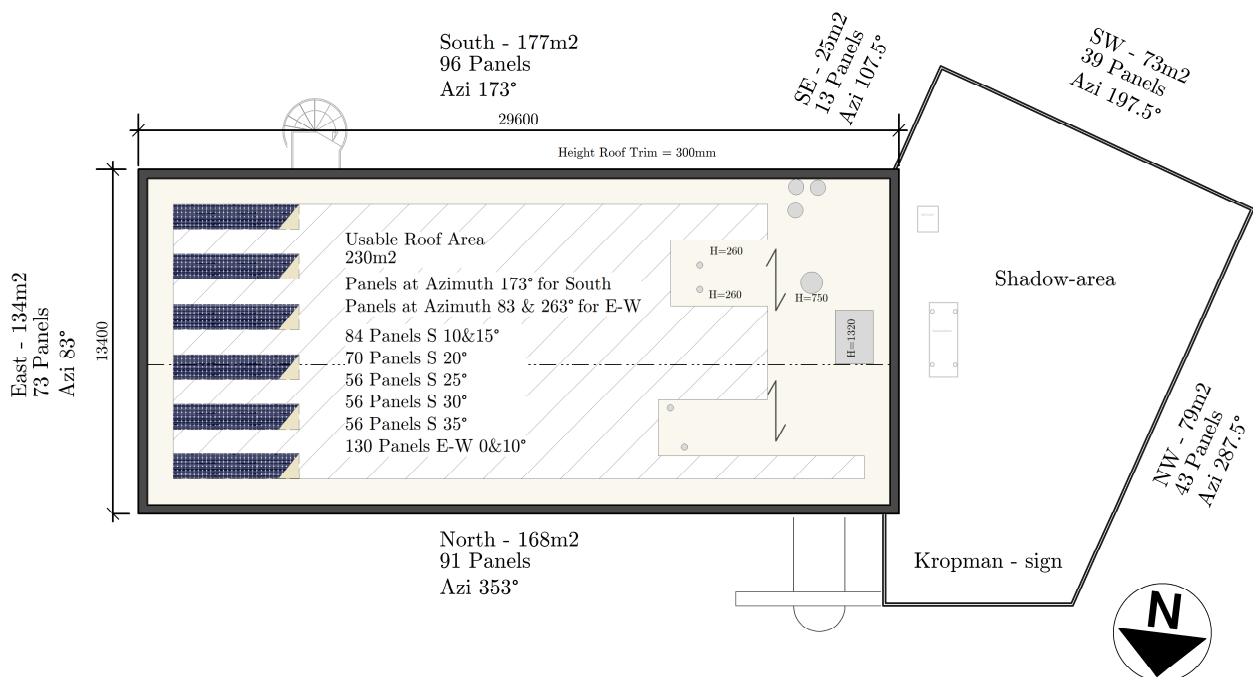

Fig. 4.2.1: Available area for PV-panel placement, on façade and upper roof. Azimuth (Azi), 0° = north, 90° = east, 180° = south 270° = west.

In this research, the focus is on the year 2014, it was the first year all energy-meter measurements were available. In this year, the electrical energy consumption accounted 83.000 kWh. The solution on the flat roof with the highest yield per panel is not always the most ideal, due the lower yield/m²-roof space ratio (longer distance between the panels to avoid shade. Panels are also mountable on the façade. In the next figures panel design configurations for the Kropman office are evaluated, the relative increase is compared to a horizontal placed panel (kWh/1.64m²) and incoming solar radiation on a square meter horizontal plane (kWh/m², typical measure for solar radiation).
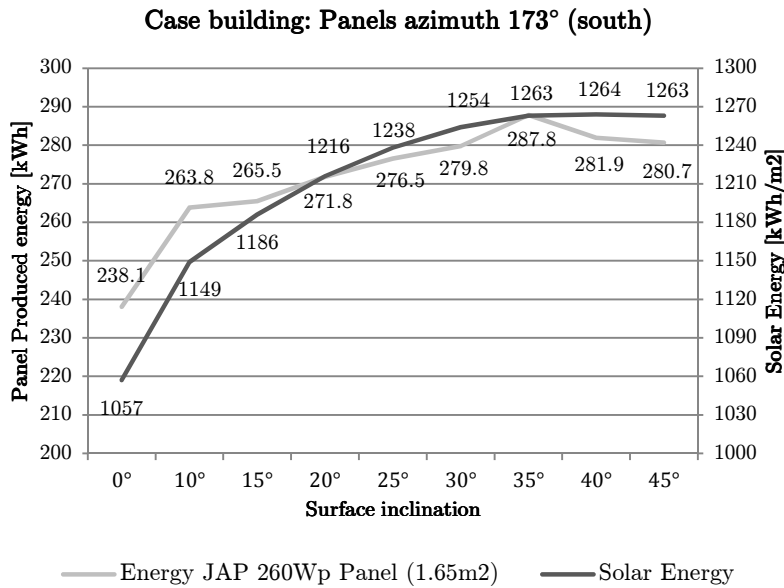
Case building: Panels azimuth 173° (south)

Relative increase compared to horizontal

Fig. 4.2.2: 2014: energy yield PV-panel JAP6-260Wp and incoming Solar-Energy *Results derived with the validated (chapter 6) PV-model (4.1.1). Simulation fixed time-step, 600sec, ODE3. A single PV-panel at an inclination angle of 35° has the highest yield.*
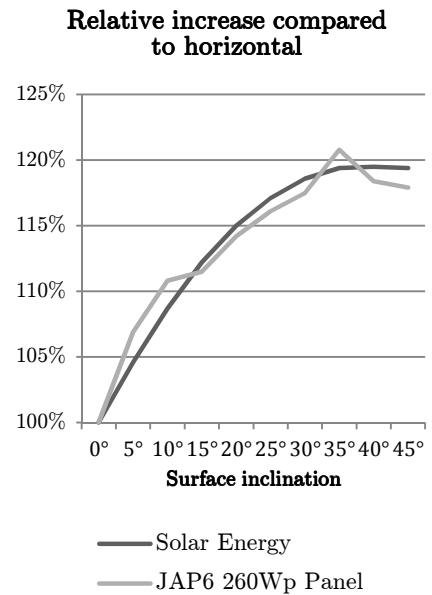
Fig. 4.2.3: 2014: Relative share compared to horizontal (100%) for solar energy and a PV-panel. *Due temperature- and conversion effects, the relative increase is not (fully) identical to the relative increase of solar yield.*

For a landscaped PV-panel, each 5 degree of surface inclination increase, require about 32cm more space between the southern faced panels. While each 5 degree increase from 15 degree (often used) only increases the PV-energy yield around the 2%.
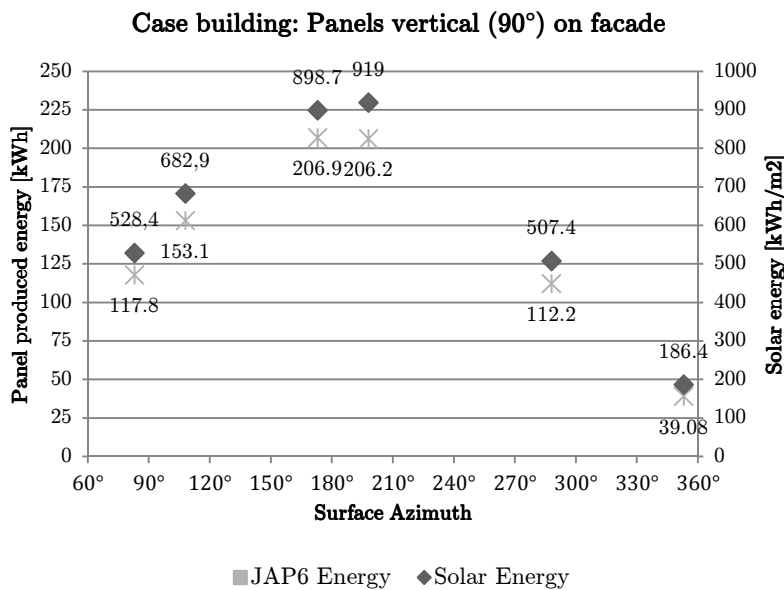
Case building: Panels vertical (90°) on facade

Relative increase compared to horizontal

Fig.4.2.3: energy yield single panel placed on Kropman office façade and incoming solar energy per m². *The yield on the eastern façade (azi: 83°) is slightly higher compared to the WNW façade (azi 287.5°). The benefit of an east-western panels is distributing the PV-power output over the day (flatten the peak-production at mid-day). PV-panel on the northern façade (353°) produces only 17% compared to the horizontal while a southern (35°) produces 116%.*
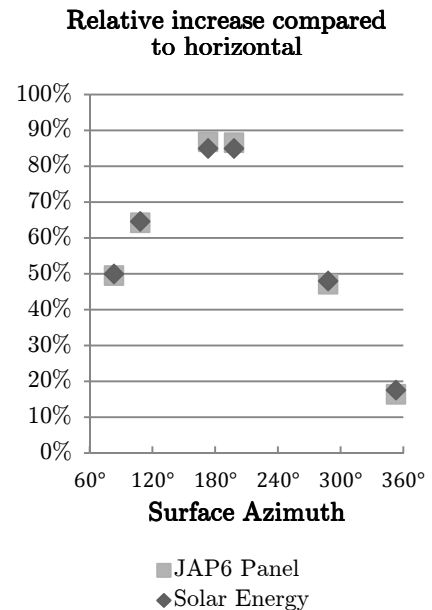
Fig. 4.2.4: Relative share compared to horizontal (100%) for solar energy and a PV-panel. *The southern faced panels (Azimuth 173° and 198°) reveal a yield decrease of 15% compared to the horizontal.*

The east (azimuth 83°, inclination 10°), west (azimuth 263°, inclination 10°), configuration provides the highest energy to roof area ratio. The incoming energy on an eastern square meter surface is 1028 kWh (97.2% compared to horizontal) and a PV panel generates 231.7 kWh (97.1% compared to a horizontal panel). For the western panel this is 1070 kWh (102.8% compared to horizontal) and 240.5kWh (100.8% compared to horizontal panel). When the eastern, southern, western façade and upper-roof surface (east/west

configuration for optimal energy surface ratio) is covered with PV-panels about 93% of the total electricity demand can be covered with renewable energy. The flat-roof provides for about 32000kWh of energy, and the panels on all façade (inclination 90°) orientations (Azimuth) 9100 kWh (83°), 2100 kWh (108°), 20800 kWh (173°), 8400 kWh (198°) and 5100 kWh (288°) is 45500 + 32000 = 77500 kWh total. This configuration (1) requires 394 panels: facilitating 102.44 kWp of PV capacity. By facing the panels on different azimuth angles (east / west), the mid-day peak is decreased. The 102.44 kWp facility peaks in 'reality' 60.6 kW, which means that only a 60kW inverter is required. In appendix E, tables are shown for all configurations.

A lay-out can be established, with the derived knowledge of PV-performance in relation to different possible panel locations for the Kropman office. There are 4 configurations chosen (final lay-out chapter 5), first one is with PV all-around the building, and 2nd to 4th is only with panels on the upper-part of the roof and scaled based on the following configuration: facing 173° south: 20% at 15°, 18.5% at 20°, 37% at 25°, 24.5% at 35°.

Table 4.2.1: facility sizing net-load analysis

Facility sizing analysis:	1: 102.4kWp (all-around)	2: 9.1 kWp (flat roof)	3: 16.9kWp (flat roof)	4: 27.3 kWp (flat roof)˙
Total demand [kWh]	83000*	83000*	83000*	83000*
Produced [kWh]	-77500	-9690	-18000	-29070
Net-load [kWh]	8000	73300	65000	53930
Renewable share [%]	93%	12%	22%	35%
Export [kWh]	-38600	-1210	-3440	-6920
Exported [%]	47%	13%	19%	24%
Self-consumed [%]	53%	87%	81%	76%

The analysis is done with the power logger measurements in the Kropman building, when this power logs are integrated for the year 2014, the energy consumption was about 75500 kWh, which is 9% less than the energy bill and hourly recorded energy measurements. This is caused by the fact that the energy logger at the case building registrates each minute, by minute 'observation' and not taken the average (energy) over that minute of time. When monthly energy registration of 2014 is summed it registrated 83245 kWh, and Kropman paid for 83132 kWh. In 2015 76901 kWh was registrated, accounted for 8% energy reduction.
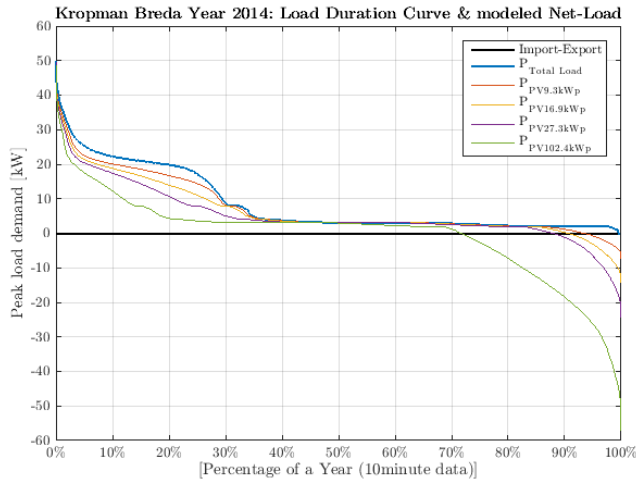

Fig. 4.2.5: 2014 load duration curves for 4 PV-configurations
By increasing the share of renewable energy, the negative-net load increases as can be seen on the right hand side of this figure. During normal operations, left hand side, the net-load reduces but peak remains (see figure on the right)
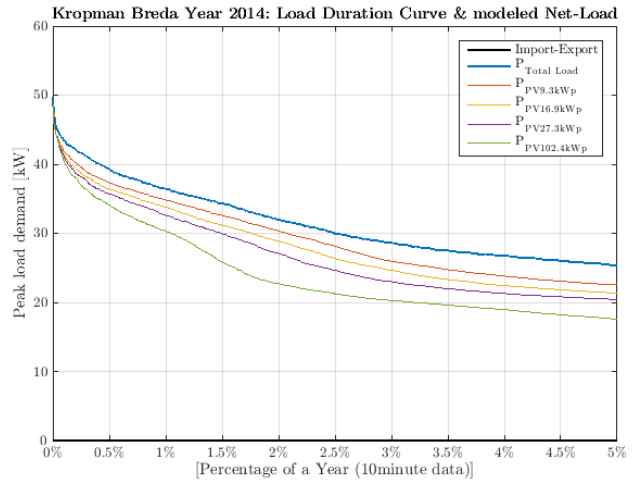

Fig. 4.2.6: Peak demand load duration curve for 4 PV-configurations

The incorporation of the PV doesn't affect the peak demand period. This peak demand period occurred during winter-time(humidifier power consumption)

$$P_{net-load} = P_{total-load} + PV_{production}$$

The Net-load is calculated for each PV-capacity, resulting in a 10minute time (from Jan. 1, 2014 to Jan. 1, 2015) series. Whereafter the resulted net-load is sorted from the highest to lowest value resulting in a load duration curve.

By increasing the size of the PV-facility, an increasing share is exported to the grid while financial benefits in relation to the cost is low (tariff structure is shown in appendix B). Only €1.93ct / kWh during

off-peak, weekends and nighttime and 3.044 ct / kWh during a working day 08:00h − 23:00h. While 2014 consumption costs are aout 3 times higher: €9.751 ct/kWh during peak and 6.301 ct/kWh during off peak.

According the research requirements (chapter 2): the PV-production shall be linked to the chiller summer operations (from the requirements a yield of about 91 kWh is required). During normal operations it has a on/off behavior from 0 to 7kW and during early morning and a hot summer day it peaks to 16/17kW.
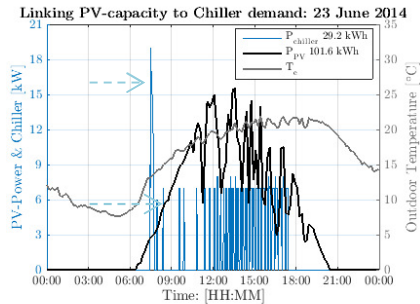

Fig.4.2.7: 16.9kWp PV-facility and chiller demand 23th of June

Fig. 4.2.8: 16.9 kWp PV-facility and chiller demand 7th of July

Fig.4.2.9: 16.9 kWp PV-facility and chiller demand 18th of July (hot summer day)

On this day the chiller consumes 29.2kWh and has 1 high peak (2nd stage chil.) when it kicks in. This peak can only be linked when the capacity is 5 times higher due the moment in time (early morning). Energy produced is 101.6kWh, resulting in a building net-load of 174.6 kWh

Again a high demand spike in the morning. An ESS could be used to service this spike. The first stage is mainly within the PV-production curve. The energy content in certain spikes is low and therefore not recommended to size the PV-facility upon these rare spikes. Energy consumed, 33.9kWh (chiller), produced 99.8kWh and resulting building net-load 230.3 kWh

This particular day is the most extreme, temperature rise to 33℃, chiller operates constantly in single stage and in 2nd stage during early morning, once, and mid-day 4 times. The chiller consumed 84.9 kWh, PV-produced 102.9kWh and the resulting building net-load is 240.2 kWh

I: 3.6 kWh 18min (7 to 16-19kW)
II: 0.6-0.9 kWh 6-8 min (7kW)

I: 4.1 kWh 20min (6-7kW to 14-17 kW)
II: 0.9 to 1.5 kWh 8-13min (6-8kW)

I: 6min 7kW, 9min 16-17kW, 6 min 7kW total of 21 minutes and 3.8kWh
II: demand 19kW, demand offset (19kW minus 8kW (single stage)) 11kW for 12 min and 3.8 kWh

Based on the available roofspace, budget, increasing-self consumption and linking the chiller capacity a size of 16.9kWp is chosen. This facility increases the case building renewable share from 0% to 22%. Whenever the whole chiller load is linked to the PV-production a facility of more than 60kW is required (figure 4.2.7 early morning peak). These peaks with a low energy- and high power content are interesting areas for the battery system to clip.

4.3   Battery Electrical Storage System capacity determination

According to the research requirements (chapter 2) the battery system should facilitate demand side operation scenarios. A BESS is capable to change the building demand profile as service to the grid without compromising the indoor building processes. The focus for the required battery capacity determination is on the demand side service related to the fluctuating chiller load, humidifier peak demand and optimize the (self-) consumption of local PV-energy production. This for the situation of a partly covered roof with PV-panels (16.9kWp).

4.3.1   Battery Sizing: Smart scenarios

The focus areas related to the design requirements are presented as three scenarios, more DSM-strategies are listed in appendix B. Numerical tests of proposed smart scenarios are provided in chapter 7.

Smart Scenario 1: Peak clipping of the humidifier peak demand

This scenario uses the basic DSM principle of peak clipping. Peaks are the main concern for utility operators; by clipping them, it can reduce the use of expensive, non-environmental friendly, (peak-demand) power plants and the utility to upgrade their infrastructure. This scenario

Smart Scenario 2: Flatten peak behavior of the chiller demand profile

This scenario flattens the day load profile, with this scenario an energy block can be bought from the utility. It shaves (I) the morning peak-demand and when the PV-system starts to generate it fills the (chiller operation) gaps through valley filling (II). It supports the grid by

can already give a financial benefit under the current contract by cutting peak demand charges. It smooths the load-profile and reduces the day-peak.

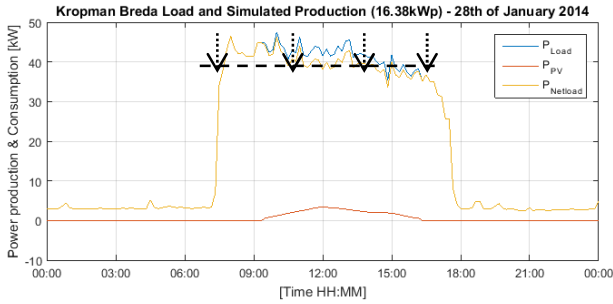smoothing the demand profile and shaving of high demand periods.

Fig. 4.3.1: Day peak due humidifier (10min avg. data)
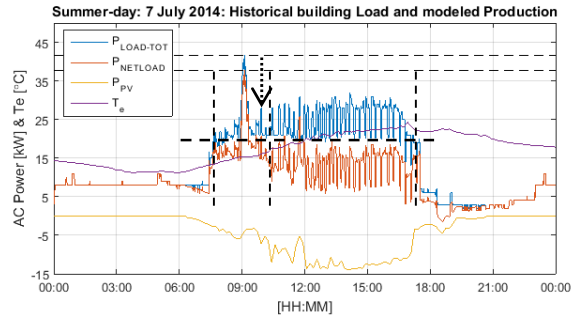*Cut peak demand charges while servicing the grid*

Fig. 4.3.2: Short interval peaks (minute load data)
Flatten the demand profile by peak shaving and valley filling

Smart-Scenario 3: increase (self-)consumption of on-site generated solar power and provide grid support during sunset

For the case building with a partly covered roof with PV-panels (16.9kWp) most energy can directly be self-consumed during the week, a surplus of on-site generated electricity is expected during weekends and after office hours (sunny spring and summer-day), see figure 4.3.4. By charging the battery during a surplus, hence a negative-net load, on-site produced-energy can be more self-consumed, where after the energy is released (battery discharged) when sunsets and/or when the net-load is positive. Discharging the battery at sunset facilitates the grid in cases of high PV-penetration.
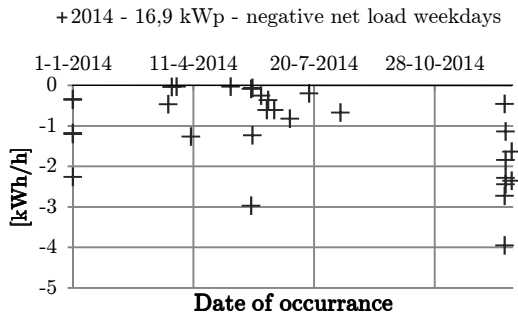

Table 4.3.3: Hourly negative net-load at weekdays
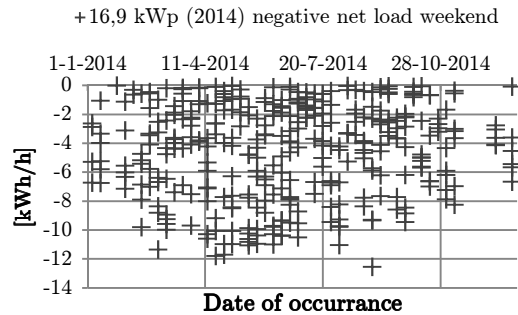*The markers on the right exist due the Christmas holiday*

Table 4.3.4: Hourly negative net-load at weekends
Surplus most of the time estimated during the weekend

In the design chapter 3, a BESS, based on NiMH-batteries was chosen. The specific battery packs are 1.2 kWh each (more information in chapter 5, final design) and configurable in steps of 6 kWh. Based on the peak demand periods of the chiller (2nd stage) and the humidifier, (early morning, day-load peak) the following BESS-capacity is required:

- Second stage peak demand (18 July) occurs about five times 3.8 kWh is **19 kWh** and about **19kW** of power (see fig.4.2.9).
- Humidifier, early morning peak require **6 to 11 kWh** and about **17 kW** of power (fig. 4.3.5)

To complete the BESS-capacity demand requirements it should also aid in a level of self-consumption. The available battery capacity is capacity was calculated as following:

Fig.4.3.5: morning humidifier peak (19 Feb 2016)

$$E_{charge} = Battery_{cap} * DoD * \frac{1}{charge\ efficiency}$$

Where:

Battery capacity = variable [kWh]

Depth of Discharge (DOD) = 80% → implies to a minimum State of Charge (SOC) of 20% SOC.
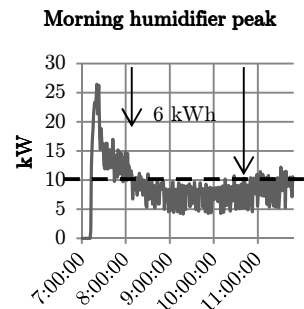
Charge efficiency = 90%

Leading in determination of the BESS-capacity to increase self-consumption on-site produced electricity are weekend energy-surpluses or negative net-load periods. Simulations show that for the year 2014 with a 16.9kWp chosen PV-capacity, a cumulative surplus of 1320 kWh occurs on Saturdays and about 1560 kWh on Sundays. The average surplus, defined as a negative-net load is shown in table 4.3.1.

Table 4.3.1: yearly, quartile, and daily average negative net-load on weekend days

Year Quarters (Q1,Q2,Q3,Q4)	Saturday [kWh]	Sunday [kWh]	Surplus [kWh]	Surplus	relative surplus	relative self-consumed
week 1 - 13	-12.9	-24.9	Saturday (30 kWh)	-474	36%	64%
			Sunday (30 kWh)	-567	36%	64%
week 14 - 26	-42.4	-50.4	Saturday (36 kWh)	-351	27%	73%
			Sunday (36 kWh)	-435	28%	72%
week 27 - 39	-29.6	-31.4	**Saturday (42 kWh)**	**-238**	**18%**	**82%**
			Sunday (42 kWh)	**-328**	**21%**	**79%**
week 40 - 52	-16.3	-13.5	Saturday (48 kWh)	-152	12%	88%
			Sunday (48 kWh)	-234	15%	85%
2014 average	-25.0	-30.0	Saturday (54 kWh)	-88	7%	93%
			Sunday (54 kWh)	-159	10%	90%

The 2014 average surplus for Saturdays is 25 kWh and on Sundays 30 kWh. Apparently, the conditions for PV-production on Sundays seem to be better for this year. By increasing the battery capacity, energy surplus can be decreased. However, if 100% self-consumption is demanded, than a battery capacity of around 100 kWh is required. With the available budget an 80/20% ratio is chosen (instead of 100), which means that a battery of 42 kWh fulfils 80% of the demand. If the last 20% is also required this would imply to more than 2.5 times this battery capacity. In relation to the smart-scenarios (1 and 2) this amount of energy is not required. In the 80/20 scenario about 20% of the weekend surplus is exported; however, this 20% is only 3.2% of the overall production. Therefore, there can be said that nearly all on-site produced energy with the 16.9 kWp facility is self-consumed with a 42 kWh BESS (96%) in 2014. 81% of the production is directly consumed due to the electrical energy use of existing building processes and about 15% by implementing a 42 kWh BESS.
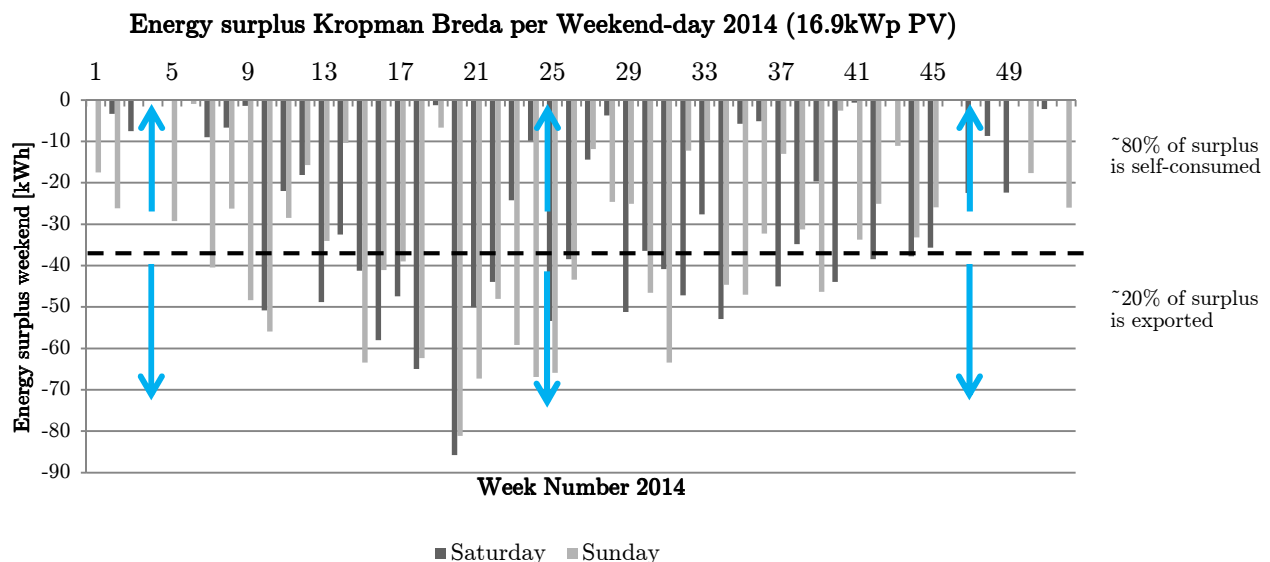

Fig. 4.3.6: Weekend energy surplus evaluation for capacity determination of battery (self-consumption)
Black dashed line represents a 42 kWh battery system (Energy AC charge: 0.8*42*(1/0.9) = 37kWh) about 2.5 times the designed capacity (42kWh) is required to 100% facilitate 'self-consumption'.

To summarize; a BESS with a nominal capacity of **42 kWh** and **17 to 19 kW** of charge/discharge power is sufficient to fulfil the research requirements. Power (kW) flexibility is more important over energy (kWh).

5 Selected PV + BESS facility

This chapter outlines the procured PV+BESS facility, in the first paragraph a schematic overview of the electric, control and monitoring system is presented. Continued with the PV-facility characteristics in chapter 5.2. In chapter 5.3 the characteristics of the procured BESS-facility are shown. In chapter 5.4, an instrumentation list for analysing the research facility is provided.
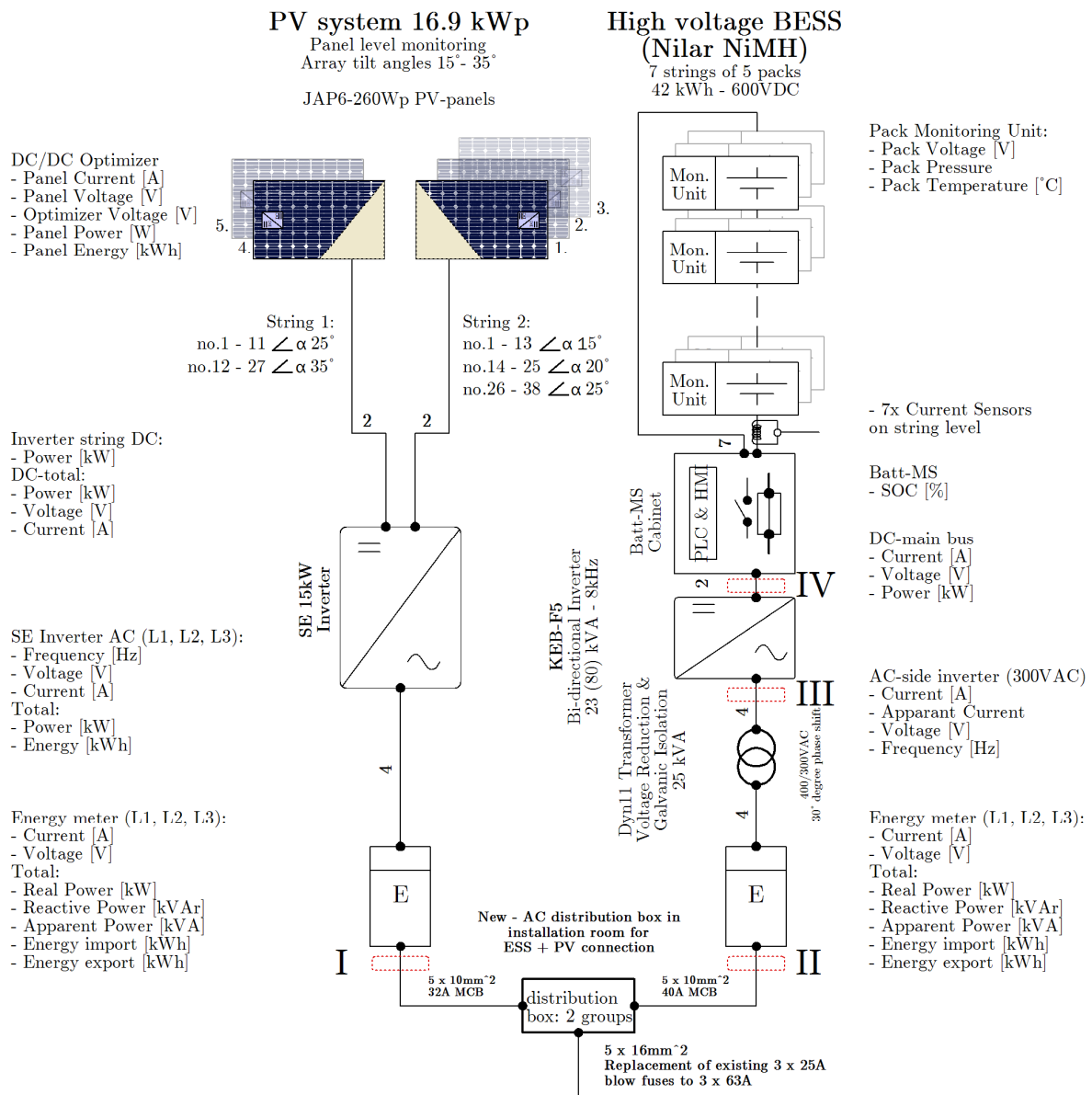
5.1 Final system design

Fig. 5.1.1: Final system lay-out
PV-facility with 16.9 kWP capaity and 15 kW inverter, ESS with 42 kWh of battery storage and 80kVA(limited to ~23 kVA) bi-directional inverter, 25 kVA transformer. All the available measurements are shown on the left- and right handside of the figure. The red-dotted lines indicates the locations of verification tests provided in chapter 6.

5.1.1 E-infrastructure

For this facility, a new distribution box is placed in the installation room where the PV- and BESS are directly connected. The BESS has a Miniature Circuit Breaker (MCB) of 40A, type D, and the PV-system a 32A MCB. Both connected with 5 * 10mm^2 cables. The distribution box located here allowing the systems to disconnect for maintenance and the unparalleled construction phases (PV-system first, September 2015 and the BESS later on in December 2015). A complete electrical one-line scheme is can be found in appendix F.

5.1.2   Construction & Safety

For the PV-system, care is taken on the accessibility of the roof and safety when working on the roof. Therefore, a safety-ladder is constructed at the lower roof. This lower roof is accessible from the second floor. Another safety aspects is on the upper-roof, where the panels are constructed, here a safety-line in the 2 meter area is placed. When a person crosses that line, he/she should be wearing a safety harness that is connected to that safety cable. This cable is fixed and can be used during future maintenance. For the installation room, care is taken on hydrogen & smoke detection, warning signs and air ventilation (more about this in chapter 5.4 instruments).

5.1.3   Control & monitoring hierarchy
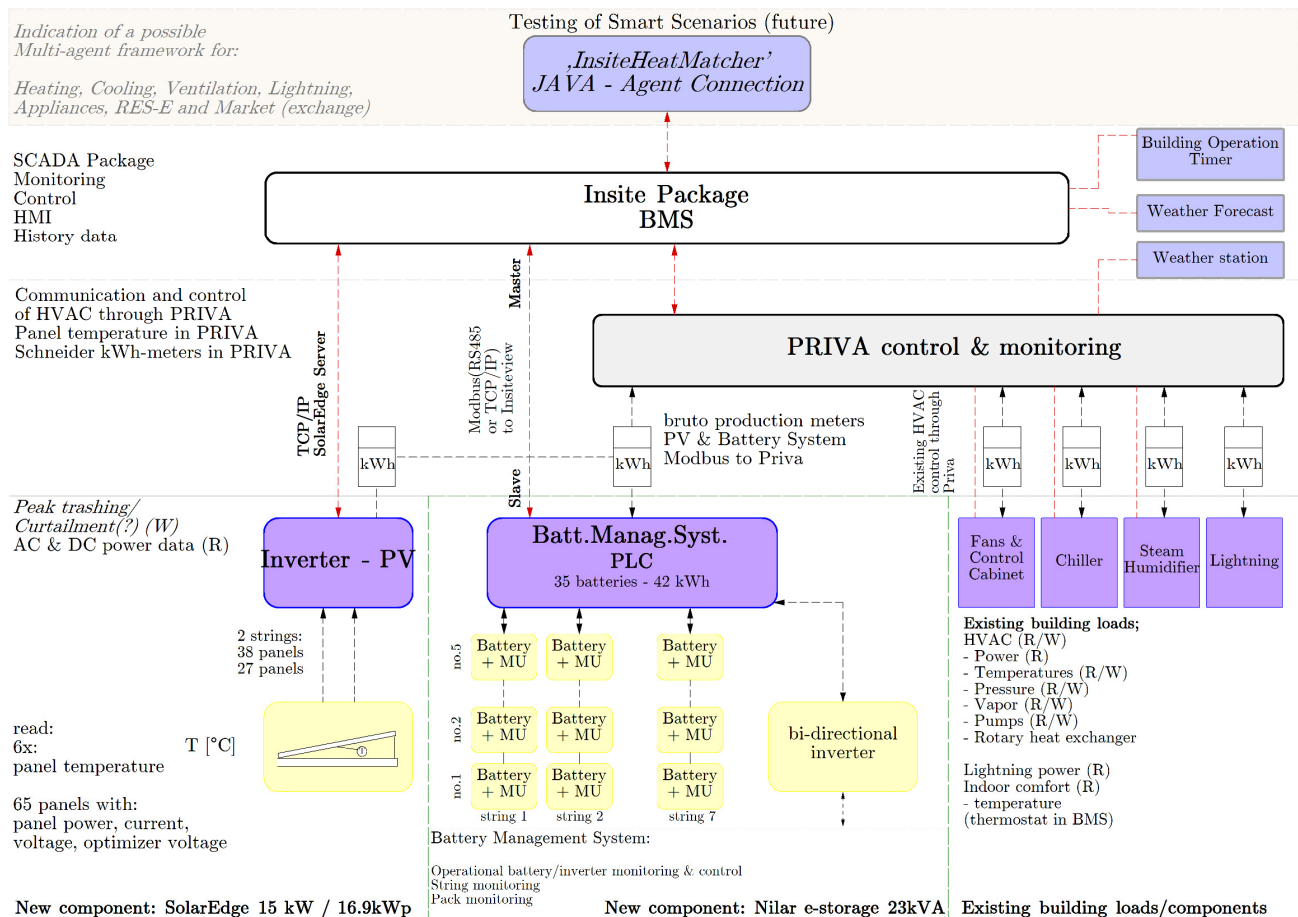
5.1.2: Control hierarchy

5.2   PV Facility system

On the building edge, wind speeds can be higher and therefore panels are on a minimal edge distance of 1 meter and require maximum weight. It is from great importance to check the state of the roof first: should it be replaced soon or is it good enough for the coming decade? In this case the roof edge needed a replacement, which gave a delay in the construction planning due unavailibity of labour during the summer period.

5.2.1   System design solution

The procured system for this design is the system from SolarEdge; this system is characterized as flexible, efficient and optimal monitoring capability. It is flexible because each panel is mountable in a different direction, since each panel is individually optimized with a DC/DC optimizer, without affecting the efficiency of the neighbouring panels in the same string. The number of panels is 65, with a size of 1.650 * 0.991m^1 = 1.635m^2 resulting in total panel area of 106.3m^2. The procured panels are 260Wp (JAP6) with a total capacity of 16.9kWp. Inverters are designed to convert the DC to an AC current. In many cases oversizing an inverter, i.e. having more DC power than the inverter AC power, may increase power output in lower

light conditions [57]. An oversize ($\frac{DC}{AC} * 100\%$) at STC of 35% (for a 15 kW inverter: 20.25kWp) is maximum allowed. Because, PV modules do not consistently perform at their nominal rating (at STC), due effects related to the weather, seasons, sun's position, local site conditions, shading, aging, soiling etc., oversizing is often considered to drive the inverter to its full capacity more often. The STC is rarely met in Dutch climate and therefore the PV-system distributor, but also the SolarEdge site designer, recommends an oversize, in this case 13% (15kW inverter). With this specific design no clips of energy is expected, according the SolarEdge site designing software. Too much oversizing would negatively affect the inverter power production and therefore in loss of energy, the inverter clips the AC power when the actual produced DC power is higher than what the inverter can invert. Oversizing SolarEdge inverters does not harm the inverter. The panel integrated power optimizers, P300, are in contrast to the inverter not over-sizable. As last, the minimal string length for a 3phase inverter is 16 panels including optimizer and a maximum of 50. They can have uneven length without compromising on the performance. The PV-facility final design is shown in figure 5.2.1 to 5.2.3.
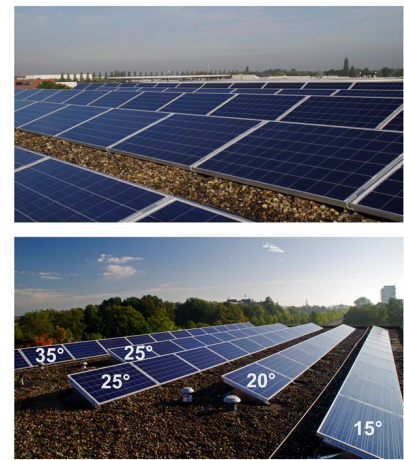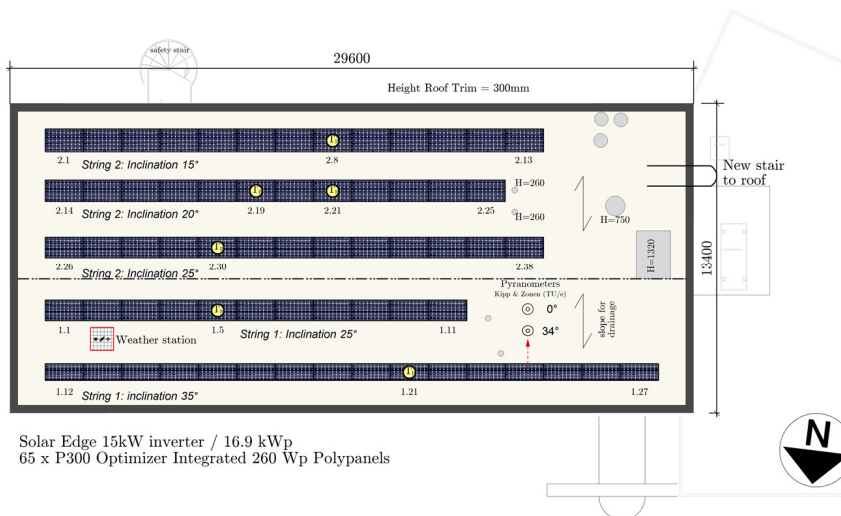

Fig. 5.2.1: Roofplan with PV − facility. *With weather station and temperature sensors location markings (yellow).*

Fig. 5.2.2: Pictures of new PV - facility

The panels are connected in two strings, one of 27 panels (string 1) and one of 38 panels (string 2). The inclination is from south to north varying from 15° to 35°, in steps of 5°, except the 30° inclination, due limited space of shade behind the panels. More manufactures performance data of the SE15k inverter, P300 optimizer and JAP6-260Wp poly PV-panels are provided in appendix F.
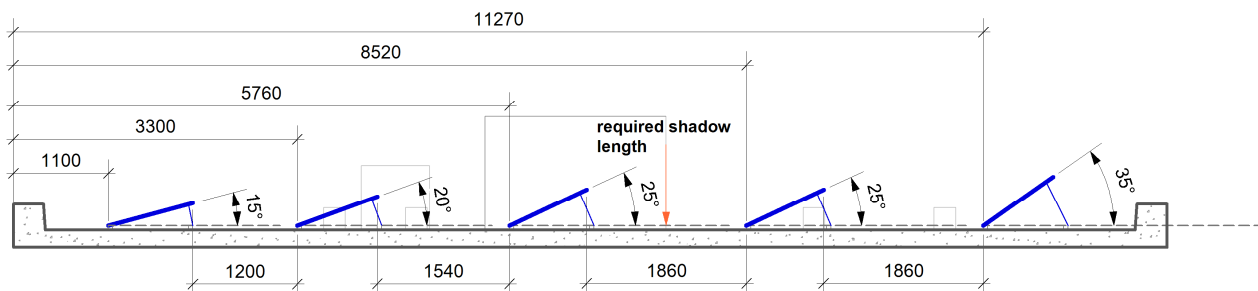

Fig. 5.2.3: Panel design sections. A dashed line represents the required shadow length (red arrow). The chosen construction is adaptable, for now 15°, 20°, 25° and 35° is used.

5.3 Battery Electrical Storage System characteristics

5.3.1 System

An advanced battery technology based on Nickel Metal Hydride form the basis of the BESS. This battery is called: 'Nilar- modular bi-polar NiMH battery'. It is 'completely' (99%) recyclable and suitable for

a large number of cycles. System nominal voltages are possible in steps of 12 VDC sizing to any required voltage. One module consist of 10 cells, of 1.2 VDC, together this is one module. On pack can made of 10modules in series for larger capacity and higher voltage to 120VDC. When these packs are placed in a series string, the nominal system voltage can be increased to any voltage requirement. Since the stack is flat, each end—plate is an electrode pole (bi-polar), figures of the battery technology are shown in appendix F.

- Energy density: 59 Wh/kg
- Power density: 317 W/kg (1000 W/kg in power cells)
- Energy density per volume: 125 Wh/L
- Power density per volume: 676 W/L (3000 W/L in power cells)
- Capacity one 12V module: 10Ah
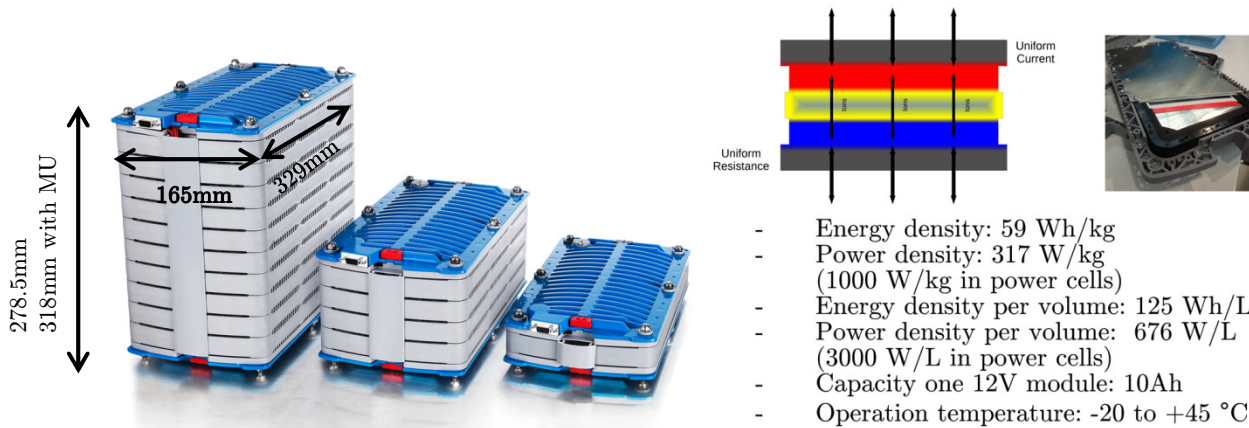- Operation temperature: -20 to +45 °C

Fig. 5.3.1: Nilar modular battery and Schematic overview of bi-polar technology [Nilar international AB]

The internal resistance between the internal cells is very low since the whole plate surface is used for a uniform current flow. High charge- and discharge rates are possible up to 3C (3 times the battery capacity). High voltage reduces Ohmic losses, in this situation the biggest package is chosen, namely the 120VDC pack, stacked with 10 modules.

In the design chapter a 42 kWh battery capacity was chosen. In the market there are no inverters for this technology available. Therefore, a complete system was developed by Nilar. The BESS consist of the following components: AC- and DC filters, capacitors, a bi-directional inverter (KEB-F5), Programmable Logic Controller (Eaton-PLC), transformer (Dyn11) and is connected to the new e-distribution box (40A, MCB type D). Thirty-five packs of 10Ah, 120V are required in order to reach a 42 kWh capacity. The developed (frequency-) inverter requires a high DC bus voltage to invert the AC current. To match the inverter to the grid a transformer is applied, this transformer works as a galvanic isolation but moreover to reduce the 3phase AC-voltage from 400VAC to 300VAC. The operating voltage range for a five-battery pack string configuration with a nominal voltage of 600VDC is between the 500V to 750V DC. A figure illustration this voltage requirement is provided in appendix F.

Table: 5.3.1: Main BESS components

AC/DC inverter (A)	Transformer (B)	Central distribution box (C)	BattMS cabinet (D)	
KEB F5 80kVA (limited to 23 kVA) 8 kHz *(23 kVA was not available)* 300VAC - measurements 500 − 800 VDC Main DC Bus to BattMS-cabinet	3KP23-25k DYN11: 25 kVA U˙primary = 400VAC U˙secondary = 300VAC	Schneider Electric MCB 40 A (type D) SE Energy meter iEM3155 AC measurements	Eaton PLC with HMI Connect battery bank Request reactive current AAC Request Direct Current: -35ADC to +35ADC Start Full charge procedure (0.3C) DC measurements Batt. Monitoring Units 7 x DC-string connection (E)	

Power loss conversion system

Power loss is depending on the current that goes thru the inverter and the filter, transformer. According the manufacture the loss is approx. a straight line between no load losses and full load losses (corresponding losses are provided in appendix F). With this, an efficiency curve was derived shown in figure 5.3.2; the relationship between AC-request and nominal power was used in the BESS-model.
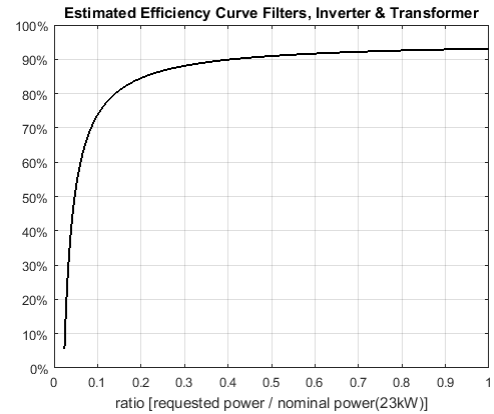

Estimated Efficiency Curve Filters, Inverter & Transformer

ratio [requested power / nominal power(23kW)]

Fig. 5.3.2: Derived efficiency curve of filters, inverter and transformer related to the maximum capacity

Battery cycle efficiency

Based on Nilar factory test measurements the average charging efficiency with 0.2 & 0.3C (0.3C is 42 * 0.3 = 12.6 kW) for each 10%-points SoC-interval, can be withdrawn see table 5.3.2. The total energy loss when charging the Kropman battery bank (35 pcs of 120V-packs) with 0.3C from SoC: 20% to SoC: 100% can be calculated to be around 5.3 kWh. Average full cycle efficiency is 87.3%. It is recommended to stay within the 20% and 80% during daily operations and perform a full charge procedure from 80 to 100% only once a day. During non-operation, the battery loses energy, during first week from 100 to 90% than from 90% to around 80% in 6 months: see the right figure in the efficiency table 5.3.2.

Table 5.3.2: Battery charge efficiency and energy loss during non-operation state according Nilar

SoC-interval	Charging time [hh:mm]	Average energy-efficiency	Average power loss [kW]
20%-30%	0:00-0:20	92%	1.3
30%-40%	0:20-0:40	91%	1.4
40%-50%	0:40-1:00	91%	1.4
50%-60%	1:00-1:20	90%	1.5
60%-70%	1:20-1:40	90%	1.6
70%-80%	1:40-2:00	89%	1.7
80%-90%	2:00-2:20	87%	2.1
90%-100%	2:20-2:40	68%	5

$y = -0.037\ln(x) + 0.9761$
$R^2 = 0.9471$
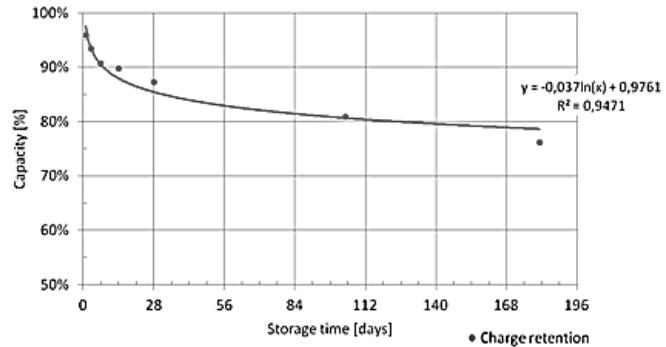
Battery Life cycle energy and theoretical cycle costs

A smaller SOC window results in a higher number of cycles. For example an operation window with a SOC window between 40% and 80% (40% window) implies to a typical number of cycles: 4221 (Appendix F). This relation is translated to a lifetime energy- and cycle cost curve.

Cycle costs are determined by dividing the investment costs by the amount of energy at a SOC window. The amount of energy is determined as following:

$$\frac{SOC\ window}{100} * No_{cycles} * \left(\left(\frac{Batt.capacity}{\left(\frac{SOC}{100}\right)}\right) * 2\right) \ [kWh]$$

Here the typical number of cycle for corresponding SOC-interval is used (No_{cycles}) and the chosen battery capacity (42 kWh). It is multiplied by 2, since a cycle contains a charge and discharge period.

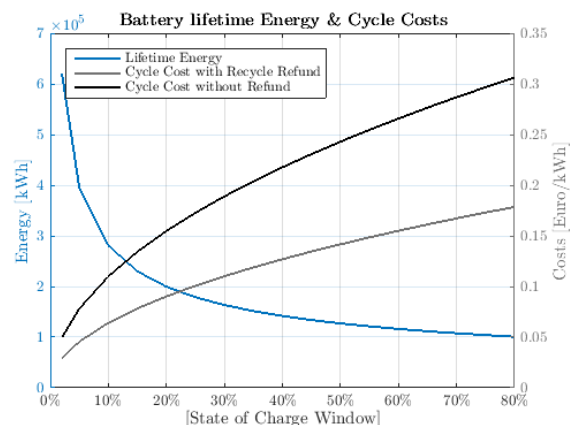*Costs excludes Kropman Labour and in- (light-gray), excludes (black) a recycling refund.*

Fig.5.3.3: Lifetime energy and cycle costs.

BESS Operational guidelines

Communication and monitoring of the ESS is achieved through a Modbus connection, this Modbus RS-485 connection is converted (with a Moxa: Nport 5200 series) to a TCP/IP port to communicate with the Insiteview Server. In Insiteview, all measurements are displayed and data is stored in the Insitehistory database. The BESS is operational as following:

1. First 'wake-up' the system from standby-state, by turning on: 'Connect Batterybank' you'll see that the system starts to consume more energy since the inverter starts to run on 8kHz. This may take about 15 seconds.
   - When you constantly run experiments than it should kept connected. If the system no longer than 15minutes (an indication) is used you should disconnect it to save energy.
2. The battery system can operate at a maximum DoD level of 80% and minimum SoC Level of 20%. However, it is recommended to stay above a 40% SOC in this early research phase. The system displayed SoC is an indication, when the battery is not used for a week it still displays 100%, while it can be on 90% (due no operation losses)
3. The system displays if it accepts charging or discharging and this is related to the SoC level because: from 20% to 80% SOC you can charge and discharge, from 100% to 80% you can only discharge, and from 80% up to 100% you can only charge according the full charge procedure.
4. The Full Charge Procedure (FCP), from 80% to 100% SOC is activated by disconnecting the battery bank (point 2) and switch on the full charge procedure. This command can be started at any SoC level. When the FCP has started and the SoC is above 80% then it should be left on until it is completely full. This full charge procedure is a constant current charge of 0.3C (DC). Each string is charged with 0.3C, which is about 3Amps, and 21Amps for total number of strings in parallel. The seven strings are independently disconnected when a string is fully charged, the system knows this by measuring the delta T (temperature gradient) and pressure in the string 120V packs.
5. During normal operations charging and discharging is simply achieved by requesting a DC-current between -35 to +35 ADC. A positive DC current implies a discharge and a negative current a charge. A second charge- and discharge option is requesting a reactive current from -35 to +35 AAC.
6. In theory the KEB inverter can run in steps of 0.1A, in practice a lowest DC-current is e.g. 1Amps, if that current is supplied to a battery bank at 600VDC, it would imply a DC-power of 550W.

Designed reaction time:
- The startup time from PLC command to operate is approx. $3 - 4$ seconds.
- Change charge to discharge is achievable within $4 - 7$ seconds.
- Changing current rates during charging and discharging is achievable within 2-3 seconds.

5.4   Instrumentation list

In this paragraph, an instrumentation list is provided; they contain a list of measurements that are withdrawn from the system components and additional sensors as the weather station. For the ESS and PV-system, the location of all measurements is shown in an earlier provided schematic overview; figure 4.1.1.

5.4.1   PV-system

Table 5.4.1: SolarEdge WebPortal: only monitors when the PV-produces energy, otherwise the system is in standby

System Component / Instrument:	Measurements: (0.00 indicates a monitored value with 2 numbers behind the 'comma')
65 Panel level optimizers with monitoring Variable inconsistent time interval: $4 - 15$minutes	Power 0.00 [W], Optimizer Voltage 0.00 [V], Panel Voltage 0.00 [V], Energy (hourly interval) 0.00 [Wh]
String measurements (2x) Constant time interval: energy 1h and power 15min	Energy 0.00 [Wh], Power [W]
Inverter-level measurements: Constant time interval: energy 1h and all others 5min	AC-energy [Wh], Frequency L1, L2, L3 0.00 [Hz], AC-Voltage L1, L2, L3 0.00 [V], AC-Current L1, L2, L3 0.00 [A] , AC-Power 0.00 [kW], DC-Voltage 0.00 [V]

Table 5.4.2: Two energy-meter integrated in Priva and transferred to Insiteview for both ESS and PV-system

System component / Instrument:	Measurements:
Schneider iEM3155 1 minute logging interval for all measurements except for the energy measurements.	Hourly, daily and monthly Energy [kWh and Wh], Current L1, L2, L3 0.0 [A], Voltage L1, L2, L3: 0 [V] Power 0.000 [kW], Reactive power 0.000 [kVAr], Apparent Power [kVA] Extra for ESS: reactive e-consumption & production 0.000 [VArh]

For all energy-meters the measurements significance increased drastically. From mid-2013 till January the 7th 2016 the logging of all Energy-meters in Priva-Topcontrol was done without any number behind the 'comma'. For example power was measured as 1, 2 or 3 kW, while from January the 7th 2016, the software is re-programmed in order to measure with values of 1.123, 2.123, 3.123 etc. This is also done for all other existing energy-meters (see one-line scheme for all energy-meters, appendix F).

5.4.2 Environmental Sensors

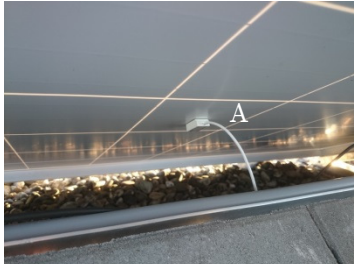Table 5.4.3: Six Panel temperature sensors for panel temperature evaluation and Pyranometers (TU/e)

Window Pane Temperature Sensor :
   A   Siemens - QAT22
        o   Accuracy 0.4 ±K
        o   Range of use -10 … 50 °C
 	
 Placed on the average performing panel for each row (5x) and 1 at a panel which performans significantly less than the average in the row (-10%). For exact location see figure 5.2.1. The sensor is placed in the mid-east center cell. Panel consist of 30 cells (width 10 cells and height of 6). Sensors are placed on cell width no. 5 and height no. 3.	

Pyranometer TU/e. Data is logged with Eltek Data Taker (manually downloadable)
   A   CMP11: Kipp & Zonen (calibrated 2 February 2010)
        o   Mounted horizontally
        o   Sensitivity: $8.65* 10^{-6}$ V/W*m^2
   B   CM10: Kipp & Zonen (Old: no exact date available, first version dates from mid 80s)
        o   Mounted on 34° (northern panel row)
        o Sensitivity: $4.26 \ 10^{-6}$ V/W*m^2	

Table 5.4.4: Weather station

Weather station from Wittich & Visser located on upper roof (north-east)
   A   Ambient temperature (1minute interval) [°C]
        o   Sensor-hut with KNMI-license
   B   Relative Humidity: HC2-S / HC2-S3 (8min. interval)
        o   Accuracy: ±0.8 % RH, ±0.1 K
   C   First Class (ISO 9060) SR-11 Pyranometer (1min) [W/m^2]
        o   Placed on an rotating arm: February 2016 (horizontal)
        o   180° field angle and 1.3% calibrated uncertainty of sensitivity
   D   DS: Wind speed (1min) [m/s]
        o   A resolution better than 0.1 m/s (pulse train 1024 Hz).
        o   Run rate (start): 0.5 m/s.
        o   Operating window 0…60m/s.
   E   DD: Wind direction (1min) [0°…360°]
        o   A higher resolution than 1°.
        o   Run rate (start): 1.2 … 1.5 m/s.
        o   Lifespan: 20×10^6 rotations.
   F   Light intensity: Lux sensor - LS
        o   on all façade orientations (4x lux sensor)
        o Operating window: 0….100.000 lux	

5.4.3 BESS

Table 5.4.5: Installation Room ambient temperature sensor and Battery management system alarms

Installation Room temperature:		
A	Siemens QAA24 with LG-Ni 1000 sensor (8minute interval)	
	o Temperature range 0…50°C	
	o Placed on upper-edge of battery rack	
B Alarms:	B Alarms:	
o Bus voltage high and low	o High ambient temperature	
o Pack voltage high and low	o LMU-communication fault	
o High Pressure	o Emergency stop tripped	
o High Pack temperature	o Smoke detector	
o Low SoC	o H2 detector	
o Tripped MCB-fuse	o Inverter fault	

Table 5.4.6: Battery-MS energy measurements

System level:	String and battery level:
o State of Charge [%]	o 7 x State of Charge (string) [%]
o Actual DC Current [0.00A]	o Current (string) [0.00A]
o Actual DC Voltage [000.0V]	o 35 x Pack voltage [000.00V]
o Actual DC Power [0W]	o 35 x Pack pressure [0.0 psi]
o Actual AC Current [0.0A]	o 35 x Pack temperature [00.0 °C]
o Actual AC Apparent[0.0 AAC]	o Min & Max allowable charge (string) [0.00A]
o Actual AC Voltage [0.0V]	
o Frequency [0.0Hz]	

Each battery string (1…7) and pack (A…E) is assigned with a unique letter and number see figure 4.4.1.
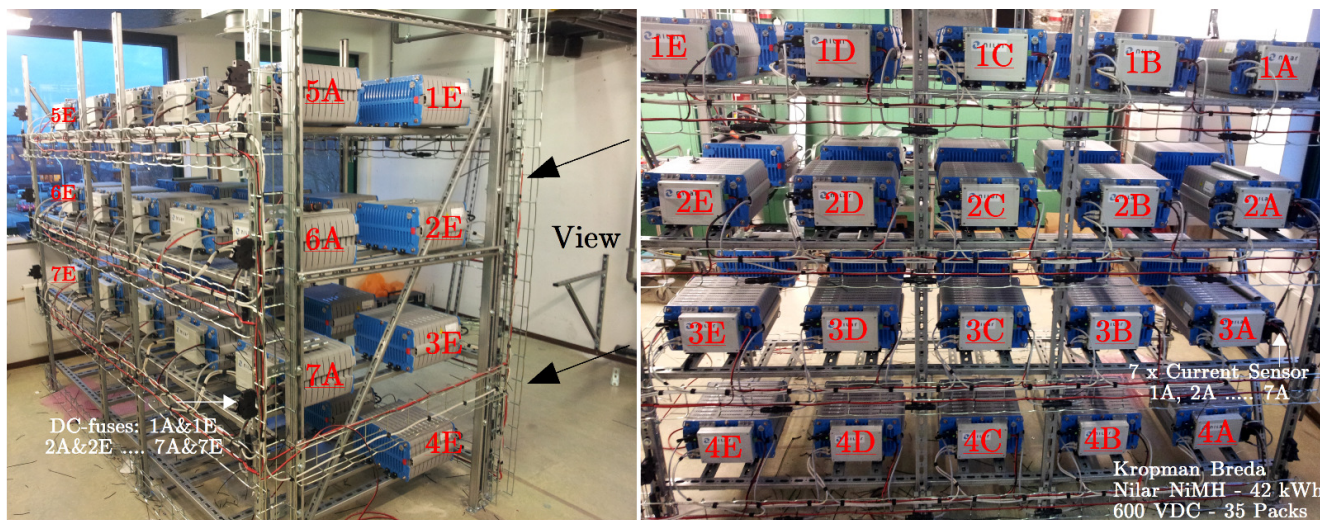

Fig. 5.4.1: Battery System lay-out
The inverter- and battery management cabinet was on this pictures not installed yet (beginning of December 2015)

Fig. 5.4.2: Safety-signs (A) & Ventilation outlet (B).*Ventilation capacity setting (unverified): 500m³, installed after cooling block north-east ventilation group*

6 Facility verification study

This chapter outlines the verification results for the developed PV+BESS facility. First in chapter 6.1, the instrumentation for energy measurements are verified using a calibrated power quality analyser. After this a comparison is made between two selected pyranometers. In sections 6.2 and 6.3, the PV-generation facility and BESS, are operational verified on energy-performance, behaviour and power quality. As last, in section 6.4, the developed model for PV-generation and BESS is validated with on-site measurements.

6.1 Instruments

The instrumentation used for the verification study is a power-quality analyser (CA 8335, for calibration see appendix J: measured accuracy of <0.3% with a 95% confidential interval. In appendix G, a measurements plan on the verification of instrumentation and BESS is provided.

6.1.1 BESS instrumentation

The building management system, stores the BESS electricity measurements data from pack-level to the AC-main connection. Due to safety reasons and accessibility of electrical connections instrument verification was only done at the primary- and secondary side of the transformer and DC-main bus. In the schematic system overview, shown in figure 5.1, these locations are marked with a red dashed line and a Greek number.

II. Verification of permanent Schneider Electric energy meter (iEM3155) was checked at primary side of transformer, between decentral distribution box and transformer
III. Secondary side of transformer (KEB-cabinet) was measured, at 3 phase connection between transformer and inverter cabinet
IV. DC-main bus, was measured at BattMS-cabinet

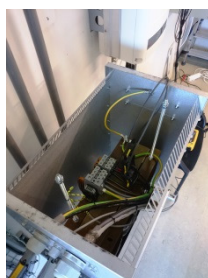Fig. 6.1.1: Accuracy measurements for central BESS energy meter (II)

Fig. 6.1.2: current clamps (II)

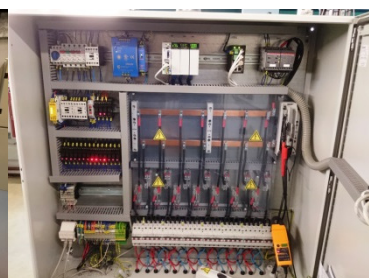Fig. 6.1.3: Accuracy measurements KEB-cabinet (III)

Fig. 6.1.4: Accuracy measurements DC-main bus − BattMS-cabinet(IV)

Charge- and discharge measurements at both sides of the transformer were tested in 10-minute intervals. In order to verify the DC-main bus measurements one point measurement was done by the inverter-representative. Due safety reasons, no 10-minute log is made of this high DC-voltage point. Difference between the measurements are accurate within 3% and any difference between the energy-meter and power analyser within the 5% are sufficient for test purposes.

Results and discussions of the instrumentation tests are provided in appendix G. Measurements at the primary side of the transformer and DC-main bus are accurate, except for the reactive power measurements [Q]. Calculating the apparent power [S], with Q and P reveals that the problem the measured apparent power of the power analyser is assumed uncertain during charging (not during discharging). Current measurements on the secondary side of the transformer were not accurate with a highest found difference of 31.2%, voltage measurements are also critical with highest found inaccuracy of 4.8% (inaccurate as instrument, but useful for BESS behaviour analysis.

6.1.2 PV instrumentation

Due limited availability of the power analyser and bad weather conditions measurements on the PV, main energy-meter (iEM3155) was only done at very low production rates. Accidently, only one unknown phase was logged from 16:00 to 16:29. Therefore, no accuracy verification could be done; however, the energy-meter was equal to the one of the BESS for now the assumption was made that this one is also accurate (iEM3155 meter can be used for energy payment with a 1% maximum inaccuracy according specs).

6.1.3   Environmental sensors

The accuracy of environmental instruments is verifiable with the new weather station, according the instrument list these sensors have very high measurement accuracy and for the ambient temperature measurement it is KNMI-licensed. The in November 2016 calibrated (pyranometer) SR11-sensor and in February 2010 calibrated CMP11-pyranometer are both horizontally mounted. Comparing minute data of on-site measurements reveals are large deviation between the two sensors, at 12 o'clock, the SR11 measures 321.8 W/m² and the CMP11 271.3 W/m², which is about 16% less than the latest calibrated SR11 sensor. The first class SR11-sensor and secondary standard CMP11-sensor are both applicable for solar energy test-applications according the ISO9060 and ASTM E2848 standards. Because it is not sure if the SR11 registers an accurate value, the output was compared with the hourly average data of the closest KNMI weather station Gilze-Rijen. By comparing these hourly values, it was concluded that SR11 measures accurate (error ˜ -2%). Some deviation in the hourly data is observed at moments of passing clouds (intermittent irradiance drops between 12:00 and 14:00 due to location difference). It is recommended to recalibrate the CMP11 sensor before using this for PV-production analysis. According the CMP-11 manufacture (Kipp & Zonen) re-calibration is recommended every 2-year.
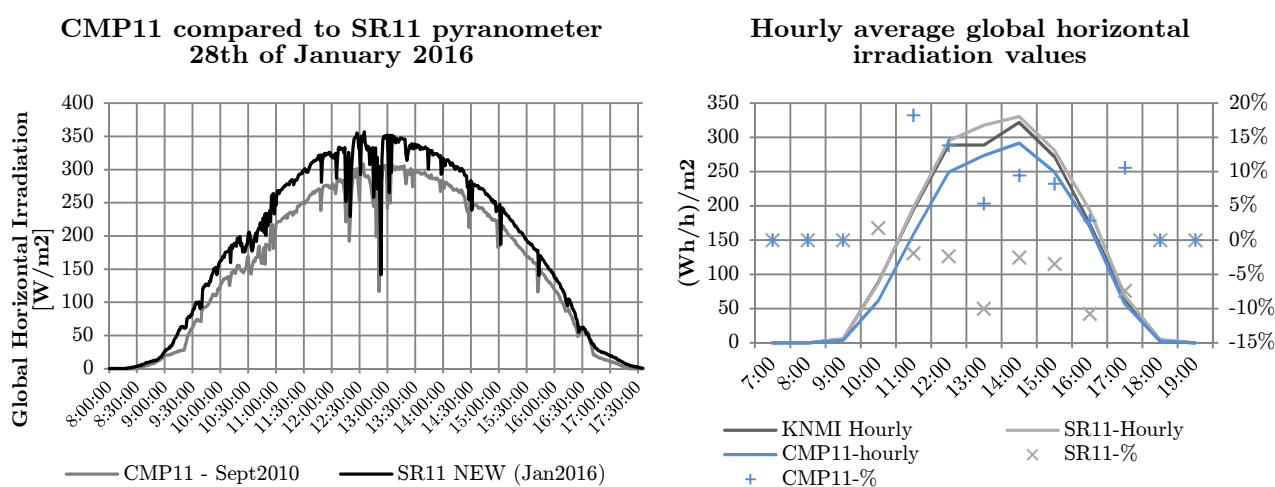
CMP11 compared to SR11 pyranometer 28th of January 2016

Fig. 5.1.4: Minute data irradiation analysis: CMP11 Pyranometer (TU/e) and newly calibrated SR11 Pyranometer

Hourly average global horizontal irradiation values

Fig.5.1.5: Comparison of KNMI-validated(Gilze-Rijen) hourly global horizontal irradiation data to case building pyranometers

Other environmental sensors are the PV-module temperature sensors, six attached to the PV-panels, two existing outdoor temperature sensors (North-East and South-West) and one attached at the new weather station. The PV-module temperature sensors are accurate, highest found difference between the sensors during a cloudy night is 0.4℃, and 0.6℃ compared to the ambient temperature sensor of the weather station. Sensors may have a difference of $+$ or $-$ 0.4℃ (range: 0.8℃). Panel temperature measurements are used to analyse PV-panel production, which efficiency is affected by cell-temperature (1℃ difference only accounts for 0.45% efficiency loss).

Two existing outdoor temperature sensors attached to the building were compared to the weather stations temperature measurements, a figure is presented in appendix G. The existing SW-measurement is not useful for PV-analysis, since it is influenced by the sun's insolation. On afternoon, February 16th, the difference compared to the weather station was +14.3℃. During a cloudy night, February the 14th, the temperature was also higher: +1.9℃. The existing NE-sensor is accurate enough for PV-analysis at a cloudy day: at February 14th the difference was only between 0.0℃ and 0.2℃. However, before, during and after a sunny day (16th) the NE-tempereature measurement lags, which means that during the day the temperature measured at NE is slightly lower (-1℃ to -1.9℃) and during nighttime slightly higher (+0.9℃ to +1.2℃) compared to the weather station. This lag is most possibly caused by the buildings thermal transmittance.

6.2   Model validation

In this section, the Photovoltaic-generation model and BESS-model are validated with the experimental PV+BESS facility.

6.2.1   PV-model

The in chapter 4 described PV-model requires climate data on outdoor temperature, Global Horizontal Irradiance (GHI) and wind-speed as input. The GHI separation model of DISC[51] is validated for hourly data. However, hourly data does not reveal the solar intermittency properly and therefore KNMI climate data with a 10-minute interval were also tested. Figures with measured- and modelled curves are provided in appendix H.

The model accuracy at sunny periods is high (figure 6.2.1 comparison); the cumulative production difference between 10minute and hourly climate data is not significant, table 6.2.1. During partly-cloudy periods the uncertainty is higher; however the relative impact on the total yield is lower due the lower production magnitude. This difference may be caused by the use of nearby climate data (KNMI station: Gilze-Rijen) and not on-site measurements, but also due the separation model for estimation of the diffuse and direct irradiance.
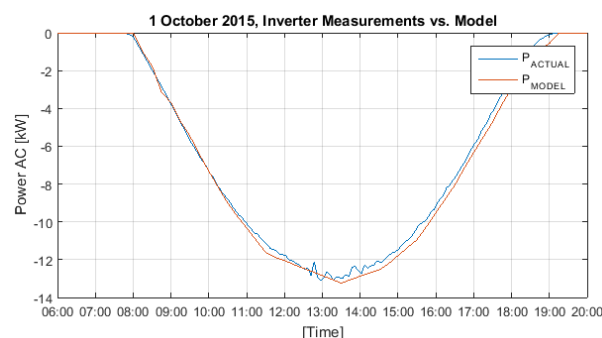

Fig. 6.2.1: central AC-power modelled and measured production with hourly data

Table 6.2.1: Cumulative error between measurements and model

	Measurements SE15k	Model Hourly	Model 10minute
	1235 kWh	1303 kWh	1252 kWh
Cumulative error	x	-5.5%	-1.4%

Each row is modelled independently; figures (appendix H) show that the model predicts the production for each row (5) accurately. For future research, it is recommended to evaluate the model validity during cloudy periods with the new on-site weather station measurements. The model is validated with 10-minute data, based on these results. 10-minute data provides a better presentation of the solar-intermittency compared to hourly data; this interval was also used for numerical operational scenario tests presented in chapter 7.

6.2.2   BESS-model

Battery model adapts actual DC-power to requested AC power. In the first experimental phase the BESS is only controllable by changing the DC-current. In the future, a controller needs to be external programmed to change the DC-current dynamically based on an active AC-power request (measured at BESS energy meter). During the verification study only one full cycle was performed, this cycle was done on a 0.3C charge and discharge capacity and is compared with modelled data in table 6.2.2. The system efficiency was slightly lower than used in the model, which was defined by the BESS design properties. In practice, an 80-kVA KEB inverter is installed instead of 23 kVA and more filtering.
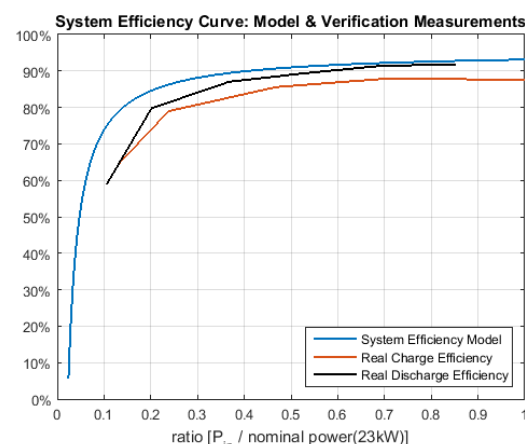

Fig. 6.2.2: Model system conversion efficiency and measured efficiency

For example during discharging the Pin = DC-power and resulting AC-power at a 0.6 ratio is 12.5kW.

6.2.2: The component efficiency curve reveals some differences:

Ratio and power in.	Charge real	Discharge real	Model
Ratio $0.2 - 4.6$kW:	74%	80%	84.8%
Ratio $0.4 - 9.2$ kW:	84%	87.5%	90%
Ratio $0.6 - 13.8$kW:	87%	90.5%	91.8%
Ratio $0.8 - 18.4$kW:	88%	91.8%	92.8%

DC-Power & SOC: Scenario 3 (AC 12kW)

Discharge 100% to 79%
E-DC = -8.82 kWh
E-AC = -7.91 kWh
η = 89.7% (only conversion loss)

Discharge 79% to 39%
E-DC = -17.65 kWh
E-AC = -16kWh
η = 89.7%

Discharge 100 % to 39%
E-DC = -26.47 kWh
E-AC = -23.91 kWh
η = 89.7%

DC-Power & SOC: Scenario 8 (full charge 20 - 100%)

Charge 39 to 79 %
E-DC = 17 kWh
E-AC = 20.75 kWh
η = 77.9%

Charge 79 to 100%
E-DC = 8.96 kWh
E-AC = 12.87 kWh
η = 56.5%

Charge 39 to 100% =
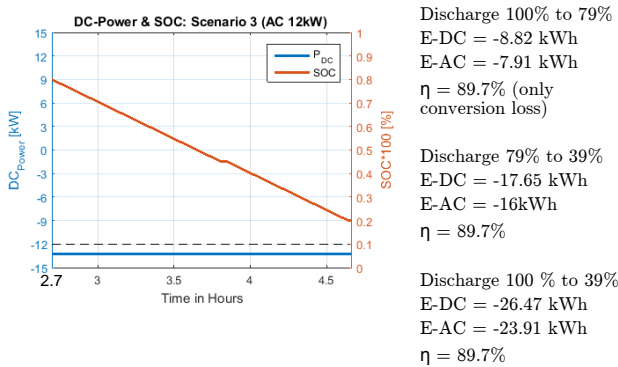E-DC 25.96 kWh
E-AC 33.62 kWh
η = 77.2%

Fig. 6.2.3: modelled discharge profile   Fig. 6.2.4: modelled charge profile
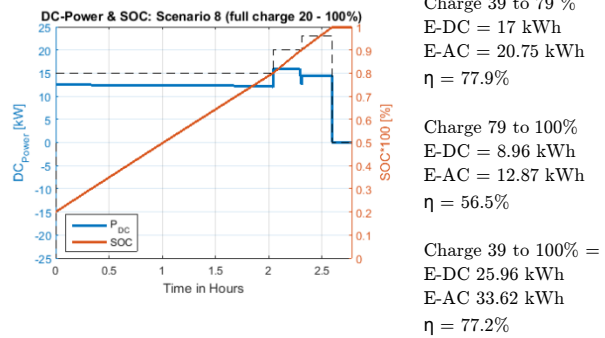
Table 6.2.3: Model vs. Measurements at 0.3C rating

Model	Measurements	Accuracy
Full cycle performance modelled (0.3C): = (23.91 / 33.62)*100% η = 71.1%	Full cycle performance measured (0.3C): = 23.9 / 35 η = 68.3%	3.9%
Discharge 100 − 39% (DC/AC) η = 89.7%	Discharge 100 − 39% (DC/AC) = 1-((26.9 - 23.9)/26.9) = η = 88.8%	1%
Charge 39 − 79% E-AC = 20.8 kWh Charge 79% - 100% E-AC = 12.9 kWh Charge 39% - 100% E-AC = 33.6 kWh	Charge 39 − 79% E-AC = 21.6 kWh Charge 79% - 100% E-AC = 13.4 Charge 39% - 100% E-AC = 35.0 kWh	3.9% 4.0% 3.9%

Model seems to be quite accurate; however non-operation losses and full charge behaviour are not taken into account. The model simulates all seven strings of the BESS to be full all at once, however in practice each string is disconnected independently whenever they are full. In the model, the full charge procedure took 54minutes while at the model it only took 36 minutes (model uses a higher charge rate during full charge procedure). More modelled figures about the BESS behaviour are provided in Appendix I. In future research, it would be useful to examine this at different situations to get a better understanding of the BESS behaviour.

6.3   PV-generation facility

Analysis of the PV-generation facility is achieved according the guidelines for monitoring and analysing photovoltaic systems, IEC 61724 [37], [58] see also appendix E. The following measurements are required: In-plane irradiance, measured with a Pyranometer directed in the same inclination and azimuth angle or estimated with the photovoltaic model (4.1) based on the global horizontal irradiance. Ambient air- and panel temperature, wind speed, array-power (DC) and total power.

In this study 4 different inclination angles were chosen as a show-case. For the study on PV-system verification and model validation real inclination angles of the 5 panel rows were measured (fig. 6.3.1). The inclination angles are slightly different than set, due a little slope at the roof (drainage). The inverter was displaced at the 8th of January since it failed to operate at the December 20, 2015.

Fig. 6.3.1: Real inclination angles

6.3.1   Behaviour of chosen cell technology: Crystalline

Between panels ±5% manufacturing loss (power production) is allowed, typical values in recent years are less than 3% [39]. A higher insolation value on a PV − panel directly relate to a higher power output, but in most cases also result in a lower efficiency, due the temperature effect. Panels *heat* up at higher insolation values and that increase *reduces* the operating *voltage* of the panel, which results in a *lower efficiency* (fig. 6.3.2). The electrical current remains relatively constant when cell temperatures increases and insolation

value is the same. Higher insolation levels correspond to an increase of electrical current. Maximum power point trackers in inverters control the voltage of a panel or array (string) in small voltage steps, to find the maximum power point (MPPT), P_{mp} (fig. 6.3.3). In this case each panel has its own MPPT tracker (DC/DC optimizer), in order that each panel operate independently at their maximum efficiency.
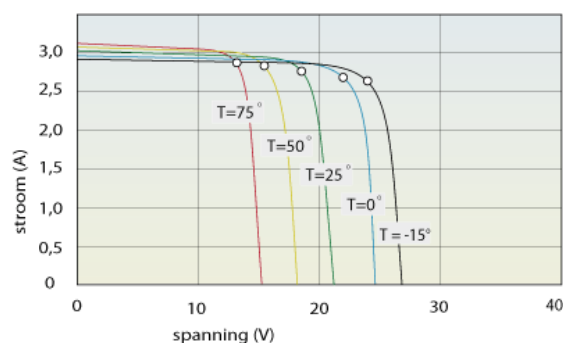

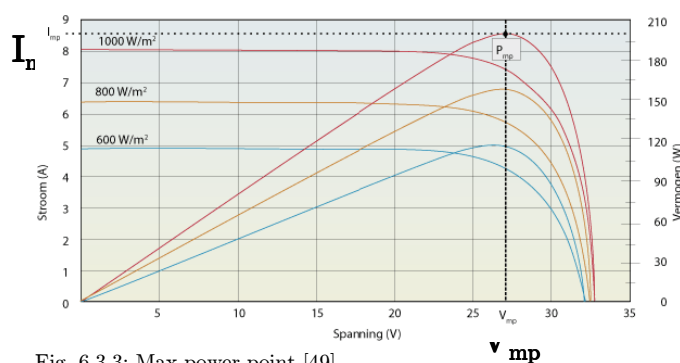Fig. 6.3.2: temperature effect on panel yield [49]

Fig. 6.3.3: Max power point [49]

Summary of factors which affect the power output of a PV-facility [39]:

- Temperature effects, higher temperature correspond to a lower efficiency
- Seasonal solar radiation differences
- Effect of dirt on PV-panels, max 5%
- Shade, inclination and orientation
- Yearly degradation (JAP6: 18% loss after 25yrs.)

- Inverter efficiency, minimum kick-in and maximum operating voltages (Volt. window S1)
- Mismatch in a string configuration (S1)
- System losses, AC and DC cabling losses
- Manufacture tolerances of maximum 5%, last year's 3% [39]

6.3.2 Panel level-analysis

In chapter 6.3.1, production differences between panels are outlined here is stated that 5% manufacture difference between panels is allowed is allowed [39], combining this with other differences due module temperature (2%), optimizer performance(1%) and dirt (1-5%) up to difference 10% is allowed. At the Kropman Breda facility, one panel is functioning way below average. In row 2, with a number of panels of 12, 1 panel is producing 12.1% less than the average for a two-month period. For all other 64 panels no significant difference between the average producing panels is measured, see table 6.3.1. for the overall panel

Table 6.3.1: Panel performance evaluation

	Row 1	kWh	Row 2	kWh	Row 3	kWh	Row 4	kWh	Row 5	kWh
Panel energy yield	1.2.1	32.97	1.2.14	33.06	1.2.26	36.12	1.1.1	34.3	1.1.12	35.3
	1.2.2	30.02	1.2.15	33.38	1.2.27	35.35	1.1.2	35.68	1.1.13	35.48
2015 Sept 25 till Oct. 12	1.2.3	32.73	1.2.16	32.78	1.2.28	35.19	1.1.3	34.89	1.1.14	36.61
and	1.2.4	30.22	1.2.17	34.57	1.2.29	37.83	1.1.4	33.48	1.1.15	36.96
2016 Jan. 8 till Feb. 25	1.2.5	30.71	1.2.18	33.66	1.2.30	35.91	1.1.5	34.73	1.1.16	36.26
	1.2.6	31.1	1.2.19	33.21	1.2.31	35.73	1.1.6	33.1	1.1.17	36.85
	1.2.7	31.47	1.2.20	33.17	1.2.32	34.86	1.1.7	33.8	1.1.18	35.84
	1.2.8	31.23	1.2.21	29.28	1.2.33	35.27	1.1.8	37.16	1.1.19	38.32
	1.2.9	32.08	1.2.22	34.62	1.2.34	35.67	1.1.9	34.83	1.1.20	39.1
	1.2.10	31.11	1.2.23	33.43	1.2.35	37.53	1.1.10	33.83	1.1.21	37.01
	1.2.11	31.12	1.2.24	33.37	1.2.36	36.1	1.1.11	36.55	1.1.22	36.44
	1.2.12	32.58	1.2.25	35.38	1.2.37	34.47			1.1.23	37.79
	1.2.13	31.76			1.2.38	36.48			1.1.24	38
									1.1.25	35.05
									1.1.26	37.09
									1.1.27	36.34
Measured inclination	**15.5°**		**20.5°**		**25.5°**		**23.7°**		**33.8°**	
average	31.47		33.33		35.89		34.76		36.78	
minimum	30.02	-4.6%	29.28	-12.1%	34.47	-3.9%	33.1	-4.8%	35.05	-4.7%
median	31.23		33.38		35.73		34.73		36.73	
maximum	32.97	4.8%	35.38	6.2%	37.83	5.4%	37.16	6.9%	39.1	6.3%
Relative yield		100%		105.9%		114.0%		110.5%		116.9%

energy yield. By investigating the P, U and I curves of panel 1.2.19, 1.2.21, 1.2.25 (figure 6.3.4) on February 16, you can clearly see that the current stays behind compared to the other two average yielding panels. Voltage is nearly equal. Basically, PV-cell current increases with higher insolation values and slightly with increasing temperatures. Voltage of panels reduces when they become warmer, this is why panel efficiency decreases with increasing temperatures (higher cell resistance, decreasing voltage). Measured voltage between panel 1.2.19, 21 and 25 are approx. equal so it is not a temperature related problem, since temperature increase decreases the cell operation voltage. However small cracks (or dirt/shade, not the case here, 6.3.1) in cells can reduce the current through a specific cell, and since the worst module is leading (in a series configuration) this can be the cause.
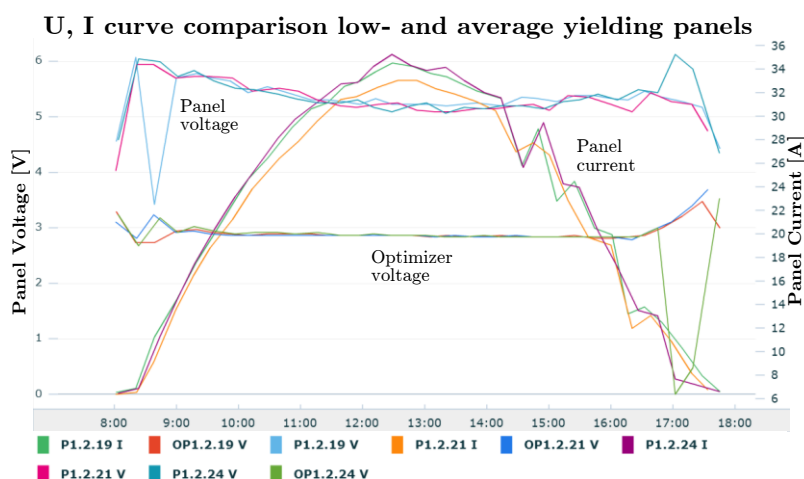
U, I curve comparison low- and average yielding panels

Fig.6.3.4: 16th of February: lower current for panel 1.2.21.

Panel voltages of all three panels are relatively the same, but the current of panel 1.2.19 is significantly (>5%) lower compared to the average.
Also shown in this figure is the optimizer output voltage, relatively constant during the day at 19.87V (string 2 = 38 panels). Optimizer voltage in string 1 (27 panels) is about 29.37V. The system automatically changes the optimizer voltage to reach a 750V string voltage.

Fig. 6.3.5: 16th of February: GHI, panel temperatures for each row average panel and panel 1.2.21.
For bad functioning panel 1.2.21 and average 1.2.19 specific cell temperature is about 1.0°C to 1.5°C warmer than average panel. This cannot explain the yield difference. On low yield periods the power output of panel 1.2.19 is about a third less and on bright days 5 to 6% less. Implies to an average energy loss of 12%.

The offset between the average energy yield and minimum / maximum performing panels is about -6% to +6%. In case of a typical string tied inverter configuration, where the lowest yielding panel is leading for the string energy yield, this implies to an energy loss.

Table 6.3.2: Absolute energy yield and minimum performing yield per row

	Row 1	Row 2	Row 3	Row 4	Row 5	All rows
Number of panels:	13	12	13	11	16	65
Lowest [kWh]	30.02	29.28	34.47	33.1	35.05	
Total worst panel [kWh]	390.26	351.36	448.11	364.1	560.8	2114.63
Total [kWh]	409.1	399.91	466.51	382.35	588.44	2246.31

For this period this implies to an efficiency improvement of at least 6%, due the application of panel level DC/DC optimizers (MPPT-panel). When the improvement exists for a whole year than it is a benefit of around 1000 kWh and €100 (0.10 ct/kWh price). Inverter costs for a typical string system is €2550 and for a panel optimized system €3150 [22]. This roughly means that the additional system costs are paid back in 6 years, which makes it a cost-effective choice.
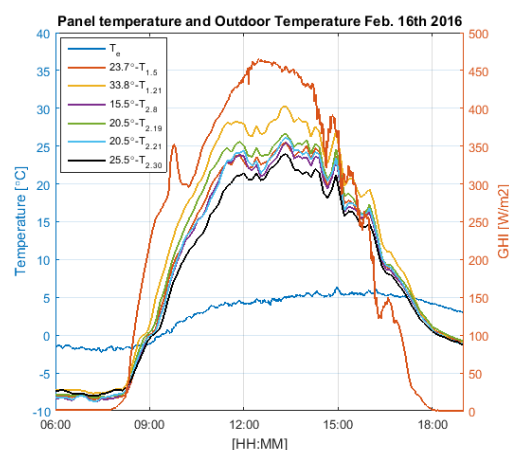
6.3.3 PV-production analysis on a clear, partly cloudy and cloudy day

Standby – energy use and on/off behaviour

The SolarEdge 15kW inverter has a measured standby power use of 3 to 4 W. At sunrise inverter wakes and start to consumes about 8W, peaking to 26W continued to a negative power value (production has started and optimizers are connected). Inverter starts production already at very low insolation values: whenever the measured GHI is 8 to 10 W/m^2 or higher and panel power output of 2.5 to 3 W. The (non-) operational behaviour is shown in figure 6.3.6 where the power and GHI are indicated.

Inverter power consumption during sunrise and sunset (Feb 16, 2016)
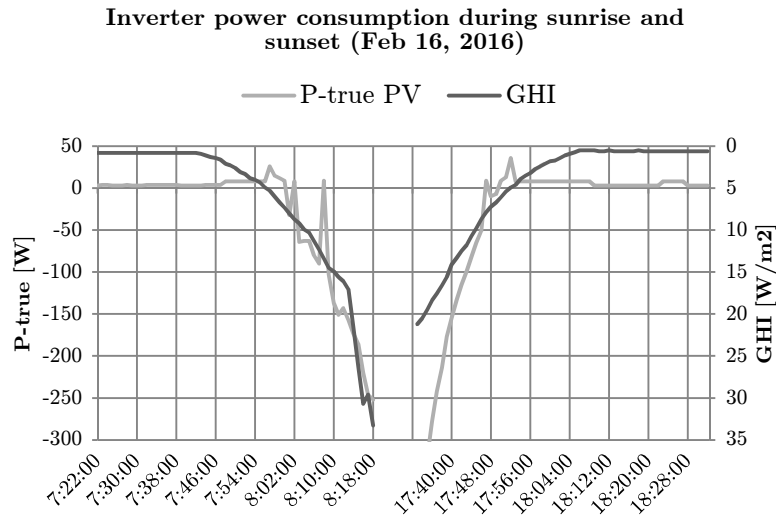
Fig. 6.3.6: Inverter day start and -end behavior (minute data: iEM3155 and SR11-pyranometer)

Highest registered peak dates from February the 25th, 2016 at 12:50 HH:MM, GHI 591.6 [W/m^2], where the 15kW inverter peaks to -15.45W.

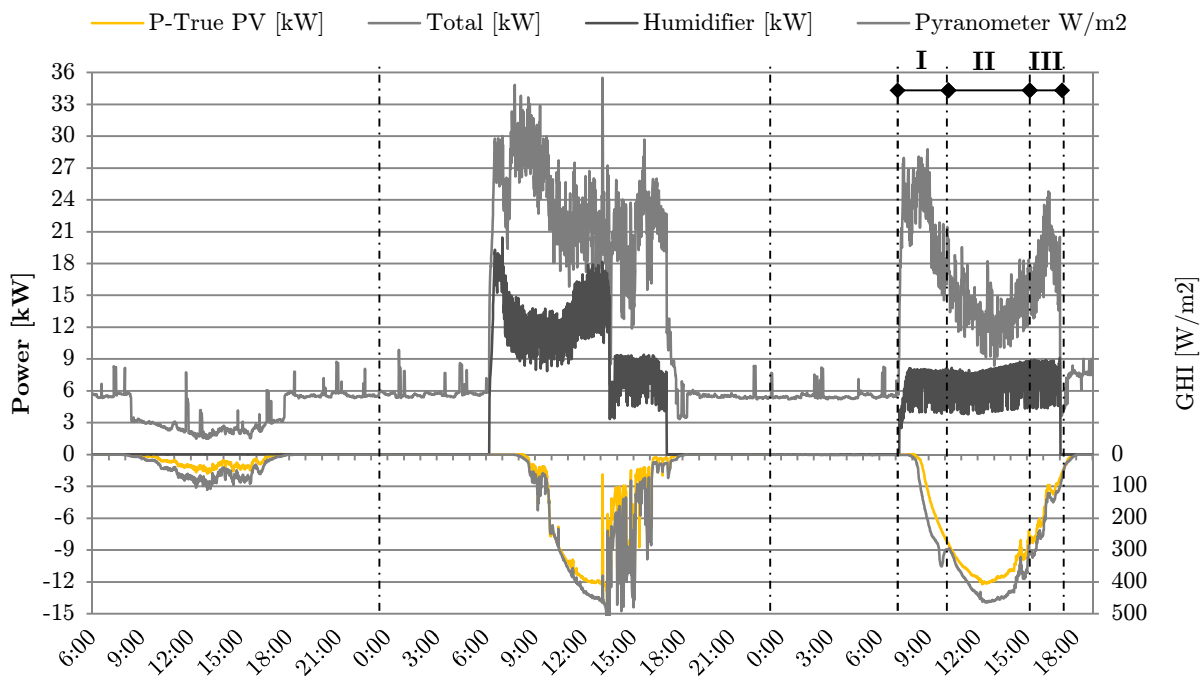**Responsiveness of inverter and resulting Net-load**

Fig. 6.3.7: PV-inverter responsiveness and behaviour due volatile GHI on a cloudy (Feb 14 2016, partly cloudy (Feb 15 2016) and clear day (Feb 16 2016)
I: at day start the building demands about 27 kW, humidifier started without peak varying around 6kW throughout the day
II: building net-load decreases due parabolic PV-production (clear day)
III: PV-production starts to decrease and a new peak demand period starts

6.4 BESS: Power Quality

In this section the following PQ-aspects are analyzed: individual harmonics (h), total harmonic distortion (THD), total demand distortion (TDD), Power factor [-] and displacement factor (DPF) often known as cos (phi). Power quality measurements were done at the primary side of the BESS-transformer; these measurements were logged in a 1sec interval. A measurements plan is provided in Appendix K: BESS system verification plan.

Fig. 6.4.1: BESS safety signs placed on rack and at room entrance

6.4.1 Power Quality requirements

The normal, AC grid-voltage is sinusoidal at 50 Hz. If a linear load (as an incandescent bulb) is connected then the <u>current</u> is pure sinusoidal and 50 Hz is the fundamental frequency. If this sinus is distorted, it is called harmonic distortion. The total harmonic distortion can be described as: the sum of more sinuses with a frequency equal to multiple of the fundamental frequency (50Hz), hence 3rd(150Hz), 5th(250Hz), 7th(350Hz),... 25th(1250Hz) or higher. Higher harmonics are caused by non-linear connected loads (electronics), in this case by the KEBF5 AC/DC inverter (8 kHz). Since it is a newly developed system with a high capacity (high current magnitude) voltage and current harmonics were analysed to determine the power quality. First PQ-requirements are provided continued with the PQ-results.

Instead of the DPF (only for fundamental frequency also known as cosines(phi)), the power factor include higher harmonics [59]:

$$Power\ factor\ (PF) = \frac{P_{real}(kW)}{P_{apparent(kVA)}} (for\ all\ frequency\ components)\ [-]$$

According the Dutch net code [35] the power factor for production units larger than 3 x 16A (this case) should be: **PF ≥ 0.90**. In order to evaluate the current- and voltage harmonic distortion, an international standard is used: IEEE Std. 519™-2014 [60]. The voltage distortion limits are displayed in table 6.4.1 and the harmonic current distortion limits are displayed in table 6.4.2.

Table 6.4.1: Voltage distortion limits according the IEEE Std. 519™-2014 [60]

Bus voltage V at Point of common coupling (PCC)	Individual harmonic (%)	Total harmonic distortion THD (%)
V ≤ 1.0 kV	5.0	8.0
1 kV < V ≤ 69 kV	3.0	5.0

Table 6.4.2: Maximum harmonic current distortion in % of I$_L$ Individual harmonic order (odd harmonics) [60]

I$_{SC}$ / I$_L$	3 ≤ h < 11 [%]	11 ≤ h < 17 [%]	17 ≤ h < 23 [%]	23 ≤ h < 35 [%]	35 ≤ h < 50 [%]	TDD [%]
< 20	4.0	2.0	1.5	0.6	0.3	5.0
20 < 50	7.0	3.5	2.5	1.0	0.5	8.0
50 < 100	10.0	4.5	4.0	1.5	0.7	12.0
100 < 1000	12.0	5.5	5.0	2.0	1.0	15.0

Where:
I$_L$ = maximum demand load current (at fundamental frequency component) at the Point of Common Coupling (PCC) under normal load operation conditions.
I$_{SC}$ = maximum short-circuit current at PCC.

At the case building the LV/MV transformer is the PCC. The transformer capacity is 630kVA and an U$_k$ of 6%, this results in a short-circuit current of 15156 KA (= 630/(0.6928*0.06)). The Isc/I$_L$ is the short-circuit current divided with the average load current during the day including battery operations is **253** (=15156KA / 60A). Limits at PCC for case building are marked in gray, table 6.4.1 and 6.4.2.

If [61] the IEEE std. 519 is being met at full capacity, then both voltage distortion and overheating (due harmonic currents) would be satisfied at all lower load levels.

6.4.2 Power Quality operational tests

Test 1: Discharge the battery with 0.1C, 0.3C and 0.5C (5 to 10minutes for each interval)

Table 6.4.3: Power quality analysis primary side transformer (building) during discharging

DC request	Active power	PF	DPF[-]	THD (I1)	THD (I2)	THD (I3)	THD(U1)	THD(U2)	THD(U3)
0.5C	-18.4 kW	-0.993	-0.997	9.4%	7.0%	10.3%	1.3 / 1.4%	1.4 / 1.5%	1.5 / 1.6%
0.3C	-11.0 kW	-0.986	-0.997	15.0%	11.4%	15.6%	1.3%	1.4%	1.5%
0.1C	- 3.6 kW	-0.978	-0.997	20.4%	16.0%	20.9%	1.4%	1.6%	1.7%

PF and DPF are during low (0.1C), average (0.3C) and high (0.5C) discharge levels within IEEE limits. The PF decreases slightly when power decreases, this is normal [61] for non-linear loads operating at partial load conditions. The voltage harmonic distortion is during all tests far below the 8.0%.

The I_{THD} normally increases as loading decreases, a non-linear load will draw less harmonic current at lighter load loads when the I_{THD} is higher [61]. This is caused to the magnitude of the individual harmonic: as percent loading decreases, I_{THD} increases but the magnitude of individual harmonic decreases (TDD) [61]. The THD is during this test not measured at the PCC, however cable lengths have a positive effect on the voltage and I_{THD}. This implies that if the TDD (current) and U_{THD}, I_{THD}, are within the limits at the BESS no problems are expected at the PCC due to the BESS. At full load the I_{THD} and individual I_{TDD} are below limits (appendix K) the TDD at 60% (0.3C) capacity and 20% (0.3C) was calculated. At full load (0.5C) $I_{THD} = I_{TDD}$, and when load drops the value of I_{TDD} relative to I_{THD} will drop proportionality with the load [61]. The TDD of the BESS was within IEEE 519 limits, table 6.4.4.

Table 6.4.4: Determination of Total Demand Distortion according IEEE [60], [61]. TDD is defined as the ratio of the RMS value of the harmonic current to the maximum demand load current.

	I_{THD} (I1)	I_{TDD}	I_{THD} (I2)	I_{TDD}	I_{THD} (I3)	I_{TDD}
Full load (0.5C)	9.4%	9.4%	7.0%	7.0%	10.3%	10.3%
60% (0.3C)	15.0%	9.0%	11.4%	6.84%	15.6%	9.36%
20% (0.1C)	20.4%	4.1%	16.0%	3.2%	20.9%	4.2%

Test 2: Charge the battery with 0.1C, 0.3C and 0.5C (5 to 10minutes for each interval)

Table 6.4.4: Power quality analysis primary side transformer (building) during charging

DC request	Active power	PF	DPF[-]	THD (I1)	THD (I2)	THD (I3)	THD(U1)	THD(U2)	THD(U3)
0.5C	27.7 kW	0.998	1	6.5 /6.6	3.9 / 4.1	6.4 / 6.7	1.4 / 1.5	1.6 / 1.7	1.7 / 1.8
0.3C	16.2 kW	0.99	1	11.9 / 12.1	7.8 / 8.0	12.0 / 12.3	1.4	1.5	1.6
0.1C	5.5 kW	0.978	1	24.8	19.3	22.1	1.3 / 1.4	1.4 / 1.6	1.5 / 1.6

The AC Power rates during charging were higher than with the same opposite DC-current control (request) value. Measured harmonics are lower than found during the discharge tests, mainly caused by a higher AC-current. All power quality aspects are within IEEE 519 limits. The highest individual current distortion was 4%, measured at the 3rd harmonic (Phase 3).

6.5 BESS: operational performance

This section outlines the results of the component (inverter and transformer) and full system performance tests. The BESS has five operation states:
1. standby
2. active / connect battery bank
3. discharge DC current request
4. charge DC current request
5. start full charge cycle

6.5.1 Standby and connected operation states: 1 & 2

A single- and three- phase group connects the complete BESS. The single-phase group for the Battery Management Cabinet (BattMS), which main energy consuming components are: a PLC-controller, LCD-

touchscreen and battery pack monitoring units. The three-phase group is used to connect the power conversion system that includes a transformer, inverter, and AC / DC filters. The BESS consumes power in standby and active operation state. The amount of withdrawn power is provided in table 6.5.1.

Table 6.5.1: Power consumption during idle and connected operation state

	Power consumption single phase BattMS-cabinet	Power Consumption three-phase Conversion System
1. Standby	103W	220W to 250W
2. Active (BESS connected)	142W	950W

The single-phase power consumption is mainly caused by the monitoring units, which uses approximately 70W (35 packs * ~2W). The cause of the standby loss of the three-phase connection is due the transformer no-load loss.   An improvement on the standby losses of the three-phase group is recommended; by electrically disconnect the whole group with a magnetic-switch installed between the decentralized electrical distribution box and the transformer unit. This switch shall be controllable through Insiteview, in order to switch the three-phase group off when the system is not operational. During active state (2.) the inverter (8 kHz) and fans in the inverter-cabinet starts to operate, this increases the demand to about 950W.

6.5.2   Component efficiency during charging and discharge operation states: 3 & 4

Conversion efficiency of transformer and inverter during <u>DC discharge request</u> of 0.05C, 0.1C, 0.2C, 0.3C, 0.4C and 0.5C (implies to 3.5, 7, 14, 21, 28, and 35 Amps) and during <u>DC charge requests</u> 0.05C, 0.1C, 0.2C, 0.3C, 0.4C and 0.5C request (is -3.5, -7, -14, -21, -28, and -35 Amps). The operational efficiency of each of these charge- and discharge intervals was tested for about 5minutes. Measurements on the primary side of the transformer was done with the iEM3155 energy meter (located at II, fig 5.1.1), secondary side of transformer was temporarily measured with a power analyser located at point III (fig 5.1.1) and as last the DC-main bus is measured at location IV (by the BattMS-cabinet).
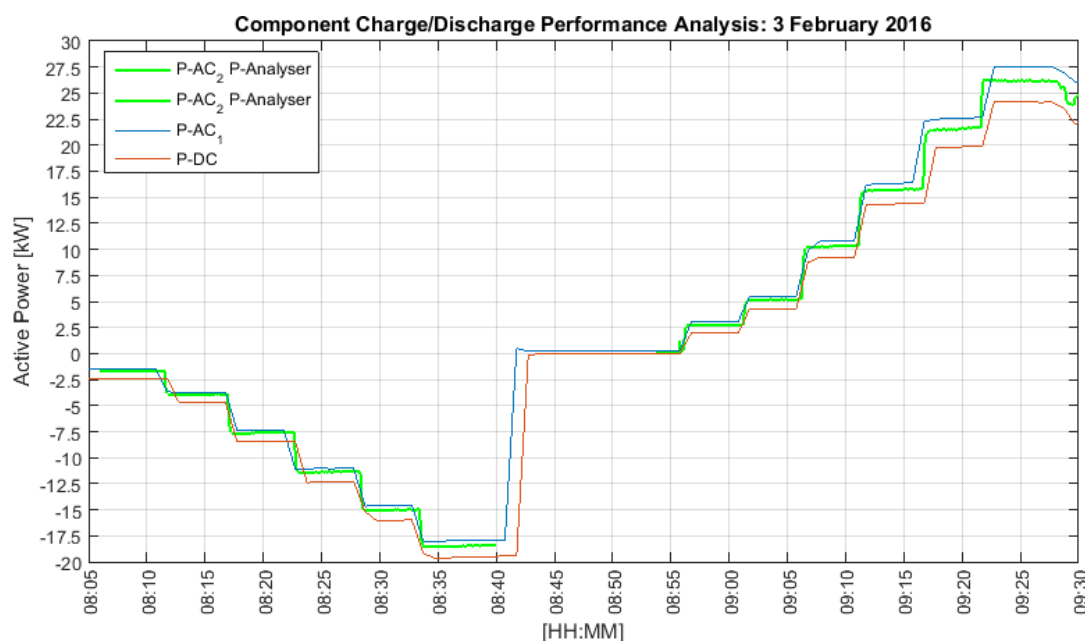

Figure 6.5.1: System and component performance tests: green line corresponds to secondary side transformer (300VAC), blue line corresponds to the primary side of the transformer (400VAC) and the brown line corresponds to the DC-power (600-700VDC)

Table 6.5.2: System, transformer and inverter charge and discharge efficiency

Setting:	1	2	3	4	5	6	7	8	9	10	11	12
P_DC [kW]	-2.43	-4.64	-8.46	-12.33	-15.98	-19.6	1.958	4.33	9.23	14.38	19.82	24.12
P_AC2 [kW]	-1.65	-3.91	-7.61	-11.36	-14.98	-18.53	2.773	5.20	10.29	15.72	21.5	26.18
P_AC1 [kW]	-1.43	-3.70	-7.37	-11.03	-14.61	**-17.98**	3.033	5.48	10.78	16.35	22.64	**27.53**
Eff. KEB	67.9%	84.4%	89.9%	92.1%	93.7%	94.5%	70.6%	83.2%	89.7%	91.5%	92.2%	92.1%
Eff. Trans	86.8%	94.5%	96.8%	97.1%	97.5%	97.0%	91.4%	94.9%	95.5%	96.1%	95.0%	95.1%
Eff. Sys.	58.9%	79.7%	87.0%	89.5%	91.4%	91.7%	64.6%	79.0%	85.6%	88.0%	87.5%	87.6%

Test results show that the system conversion efficiency is low for setting 1 & 2 and 7 & 8 due to the low current request and corresponding loss due to the KEB-Inverter including filtering and transformer. For building operational flexibility in the 0 to 5 kW range it would be interesting to use the existing building processes as much as possible to avoid this inefficient settings/operational range. In figures 6.5.3 and 6.5.4 the system efficiencies in relation to the incoming power are displayed.
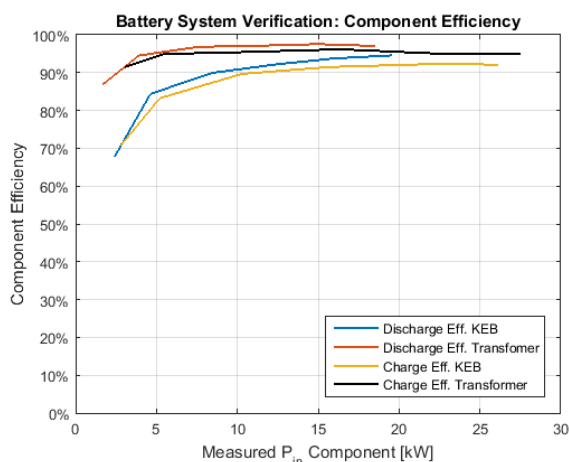

Fig. 6.5.2: Transfomer and Inverter + Filters operational efficiency
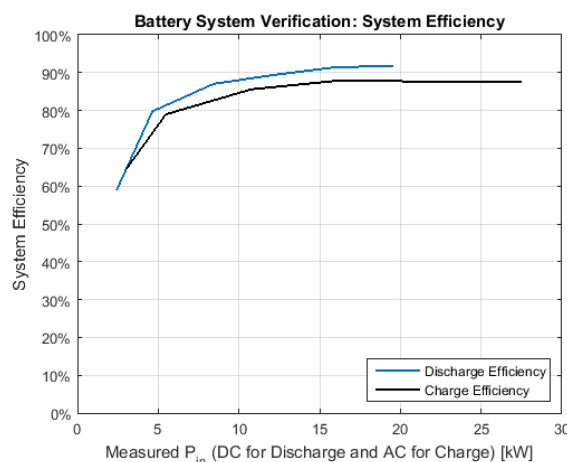
Fig. 6.5.3: Total system operational efficiency, during normal operations around the 90%.

After finishing these component performance tests a full charge procedure was initiated to make sure the battery was at 100% SOC level (avoid non-operation loss). A full cycle experiment was initiated at 0.3C to investigate the chemical- and system energy losses between a SOC of 100% and 39%. Performance analysis was done using the SOC indicator, DC-main bus measurements and AC-energy meter (iEM3155) power measurements (1minute interval). Energy was calculated with 1 minute power data, power deviations 'in' the 1minute interval were not taken into account. The complete experiment day is shown in figure appendix L and the found cycle efficiencies are shown in table 6.5.3.

Table: 6.5.3: Full cycle BESS performance

Experiment at 0.3C = 60% of system capacity	Energy [kWh]	SOC interval [%]	Efficiency	Notes:
E-DC discharge full	-26,9	100 − 39%		131 min discharged and 133 min charged
E-AC discharge full	-23.9	100 − 39%		
E-DC charge full	30.9	39 − 100%	86.9%(cycle)	Mainly due chemical energy loss
E-AC charge full	35.0	39 − 100%	68.3%(cycle)	System full cycle efficiency
E-DC discharge 40%-interval	-17.1	79 − 39%	100% (disch.)	85 min discharged and 77 minutes charged
E-AC discharge 40%-interval	-15.3	79 − 39%	89.5% (disch.)	
E-DC charge 40%-interval	18.8	39 − 79%	90.6%(charge)	Most efficient region for charging and discharging the BESS
E-AC charge 40%-interval	21.6	39 − 79%	71.1%(cycle)	
E-DC discharge (full charge procedure)	-9.8	100 − 79%		Full charge procedure took 56 minutes
E-AC discharge (full charge procedure)	-8.6	79 − 100%		
E-DC charge (full charge procedure)	12.1	79 − 100%	81%	Efficiency during the full charge procedure from SOC 80 to 100%
E-AC charge (full charge procedure)	13.4	100 − 79%	64%	

During a full cycle (between 100 and 39% SOC) most energy is lost due to the component conversion efficiency (inverter and transformer). The DC cycle efficiency in this interval at 0.3C is 86.9%, mostly due exothermic charging losses (packs built up heat). This tested efficiency is higher than written in literature [45] where the reported cycle efficiency of a NiMH-battery was 70-75%. The full system cycle efficiency is 68.3% (which includes DC/AC conversion losses). The most efficient region for charging and discharging the battery is between the 39 and 79% SOC. Verification results at 0.3C charge rate reveals a DC/AC efficiency of 89.5%, it also indicates that during discharging no energy is lost in the DC-process. Charging in this interval resulted in a DC-efficiency of 90.6%. Overall cycle efficiency, which includes inverter and transformer component conversion losses (between 39 and 79% SOC) is 71.1%. During the full-charge-procedure (80 to

100% SOC) the DC-efficiency was 81% and a total system efficiency of 64%. During daily operations, it recommended to stay within the 40 to 80% region for most efficient operation. Full-charge-procedure: on once a day (highest chemical energy loss). The BESS efficiency and power-quality improves at higher current requests, based on the verification tests it is recommended to only operate the battery whenever the AC-charge/discharge request is higher than 4kW.

Two full charge cycles (to 100% SOC) were performed during these second experiment day, which increased the highest pack temperature to 39.5°C after interval II (1st full charge, appendix L) and 47°C after interval V (2nd full charge). The normal operational battery temperature should be between -20 and 45°C. The software was adapted based on this result and a full charge can only be initiated when the temperature of the battery banks is below 30°C. Other charge and discharge cycles were calculated (table 6.5.4), based on the earlier verified component conversion- and chemical efficiency results at 0.3C. For the charge cycle the chemical loss is only verified for a 13.8 AC-power request, chemical loss at higher/lower charge rates was assumed to be equal to the 0.3C rate (table 6.5.5).

Table 6.5.4: Estimation of time, energy and power during a 100 to 30% **discharge** cycle (not experimental tested)

DC power	Discharge efficiency (verified)	AC-power	Expected time (100 − 30% SOC)	Expected AC energy
4.6kW − 0.11C	80%	3.7 kW	06:20 HH:MM	23.52 kWh
9.2kW − 0.22C	87.5%	8.1 kW	03:10 HH:MM	25.7 kWh
13.8kW − 0.33C	90.5%	12.5kW	02:07 HH:MM	26.6 kWh
18.4kW − 0.44C	91.8%	16.9 kW	01:35 HH:MM	27.0 kWh

Table 6.5.5: Estimation of time, energy and power during a 30% to 80% **charge** cycle (not experimental tested)

AC power	Charge efficiency (verified)	DC power	Chemical energy loss verified for 0.3C	Expected time (30 − 80% SOC)	Expected AC energy
4.6kW	74%	3.4 kW = 0.08C	90.6%	06:49 HH:MM	31.4 kWh
9.2kW	84%	7.8 kW = 0.19C	90.6%	03:58 HH:MM	27.3 kWh
13.8kW	87%	12.0 kW = 0.29C	90.6%	1:56 HH:MM	26.6 kWh
18.4kW	88%	16.2 kW = 0.39C	90.6%	01:26 HH:MM	26.3 kWh
23kW	88%	20.2kW = 0.48C	90.6%	01:09 HH:MM	26.3 kWh

At maximum AC discharge rate of -19kW the BESS can be discharged to a SOC of 30% in 01:26 HH:MM. Charging from 30% to 80% SOC at maximum capacity (AC-power of +27kW) is possible in 59minutes and the last 20% (full charge procedure) in 54 minutes. From 30 to 100% this implies to a quickest possible charge time of 01:53 HH:MM.

A **Full charge procedure** from 80 to 100% (8.4kWh) takes about 54minutes and requires 13.4 kWh of AC-energy and 12.1kWh of DC-energy. A battery string (7 strings in total) is full charged when the measured temperature increase is higher than 0.3 °C in 2 minutes and relative measured pressure is 50 psi. During a full-charge procedure the BESS is charged with 21A-DC and each string is disconnected separately when string meets delta T and pressure limit (DC-main bus step down: 21, 18, 15, 12, 9, 6 and 3 Amps), figure is shown in appendix M.

7   Demand side flexibility for SG-integration

In this chapter, demand side flexibility for the designed- and built facility is evaluated as a possible future SG-service. First numerical assessments on smart operation scenarios are done, with the in chapter 4 described models. Followed by an evaluation of the experimentally found results (verification chapter 6) related with possible future demand side service.

7.1   Numerical assessment on smart operation scenarios i.r.w. design requirements

At the design phase (chapter 4), there was decided to install a PV-facility with a capacity of 16.9 kWp and a BESS capacity of 42kWh with a power flexibility of 19kW (AC). At the developed facility, power flexibility can be set slightly higher during charging (about 27.5lW) and equal for discharging (-19kW). In the developed and validated BESS-model, the inverter is simulated as a 23 kW-inverter (from the design phase: KEB-23kVA), which is representative for the on-site built battery storage facility. The in chapter 2 described research requirements are translated into three smart operation scenarios:

1. Optimize self-consumption of PV-surplus, presented in figure 7.1.1
2. Clip summer peak demand due power consumption of the chiller, presented in figure 7.1.2
3. Clip winter peak demand due to the electric steam humidifier, presented in figure 7.1.3 and 7.1.4.

For each scenario figures are made about efficiency, charge command, state of charge and DSM (all figures can be found in appendix N). Here only the net-load (which includes the simulated PV-production) and resulting DSM curve are presented. The modelled 'DSM net-load controller' controls the new DSM load curve (dark black line). These scenarios are indicative as a possible future smart-grid service.
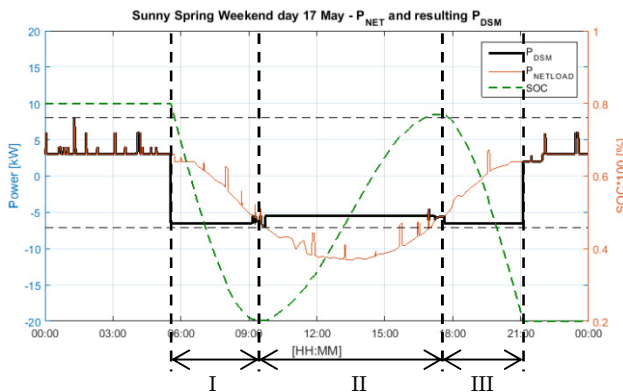
Fig. 7.1.1: DSM-scenario test for optimized self-consumption on sunny weekend day, 17th of May 2014
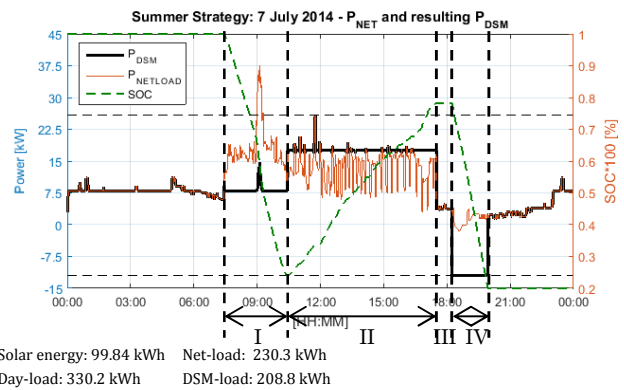
Fig. 7.1.2: DSM-scenario test at warm summer day, 7th of July

During this day the chiller operated and night ventilation was active from 23:00 to 07:00. The battery was assumed to be full charged during the weekend (with PV-production surplus).

I: Discharge: Grid support activity during morning peak
II: Charging: Negative peak shaving
III: Discharge: Grid support activity during evening peak
Initial SOC 80%, dark-green dashed line.

I: Discharge: Grid support activity: peak shaving. In line with night ventilation consumption (to flatten the demand profile)
II: Charging: Valley filling, power fluctuations of chiller. Fluctuations are approximately 12-13 min each.
III: IDLE state
IV: Discharging Grid support activity, due peak demand in grid from 18:00 to 20:00 (Belly-of-duck)

	Net-load setting	Time interval [HH:MM]	Minimum charge/discharge threshold		Net-load setting	Time interval [HH:MM]	Minimum charge/discharge threshold
Period I	-6.5 kW	$05:35 - 09:45$	1 kW	Period I	7.5 kW	x	1 kW
Period II	-5.5 kW	$09:45 - 17:30$	1 kW	Period II	17.5 kW	x	1 kW
Period III	-6.5 kW	$17:30 - 21:15$	1 kW	Period III	nothing	x	1 kW
				Period IV	-12kW	x	1 kW

Average Discharge efficiency = -42.99 kWh (DC) divided with 49.05 kWh (AC) = **88%**

Average Discharge efficiency = -51.37 kWh (AC) divided with -56.45 kWh (DC) = **91%**

Average Charge efficiency = -23.85 kWh (DC) divided with 31.82 kWh (AC) = **75%**

Average Charge efficiency = -22.85 kWh (DC) divided with 29.82 kWh (AC) = **77%**

P-load (without PV) max / min	P-Netload max / min	P-DSM max / min	P-load (without PV) max / min	P-Netload max / min	P-DSM max / min
8 kW / 2 kW	8 kW / -11.6 kW	8 kW / -7 kW	41.6 kW / 2 kW	37.6 kW / -1kW	25.8 kW / -12 kW

The first scenario provides (figure 7.1.1) grid-support by clipping the PV production peak by charging the battery system from 09:45h to 17:30h. In cases of high PV-penetration, this mid-day peak could become a huge management challenge on neighbourhood- and national level (or even international). On national level this problem can be called as the 'belly of the duck [62]', in *California solar additions have the effect of shifting the minimum net load from early morning (03:00h) to the middle the afternoon (2pm).* High level of PV-penetration contributes to a steep ramp to meet peak net demand after the sun sets. The ramp can be reduced by charging the battery during mid-day and discharging the battery when the sun sets, as presented in the first simulated scenario. With prediction models, load and production can be estimated and an energy block can be bought or sold on the market in advance.

The second scenario aims at clipping a typical 2nd stage behavior of the chiller when it starts to operate. The discharge rate of the battery is set to the night-ventilation load rate. It provides a continuous load profile from midnight till 10:30h. Combined with the simulated PV-production the day peak reduced from 41.6 kW to 25.8 kW, however this can be lower when the battery was shortly discharged at 12 o'clock resulting in a peak demand of only 17.5kW. In practice charging, discharging and charging the battery can be shortly after each other, while in the model the second interval was adapted for valley filling (by charging the BESS). At the end of the day when the national demand increases and renewable production decreases grid-service is provided by discharging the BESS from 18:00h to 20:00h.
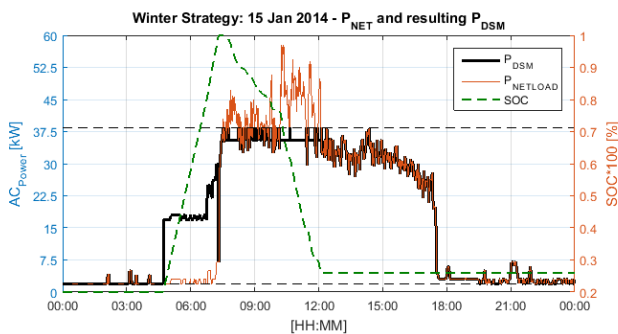
Fig. 3.6.x: Peak clipping during winter time: Jan.15
E-demand day = 403.4 kWh
Net Load = 401.2 kWh

Minimum shave battery starts when AC request > 3kW
Full Charge is performed during early-morning

Peak demand without PV: 57.8 kW
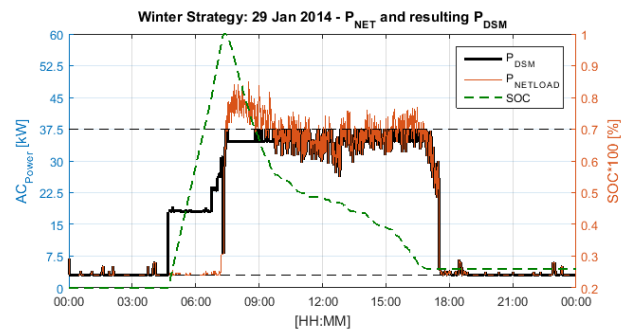**Peak demand with PV: 57.8 kW**

Peak demand with BESS: 38.5 kW

Fig. 3.6.x: Peak clipping during winter time: Jan.29
E-demand day = 464.7 kWh
Net Load = 420.3 kWh

Minimum shave battery starts when AC request > 3kW
Full Charge is performed during early-morning

Peak demand without PV 50.9 kW
Peak demand with PV 48.8 kW

Peak demand with BESS 37.5 kW

The third simulated scenario (figures 7.1.3 and 7.1.4) shows the effectiveness of the designed and built BESS during two winter-days where the humidifier operated. There is assumed that the battery was empty due to the previous day and it is fully charged during night-time. In this case, just before the building started to operate from about 05:00h to 07:00h. Dependent on the required grid-service, full charges can be initiated earlier as well (for example from $01:00 - 03:00$, dependent on SOC, electricity rate and current request). Those two days are representative for a cold winter-day scenario and therefore there can be concluded that the contracted power, using the BESS for peak clipping, could be limited to 40kW, instead of 53kW (mainly due to the peak demand period of the building and steam humidifier).

This measure could already save in the yearly electricity costs (for electricity tariffs see appendix B):

- Standing charge: from €441.00 to €18.00 saves **€423.00** a year.
- Contracted power: from 53kW to 40kW: from €1177.13 to €212.00 saves **€965.13** a year
- Maximum measured extracted power: average extracted power of 35kW (before) costs 1.44 per kW. In the new (40kW) transportation category (I) no costs are charged: approx. **€50.40** can be saved
- **Total yearly saving** using the BESS for peak clipping under 2015 contract conditions is **€1438.53**

7.2   Experimental assessment on building side flexibility

In this section, the power behaviour of the BESS is presented, starting with response- and recovery time for reaching a requested power demand for building side flexibility and continued with a possible SG-service. The BESS starts to change current in about 5 to 6 seconds and then ramps up (charge) or down (discharge) power. Measured behaviour characteristics are outlined in the next figures 7.2.1 to 7.2.4.
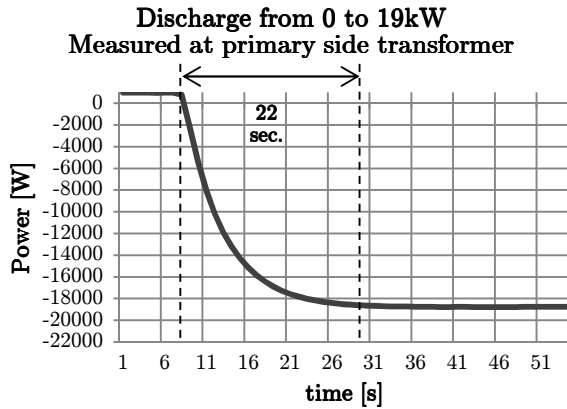
Fig. 7.2.1: Discharge start-up behaviour (2 Feb) start at +970W
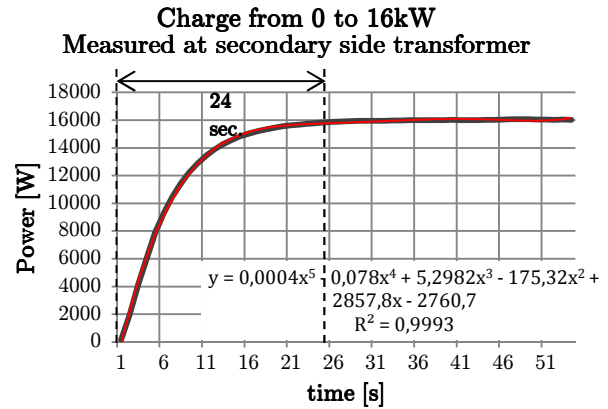
Fig. 7.2.2: Charge start-up behaviour (3 Feb)
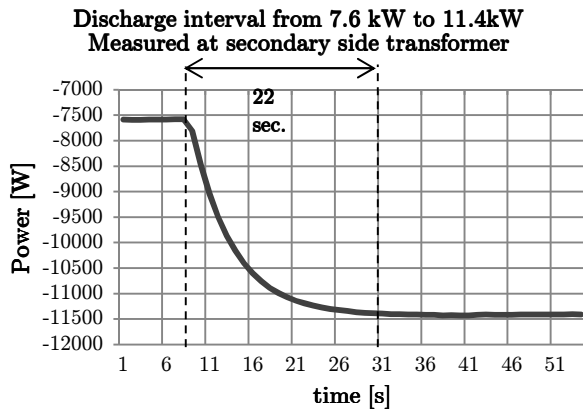
Fig. 7.2.3: Change of discharge current during operation (3 Feb)
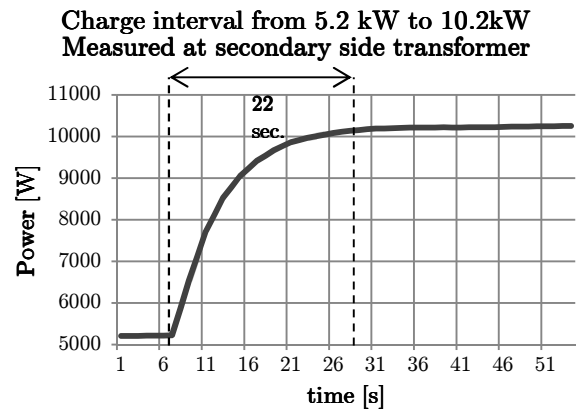
Fig. 7.2.4: Change of charge current during operation (3 Feb)

The recovery time after requesting a current is about 22seconds independent to the operation state, current rate and direction. The BESS response time to change current is 5-6 seconds, which mean that in 28 seconds a requested demand can be met. Further research is required to explain this 'identical' recovery time delay. In relation to existing reserve markets on TSO scale, this time is still within the quickest reserve market for primary control (PC). PC: to be activated in 30sec and time period per single accident $0 < t < 15min$ [63].

Secondary Control: to be active within 5min and time period per single incident $30s < t < 15min$. In balance markets, relatively high prices are paid for power and energy flexibility, however the end-users cannot participate in those markets (yet). Future SG-mechanisms could facilitate this, when buildings become part of a virtual power plant, managed by a central aggregator. The maximum measured AC-discharge support-activity by the battery was -19kW, and during charging +27.5kW. This implies to a maximum flexibility range of 46.5kW. With respect to the performance, it is recommended to use the BESS whenever the requested power flexibility is higher than 4kW to remain a reasonable system conversion efficiency and power quality. In cases of lower flexibility requests, it is recommended to actively approach the building processes.

8   Discussion

The graduation research aims to design, develop and commissioning a Photovoltaic-generation and Battery Energy Storage System (BESS). Designing a demand side BESS for grid-support activities in office buildings is new in the building sector and systems for active grid-participation are not commercially available yet. There is no best design solution to fulfil all the demanded research design requirements, however an optimal concept design solution is found using the Kesselring-S [29] assessment methodology. This method is easy understandable and sufficient during the pre-feasibility study at the conceptual design stage. There are no examples available in the literature [27] using the Kesselring-S method for hybrid-system (hybrid: PV-production, BESS and e-Grid) design assessment. With the Kesselring design assessment methodology only care is taken on the initial costs and not on life cycle costs, while often [27] used software tools as HOMER[27] could enable that for the proposed design configurations. Costs and benefits, hence cost-effectiveness, is taken into account through comparing the initial costs and functional scores in the Kesselring-matrix. The advantage of this method is the easy understandable comparison of different design concepts before getting into too much detail (which is the case for software tools as HOMER).

For facility sizing, models are used and developed in a Matlab-Simulink environment, the PV-generation model mainly consists of functions developed by Sandia National Laboratory [31], also mentioned in the hybrid system analysis software review [27]. Building loads are simulated with empirical data, and the BESS is self-developed in Simulink using manufactures data for battery and mathematical operations (inspired by [32]). With this there are no limitations due to preprogramed settings in externally developed programs, all type of time series can be imported/exported and anything can be added to the model for analysis.

The Photovoltaic-model provides accurate predictions based on the climate data, wind speed, global horizontal irradiation and ambient temperature. The solar separation model, for GHI into direct and diffuse radiation is validated [51] for hourly values, however monthly cumulative comparison and daily profile show that the 10minute data also provides accurate outcomes.

The BESS-model is a simplified representation of the constructed NiMH BESS-facility, it shows accurate results for large SOC intervals for example between 40 and 80% SOC or 40 and 100% SOC, however improvements based on the found efficiency curves in the verification study are required in order to model the conversion system (transformer and inverter) more accurately. The model also does not take any response time into account; it directly changes power if that is requested by the DSM-controller. It also excludes the real full charge procedure behaviour, with the found step by step string disconnection, and as last it doesn't take non-operation losses into account. For the research objectives this model was sufficient to determine the PV-facility- and BESS-size and numerical assessment on DSM-scenarios (chapter 7). The PV-facility capacity is determined, in relation to the available roof space, budget and more importantly to the chiller power- and energy demand on a summer-day for DSM-scenario.

If all the available area on the building roof and façade was used for installing PV-panels, the office would become nearly electrical energy neutral (90%), however almost 50% of the produced energy would have been exported. The same photovoltaic-model was used to determine the energy surplus due the existence of a PV-facility at the Kropman Breda office building during the year 2014. A remark on the used empirical building loads data should be made, the data used in the model is power data, at 1minute interval, in 2014 it was logged in kW steps (for example 0,1,2,3,4 kW), calculating the yearly energy content with this power data and comparing it with the measured energy the (low resolution power) energy consumption was 9% lower. For the numerical DSM scenario analysis with the developed DSM-controller (PV, BESS and building loads), it is used in order to analyse the behaviour of the loads (0...60minutes). The measurement logging registration is improved in the BMS, so it logs power with 3 decimals now.

After a system- configuration and capacity was chosen (by modelling), procured and constructed a verification study is done in order to test the operational behaviour and performance of the PV+BESS-facility in relation to the research requirements. The PV-facility operates according the product specifications, production starts already at a GHI of 8 to 10W/m² and it responses directly to the intermittent insolation changes. The production is compared with the model and independently monitored panels, and except for one panel, which produces about 12% less compared to the row average, the system performs well. This panel produces a lower DC-current compared to the other in the row, which may be caused by a bad operating PV-cell, more analysis is required to found the threat behind this problem. Only by modelling, there is found that the PV-facility energy yield can be linked to the chiller operations, since

measurements of a summer period are not there yet. However during autumn and winter the facility already peaked to 15kW (24 Feb) and produced about 92kWh on the 27th of September, so it is expected that that research requirements (summer yield of: 91 kWh) are met. At summertime the daily yield will be higher due longer days and higher insolation values.

The BESS uses a NiMH based technology, according literature the cycle efficiency is between $60 - 66\%$ [44] and $70 - 75\%$ [45]. At the verification tests, with a SOC window between 39 and 100%, the measured battery cycle efficiency ($E_{\text{DC,in}}/E_{\text{DC,out}}$) was significantly higher namely: 86.9%. The determined battery efficiency does not take the system conversion loss into account. At operations with a 0.3C rate, the charge conversion efficiency (AC➔DC) was 87% and during discharging (DC➔AC) 90.5% this implies to a cycle (AC/DC and DC/AC) conversion efficiency of 79% and a full system cycle efficiency of 68.3% (includes chemical loss). In other words during a full cycle almost a third of the energy is lost, with the largest loss contribution due to the system conversion efficiency. It is recommended to perform more cycle tests at different C-rates to verify these results.

With regards to the research requirements the system must be capable of clipping the intermittent spikes of the chiller and humidifier demand, they demand a power flexibility of -19 and -17kW respectively. The BESS verification results show that it is capable of consuming an AC-power of about 27kW and supplying -19kW, which means that it meets the power flexibility design requirements. It is also capable of consuming the peak production of the inverter which is about 15kW. During the early morning experiments (08:15) on February 3, the building became electrical energy neutral while the BESS operated at maximum discharge capacity and the PV-production and steam humidifier was not active.

The power-quality aspects at a nominal and normal capacity (0.5C and 0.3C) in relation to the; power factor, displacement factor and current and voltage total harmonic distortion are within limits in according to the IEEE 519 std. [61]. The individual voltage and total harmonic distortion (U_{THD}) at lower rates (0.1C) is within limits, only the current THD was not within IEEE 519 requirements. However, due the low current magnitude at these low charge/discharge rates the calculated total demand distortion (TDD) is within TDD power quality requirements. The Power Quality-analyzer was in this case located at the BESS, for optimal PQ-analysis in accordance with the IEEE 519, it should be connected at the point-of-common coupling (in this case at the Low Voltage side of the transformer (LV/MV) building). For an efficient system power conversion (AC/DC) and better power quality, it is recommended to use the battery system at AC-power rates above: 4 to 5kW.

Performance analysis of the developed facilities during the commissioning period was done with facility integrated and additional instrumentation (chapter 5.4). Additional installed instruments are: a weather station (which includes wind speed/direction, adaptable pyranometer, outdoor temperature and light intensity) separate pyranometers, AC-energy meters and panel- and room temperature sensors. Comparing measurements of the in 2010 validated, CMP10 pyranometer with the new SR11-pyranometer and KNMI-station Gilze-Rijen, there is found that the CMP10 is not accurate anymore; new calibration is required in order to use it for this research. The lighting intensity on four façade directions is not mentioned in the verification study, this because the LUX-sensors were not functioning yet.

Life after research: The PV-facility is constructed with staff of Kropman; this was for them a knowledge advantage, but also a sustainable benefit. During the (minimum) 25-year lifespan, only little care is required as on cleaning. Water droplets are naturally used to wash dust and sand of the panels, these droplets does not significantly affect the performance of the PV-panel [64]. However, it is recommended to clean the panels at least once a year to avoid dirt-losses. The PV-inverter has a product guarantee of 12 years, it is expected that it should be replaced at least once during the 25 years life span of the facility. According a literature review [65] about 40 years of PV-cell technology field tests there was found that poly crystalline-cells have a yearly average degradation rate of 0.61% (constructed before 2000) and 0.64% (constructed after 2000). At the developed PV-facility, JAP6-poly panels were chosen which according specifications provide a linear power warranty of 0.7% a year. After 25 years the panel average degradation rate still allows reasonable performance after the life span of 25 years [65]. Panel integrated optimizers have a product warranty of 25 years, there is only 10 years field experience with the optimizers, so no statements on the 25 years lifespan can be made.

9   Conclusion

The aim of this research is to develop a Photovoltaic- and Electrical Storage System for investigation of Smart Grid facilitating demand side management strategies for an office building in Breda. The work was done within the framework of PhD research project entitled: 'Smart-Grid Building Energy Management System [13]'. This promotional research aims at developing a building control framework for sustainable energy exchange between office building and futuristic Smart-Grids.

1. Which are the desirable properties of PV + BESS facility that comply with SG-BEMS research requirements?

The required capacity for this research is basically categorized into four demand side scenarios: peak power capping by linking the chiller operations to the PV-facility production, peak power capping by clipping 2nd stage chiller demand and by clipping early morning peak of humidifier with BESS, optimize self-consumption of local-generated renewable energy and participate in smart grid-support activities. Smart-grid support activities with specific reference to short-term power flexibility services of less than an hour. Other general requirements are about available budget, safety during and after facility construction, instrumentation for facility analysis, the integration of the facility in the existing electrical infrastructure and building management system (Insiteview).

2. What is the best suitable PV- and BESS facility available in the market?

There can be concluded that there are only few BESS systems in the market (2015), which are mainly developed for optimizing self-consumption of on-site produced electricity. These hybrid systems have the advantage of efficiently charging solar surpluses, however for demand side scenarios as above this makes it a disadvantage, since these hybrid systems with bi-directional inverters limits the batteries discharge capability for power flexibility while PV-production is active. Contrary to decentralized BESS, PV-systems are widely available, from systems based on string-inverters, to panel level optimized systems with micro-inverters or DC/DC optimizers. Due the rare existence of useful market ready hybrid (PV+BESS) solutions and the required operational independency to facilitate demand side scenarios there is, based on the Kesselring-S assessment diagrams, decided to have two independently operating systems, one for PV-generation and one for BESS.

The chosen PV-facility is made out of 65, 260Wp panels facilitating 16.9kW peak capacity connected to a 15kW inverter (SE). These polycrystalline modules are panel-level monitored and individually optimized to its maximum power point. In the modelled reference year 2014, it produces (simulated) about 18.000 kWh. This covers 22% of the total electrical energy demand, from which 19% of the production is exported also called a negative net-load. The designed BESS is capable of linking the chiller demand requirements illustrated at peak day 18th of July 2014, where the chiller demanded 84.9 kWh and the modelled PV-facility produced 102.9 kWh. Second stage operations of the chiller exceeded the PV-production, but in that specific situation the BESS can be used for peak clipping by shortly discharging the battery. In this case flexible power is more important than energy, since the energy content in those spikes (4 times) is relatively low.

The best suitable BESS facility chosen for this research is the independently operating and completely recyclable (99%) NiMH-battery technology developed by Nilar. The bi-polar design (of the NiMH-battery) is capable of delivering high capacity charge and discharge rates up to three times the battery capacity. It is not a market-ready BESS-solution and therefore a complete system is newly developed with respect to the research requirements. One of these requirements was clipping the humidifier morning peak demands which accounted for 6 to 11 kWh (day dependent) of energy and 17kW of power capacity. Other requirement was clipping 2nd stage demands of the chiller which requires 19kWh of usable energy (a day) and a peak power of 19kW. The developed BESS will also contribute to an improvement of PV-production self-consumption. With the available budget there is decided to optimize self-consumption of exported energy (19% of total) with 80%. Compiling these requirements for the year 2014, there is concluded that 42 kWh of nominal battery capacity and 19kW charge/discharge power is required in order to obtain a self-consumption of 96% and to clip the peak demand periods of the chiller and humidifier.

3. How can the selected PV- and BESS facility be adapted for installation and operation with the existing electrical infrastructure, building management system and building?

The selected research facility is built in the existing installation room of the Kropman Breda office, to facilitate the high power rates the electrical infrastructure needed to be adapted. Both the PV-facility and BESS are connected to a new decentral distribution cabinet located in the installation room. The chosen NiMH-battery system has the advantage that it does not emit any hydrogen gasses or other during any normal use. It *could* be placed inside a building without any additional safety measures, however for some additional safety; detection sensors (hydrogen, smoke and temperature: in case of short-circuit, fire or ..) are mounted and some ventilation is provided for heat removal. Compared to lead-acid batteries, which should always be placed in a well ventilated room due to their hydrogen-gas emission. The PV- and BESS facility is completely controllable and monitored with all required instruments in the Insiteview building management system. Insiteview can be used as a gateway for intelligent BESS operational control through JAVA (agent-based, Remote-Control-Agent). Future software changes can easily be adapted since it is an in-house developed BMS-program.

4. How to verify the performance of the PV and BESS facility for fitness of purpose?

To verify and experiment with the PV- and BESS facility instrumentation was installed. For the PV-facility instrumentation is installed in accordance with the IEC61724 [37]: environmental sensors which measures the outdoor temperature, solar irradiance, wind-speed and panel temperatures. Electrical energy and power is measured from panel- to inverter level. Additional measurements are light intensity in all façade directions, relative humidity, wind direction and energy measurements on panel level. For the BESS energy- and power is measured from individual pack, to string level, to the central AC-connection of the 40A group. These instruments are used during the facility verification study. PV-facility verification is achieved by analysing the power output related to the GHI, PV-model and yield of individual panels. There can concluded, that expect for one panel, the PV-facility performed according manufactures product specifications. The energy yield of one panel stays behind the rest, measured in the second row at 20.5fl (about 12% less production) this problem is related to a lower panel current, which may be caused by a small-crack in a cell, further analysis is required. The chosen panel optimized PV-system shows a 6% energy improvement compared to typical string-tied inverter systems.

The BESS-facility is verified by analysing the power-quality, cycle performance and charge/discharge behaviour. The BESS conversion efficiency and power-quality improves at increasing power rates. During the verification study there can be concluded that most energy, during a full cycle (39% and 100%SOC) is lost due the component conversion efficiency (inverter and transformer). During a full charge the battery packs built up heat and more energy is lost, these full charge should be limited to once a day. Power quality of the BESS was sufficient in accordance with the IEEE-519 limits (chapter 6.4.2). For a reasonable efficiency and better power-quality: charge and discharge rates of 4kW and higher are recommended. The most efficient region for charging the battery was between 39 and 79%.

5. What is the operational performance of the developed system in relation to the SG-BEMS requirements and operational flexibility?

Numerical demand side management tests i.r.w. the research requirements show that the facility is capable of clipping the peak demand periods during a summer-day. Simulations for the 7th of July 2014 show that the day peak is reduced from 41.6 kW without PV-production, reduced to 37.6kW with PV-production, and to a peak of 25.8kW with the use of the BESS. On the 15th of January peak clipping by BESS operations decreased the winter day peak demand from 57.8 kW to 38.5 kW. On the 29th of January 2014 the peak demand was, 50.9 kW reduced to 48kW due the existence of a 16.9kWp PV-plant and clipped to 37.5 kW by BESS operations. These scenarios are not operational tested and are part of future research. Under existing contract conditions, electricity costs can be saved by decreasing the contracted power. With the numerical found results there can be concluded that already €1450 on yearly basis can be saved on the transmission costs by adapting the existing contract.

Operational tests reveal that the BESS is capable for servicing the grid to meet a requested AC-power in 28 seconds. About 6 seconds due to a control-delay and 22 seconds ramp-up/down time to reach a power-request. The observed time period is quick enough to participate in a primary control reserve market. In balance markets, relatively high prices are paid for power and energy flexibility, however end-users (as commercial buildings) cannot participate in those markets (yet). Future SG-mechanisms could facilitate this, when buildings become part of a virtual power plant, managed by a central aggregator. The maximum power flexibility service is -19kW and + 27.5kW, which implies to a 46.5kW flexibility range. The found power flexibility at continuous maximum (charge or discharge) capacity can last for more than 1.5hour which means that the SG-service requirement on demand side flexibility time period of 0 to 60min has been met. With respect to the performance, it is recommended to use the BESS whenever the requested power flexibility is higher than 4kW to remain a reasonable system conversion efficiency and power quality. In cases of lower flexibility requests, it is recommended to actively approach the building processes. Combining the newly developed BESS and existing building processes (as active use of fans, steam humidifier and chiller) could even provide larger demand side flexibility service.

9.1   Acknowledgements

10   Further research

Experimental facility related:
- Test proposed demand side scenarios in practice.
  - Peak clipping of 2nd stage chiller demand during summer time
  - Peak clipping of morning peak demand electrical steam humidifier
  - Optimize self-consumption of solar-energy surplus
    - Increase self-consumption by charging the BESS during production surpluses
- Develop an agent-control-framework for intelligent operations of the BESS i.r.w. comfort based loads.
- Develop intelligent control algorithms for testing parallel demand side flexibility requests. For example lowering the set point of the humidifier whenever a demand of 0 to 4kW is requested and use the BESS for higher requests.
- Fire-safety of NiMH technology compared to other technologies
- BESS cycle performance analysis at different charge and discharge rates and SOC-intervals

Performance:
- BESS performance improvement: Install a three-phase contactor (Magnetic Switch), which can disconnect the transformer from the grid when the energy storage system is not in use. Due to transformer no-load losses the BESS-group consumes about 240W. It is a waste of energy to have the transformer energized when it is not in use. This contactor should be controllable through Insiteview BMS.
- PV-production analysis with newly installed weather station during all seasons.
- Further analyses on panel 1.1.19, for example with a thermographic camera to see if a probably broken individual cell built up heat.

PV-Model related:
- Test PV-model accuracy by using the on-site weather station and panel temperature sensors.
- Use the PV-model to forecast PV-power production for coming day.
- Based on 3 parameters a prediction can be made:
  - Global Horizontal Irradiance [W/m^2]
  - Wind Speed [m/s]
  - Outdoor temperature [°C]

Improve BESS-model:
- Integrate a time-delay
- Full-charge-behavior, independent disconnection of the strings (7strings, 3A each)
- Include non-operation-losses
- Implement validated models in agent-control system as a black box

BMS Software related:
- Update Insiteview software (BMS) with newly received BESS communication list in order to store all data on string and pack level as well
- Program simple logic in order to:
  - Charging the battery without agents structure energy during negative net-load periods
  - Set charge/discharge rates and SOC-levels. For example on a winter day, automatically shave the early morning peak by setting an energy consumption limit. Discharge the battery if P-building > 25 kW for example.
  - Turning a full-charge procedure on, for example start-full-charge procedure during off-peak hours

11 References

[1]   D. Staniaszek, *RENOVATION STRATEGIES OF SELECTED EU COUNTRIES A STATUS REPORT ON COMPLIANCE WITH ARTICLE 4.* 2014.

[2]   M. Hekkenberg and M. Verdonk, "Nationale Energieverkenning 2014," 2014.

[3]   CIBSE, "CIBSE Briefing The Recast Energy Performance of Buildings Directive," no. Article 10, p. 16, 2011.

[4]   SER, "Energieakkoord voor duurzame groei," *Rep. From Http//Www.Energieakkoordser.Nl/*, no. September, pp. 1–146, 2013.

[5]   European Commission, "Energy RoadMap 2050," 2011.

[6]   R. Venekamp, Gerben, J. Kamphuis, M. Laarakkers, and van den Berge, "OS4ES : Increasing awareness of DG-RES and demand response processes by registry enabled services," *PowerTech*, 2015.

[7]   AGORA Energiewende, "12 Insights on Germany ' s Energiewende 12 Insights on Germany ' s," no. February, 2013.

[8]   RVO,   "Cijfers   elektrisch   vervoer,"   2015.   [Online].   Available: http://www.rvo.nl/onderwerpen/duurzaam-ondernemen/energie-en-milieu-innovaties/elektrisch-rijden/stand-van-zaken/cijfers.

[9]   P. B. L. Planbureau, D. Leefomgeving, and D. N. V Gl, "Het potentieel van zonnestroom in de gebouwde omgeving van Nederland," 2014.

[10]   H. Farhangi, "The path of the smart grid," *IEEE Power Energy Mag.*, vol. 8, no. 1, pp. 18–28, 2010.

[11]   S. Grijalva and M. U. Tariq, "Prosumer-based smart grid architecture enables a flat, sustainable electricity industry," *IEEE PES Innov. Smart Grid Technol. Conf. Eur. ISGT Eur.*, 2011.

[12]   IRENA, "Case studies: Battery storage," *Int. Renew. Energy Agency*, 2015.

[13]   E. Mocanu, K. O. Aduda, P. H. Nguyen, G. Boxem, W. Zeiler, M. Gibescu, and W. L. Kling, "Optimizing the energy exchange between the Smart Grid and Building Systems," *2014 49th Int. Univ. Power Eng. Conf.*, pp. 1–6, 2014.

[14]   K. O. Aduda, E. Mocanu, G. Boxem, P. H. Nguyen, W. L. Kling, and W. Zeiler, "The potential and possible effects of power grid support activities on buildings : an analysis of experimental results for ventilation system."

[15]   K. O. Aduda, W. Zeiler, G. Boxem, and K. De Bont, "On the use of electrical humidifiers in office buildings as a demand side resource," *Procedia Comput. Sci.*, vol. 32, pp. 723–730, 2014.

[16]   K. O. Aduda, W. Vink, G. Boxem, Y. Zhao, and W. Zeiler, "Evaluating cooling zonal set point temperature operation strategies for peak load reduction potential : case based analysis of an office building," *PowerTech*, pp. 4–8, 2015.

[17]   K. O. Aduda, T. Thomassen, G. Boxem, and W. Zeiler, "Adaptability of office buildings for improved energy intelligence : a case analysis for operations in electrical power grid," pp. 5–12, 2015.

[18]   D. Bank, "F . I . T . T . for investors Crossing the Chasm," 2015.

[19]   P. T. Moseley and J. Garche, *Electrochemical Energy Storage for Renewable Sources and Grid Balancing Edited by*. Elsevier, 2015.

[20]   R. Dufo-López and J. L. Bernal-Agustín, "Techno-economic analysis of grid-connected battery storage," *Energy Convers. Manag.*, vol. 91, pp. 394–404, 2015.

[21]   G. Mulder, D. Six, B. Claessens, T. Broes, N. Omar, and J. Van Mierlo, "The dimensioning of PV-battery systems depending on the incentive and selling price conditions," *Appl. Energy*, vol. 111, pp. 1126–1135, 2013.

[22]   W. van Sark, P. Muizebelt, and J. Cace, "Inventarisatie PV markt Nederland," 2014.

[23]   W. Sinke, "Zonnestroom : van niche naar impact," 2015.

[24]   IEA, "Technology Roadmap," 2013.

[25]   Fraunhofer ISE, "Current and Future Cost of Photovoltaics. Long-term Scenarios for Market Development, System Prices and LCOE of Utility-Scale PV Systems," 2015.

[26]   IRENA, "Renewable Power Generation Costs in 2014," 2015.

[27] S. Sinha and S. S. Chandel, "Review of software tools for hybrid renewable energy systems," *Renew. Sustain. Energy Rev.*, vol. 32, no. February, pp. 192–205, 2014.

[28] S. Nuchprayoon, "Optimum Scheduling of Non-utility Facility with Battery Storage Under a Price-taking Scheme."

[29] W. Zeiler, P. Savanovic, and E. Quanjel, "Design Decision Support for the Conceptual Phase of the Design Process," *Int. Assoc. Soc. Des. Res.*, pp. 1–15, 2007.

[30] W. Zeiler, *Basisboek Ontwerpen*, 1st ed. Noordhoff Uitgevers B.V., 2014.

[31] PVPMC, "PVPerformance Modeling Collaborative," 2015. [Online]. Available: https://pvpmc.sandia.gov/.

[32] M. Zisler, S. Spann, and M. Tragner, "Modelling of decentralised grid-connected electricity storage," *Symp. Energyinnovation*, vol. 13, pp. 1–11, 2014.

[33] G. Benetti, D. Caprino, M. L. Della Vedova, and T. Facchinetti, "Electric load management approaches for peak load reduction: A systematic literature review and state of the art," *Sustain. Cities Soc.*, vol. 20, pp. 1–18, 2015.

[34] T. P. W. Thomassen, "Smart Grid Building energy management," 2014.

[35] ACM, "Netcode Elektriciteit," 2014.

[36] NEN 1010 (nl), "Safety Requirements for low-voltage installations," 2015.

[37] British Standard, "IEC 61724:1998. Photovoltaic system performance monitoring — Guidelines for measurement , data exchange and analysis," 1998.

[38] P. Savanovic, "Integral design method in the context of sustainable building design: Closing the gap between design theory and practice," University of Technology Eindhoven, 2009.

[39] IRENA, "Design of Grid-connected PV Systems," 2013.

[40] G. Knier, "How do Photovoltaics Work? - NASA Science," *NASA*, 2002. [Online]. Available: http://science.nasa.gov/science-news/science-at-nasa/2002/solarcells/.

[41] MPowerUK, "Electricity Generation from Solar Energy, Technology and Economics," 2015. [Online]. Available: http://www.mpoweruk.com/solar˙power.htm#domestic˙pv. [Accessed: 15-Oct-2015].

[42] MPowerUK, "How Energy Cells Work," *Electropaedia*. [Online]. Available: http://www.mpoweruk.com/chemistries.htm. [Accessed: 18-Jan-2016].

[43] T. Kousksou, P. Bruel, A. Jamil, T. El Rhafiki, and Y. Zeraouli, "Energy storage: Applications and challenges," *Sol. Energy Mater. Sol. Cells*, vol. 120, pp. 59–80, 2014.

[44] H. L. Ferreira, R. Garde, G. Fulli, W. Kling, and J. P. Lopes, "Characterisation of electrical energy storage technologies," *Energy*, vol. 53, pp. 288–298, 2013.

[45] A. Chatzivasileiadi, E. Ampatzi, and I. Knight, "Characteristics of electrical energy storage technologies and their applications in buildings," *Renew. Sustain. Energy Rev.*, vol. 25, pp. 814–830, 2013.

[46] M. Vetter, "Battery system technology," 2011, no. April, p. 34.

[47] R. van Herpen, "Brandgevaar van Lithium-Ion batterijen," *Eén Vandaag*, 2015. [Online]. Available: http://www.fellowfse.nl/news/ruud-van-herpen-over-het-mogelijke-brandgevaar-van-lithium-ion-batterijen. [Accessed: 17-Feb-2016].

[48] KNMI, "Uurgegevens van het weer in Nederland." [Online]. Available: https://www.knmi.nl/nederland-nu/klimatologie/uurgegevens.

[49] ISSO, "ISSO-HANDBOEK ZONNE-ENERGIE," p. 472, 2012.

[50] I. Reda and A. A. Nrel, "Solar Position Algorithm for Solar Radiation Applications (Revised)," *Nrel/Tp-560-34302*, no. January, pp. 1–56, 2003.

[51] E. Maxwell, "A quasi-physical model for converting hourly global horizontal to direct normal insolation," *Unknown*. 1987.

[52] D. R. Myers, "Solar radiation modeling and measurements for renewable energy applications: Data and model quality," *Energy*, vol. 30, no. 9 SPEC. ISS., pp. 1517–1531, 2005.

[53] R. Perez, P. Ineichen, R. Seals, J. Michalsky, and R. Stewart, "Modeling Daylight Availability and Irradiance Components From Direct and Global Irradiance," *Sol. Energy*, vol. 44, no. 5, pp. 271–289, 1990.

[54]   C. a. Velds, *Zonnestraling in Nederland*. 1993.

[55]   D. Faiman, "Assesing the Outdoor Operating Temperature of Photovoltaic Modules," *Prog. Photovoltaics Res. Appl.*, vol. 16, no. 4, pp. 307–315, 2008.

[56]   SBRCURnet, "Plaatsing van pv-panelen op platte daken," 2015. [Online]. Available: http://www.sbrcurnet.nl/producten/infobladen/plaatsing-van-pv-panelen-op-platte-daken. [Accessed: 12-Aug-2015].

[57]   SolarEdge, "Oversizing of SolarEdge Inverters , Technical Note," 2014.

[58]   T. P. and M. W. Jessie Copper, Anna Bruce, Ted Spooner, Martina Calais, "Australian Technical Guidelines for Monitoring and Analysing Photovoltaic Systems," 2013.

[59]   A. Pit, "White paper: Hogere harmonischen," 2013.

[60]   "Power Quality: IEEE Std . 519 ᵀᴹ -2014." 2014.

[61]   T. Hoevenaars, P. Eng, K. Ledoux, W. Little, and Y. Rd, "Interpreting IEEE Std 519 and Meeting its Harmonic Limits in VFD Applications," *IEEE*, 2003.

[62]   D. Howarth and B. Monsen, "Renewable Energy Faces Daytime Curtailment in California," 2014. [Online]. Available: http://www.nawindpower.com/issues/NAW1412/FEAT˙04˙Renewable-Energy-Faces-Daytime-Curtailment-In-California.html. [Accessed: 08-Jul-2015].

[63]   Amprion, "Procurement of control power and energy in Germany," *Control Energy*. [Online]. Available: http://www.amprion.net/en/control-energy. [Accessed: 04-Feb-2016].

[64]   S. A. Sulaiman, A. K. Singh, M. M. M. Mokhtar, and M. A. Bou-Rabee, "Influence of dirt accumulation on performance of PV panels," *Energy Procedia*, vol. 50, pp. 50–56, 2014.

[65]   D. C. Jordan and S. R. Kurtz, "Photovoltaic degradation rates - An Analytical Review," *Prog. Photovoltaics Res. Appl.*, vol. 21, no. 1, pp. 12–29, 2013.

Author
K.F.M. de Bont

Student ID:
0831181

Master Thesis

Date
March 2016

Development of a Photovoltaic- and Electrical Storage System for Investigation of Demand Side Management Strategies in Office Buildings

Appendix

TU/e Technische Universiteit
Eindhoven
University of Technology

Where innovation starts

Content

A National and international energy consumption statistics

The world is in an energy transition that is a fact, this is because the climate is changing, and global temperatures are rising, often related to the rising greenhouse gas concentration in the atmosphere. Measurements in Hawaii Mauna Loa reveals an increase from about 317 ppm (parts per million) in 1958 to around 400 ppm today [1] (graphs appendix C), when this rapid rise continues carbon dioxide concentrations will reach 450 ppm by the year of 2040. At the dawn of the first industrial revolution carbon dioxide concentrations was around 280 ppm [1]. Only the most ambitious scenarios could have a reasonable chance to limit the global temperature rise to 2°C. There is a 50% chance that we stay within this limit, whenever carbon dioxide concentrations not exceed 530ppm by 2100. For a bigger chance, of two third, a maximum concentration of 450ppm is allowed [2]. For the 530 ppm scenario, this means that global emission in 2030 should be at the same or lower level of 2010, after this it should be reduced with 3% each year. In comparison, global emissions increased from 1990 to 2010 with 1 to 4% each year. When before 2030 no emission reduction is achieved, than a concentration level of 530 ppm or lower is practical infeasible according this research [2]. About a quarter of these emissions are contributed by the heat and electricity sector (as coal fired power plant).

Not only because of these indicators for climate change we are transitioning our energy system, but also because fossil fuels are depleting. One of the global approaches to fight against this renewable energy sources is increasing the share of our global energy usage. In the Netherlands this actions are written in a national energy agreement [3]. In 2014 this accounted in a renewable energy share of 5.6% [CBS-Statline] compared to the national energy demand. In 2020 14% (2023: 16%) of the national and 20% of the European demand should be fulfilled by renewable energy sources. In the Netherlands most energy is consumed by the built environment, 35%, followed by the industry, 28%, and traffic sector, 24%. Only a fraction, 17%, of this demand is consumed by electrical energy. Only about 10% (2014) of this electrical power is produced with renewable energy as wind, solar and biomass. Graphs and tables about the national energy production- and consumption current and future contributions are shown in appendix C. Our national energy demand for the coming years will stay pretty constant around the 2150 PJ a year, if current stimulation resources remain after 2020 than the share of renewable energy will substantially stay increasing also after 2020. See figure 2.1.

Available capacity (GW) — share of national electricity demand		
Wind 2014	2.847	4.98%
Wind 2020	6,0(land)	x
Wind 2023	4.45(sea)	x
PV Sept 2014	1.0	0.8%
PV 2020	6.0	4 − 5%
PV 2030	20.0	12–15%
Biomass 2014		4.34%
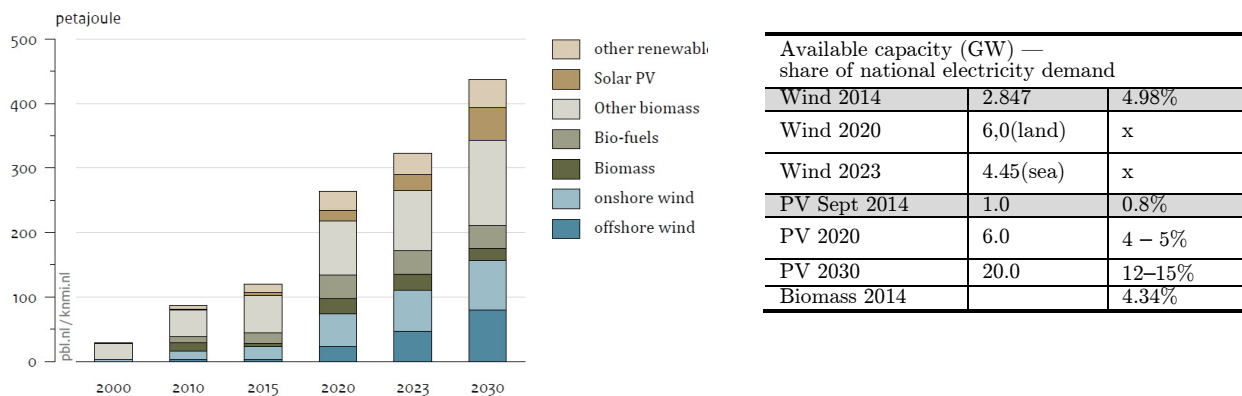
Fig. A.1: Contribution of different renewable energy sources in the Netherlands [pbl.nl/knmi.nl]

A.1 Renewables and the power grid

A.1.1 Wind

Wind is an intermittent source of energy which provides one of the largest RES-share of our national demand. To show an example of the variability of available wind power-feed in for our 2020 wind capacity situation, see the German E-on situation end 2004 (fig A.1.1) On Christmas evening a down gradient of 16 MW/Min was measured, this means a capacity of 1 coal fired power plant (500MW) every 32 minutes. In two days the drop in energy production is almost 6 GW which can be compared to 12 coal-fired power

plants. These and other earlier mentioned events pose major challenges for the grid operators, which form the basis of the problem.

A.1.2 Photovoltaic-generation

From the first made PV-module in 1954, to application in the space industry [5] during the 60s and now-a-days world-wide application at islands, rural areas and grid connected systems at buildings (behind the meter) and various large scale power plants (before the meter) with peak capacity rating to 575MW [6] . From 2000 to 2011 a global

Fig. A1.1: Wind power feed-in E-On, Germany 2004 (7GW capacity) [4]

growth rate of 44% per year was found and it is expected that during the coming years the installed capacity remain increasing [7]. For the future, 2050, it is expected that the worldwide installed capacity of solar power increases to 5TWp [8]or at the most optimistic scenario 35 TWp (is 200 times the current capacity).   For the Netherlands the 1 GWp milestone was reached in September, 2014 (is 0.8% of total yearly elec. consumption, about 265.000 households). Further Dutch national targets are; in 2020: 6GWp (4-5%) and in 2030: 20 GWp (12-15%) [3]. To put this in perspective in the second quarter of 2014 about 24.8GW plant capacity was registered at Tennet in the Netherlands. The Netherlands has one of the lowest share of solar power, instead of Germany (February 2015) where solar accounts for a nominal installed power of 38.5 GWp. According Netbeheer Nederland the assigned (energieleveren.nl) PV capacity at the end of 2015 was 1.32 GW.

Research [9] on the implementation of solar-PV at the Dutch national grid expects the following implications:

- 4 GWp PV is without grid upgrades possible if PV is *evenly distributed* in the Netherlands, however at local concentration grid upgrades are already necessary.
- From 4 to 20 GWp is a turning point, where grid upgrades are necessary, with *evenly distributed PV* in the grid the turning point will be around 16 GWp.
- From evenly distributed *PV* other methods are necessary on grid level: as peak trashing/curtailment (30% levelled). With this strategy the *evenly distributed PV* can be installed up to 27 GWp without additional grid upgrades. This only result in a 2-3% lower yearly energy yield.

- Another additional method which is proposed to prevent high investment costs due grid upgrades is DSM, which can give an additional PV capacity of 8GWp.
- Another additional method which is proposed is implementing e- storage.
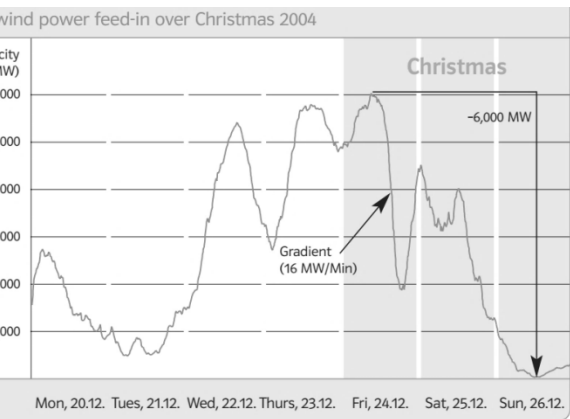
The ECN [10] states similar approaches towards the implementation of PV in the built environment and grid:

1. Spreading of locations and orientations
2. Match supply and demand
3. Curtailment or peak trashing
4. Local electricity- or heat storage
5. Large-scale storage / power-to-fuel

When the installed capacity of solar-PV facilities remain growing, sunny periods could become a challenge in the future. This challenge is sometimes called as the 'belly of the duck' figure A.1.2. In California, where solar-energy is one of the main RES-E producers, this result in shifting the minimum net load from early morning to the middle of the afternoon (that is, from 3 a.m. to around 2 p.m.). The growing belly also contributes to the steep ramp to meet peak net demand after the sun sets [11]. Within this scenario, load shifting strategies are made to cope with this problem and increase the self-consumption of the on-site generated solar-energy. Charge the battery during the day and discharge it during the evening peak (at sunset).
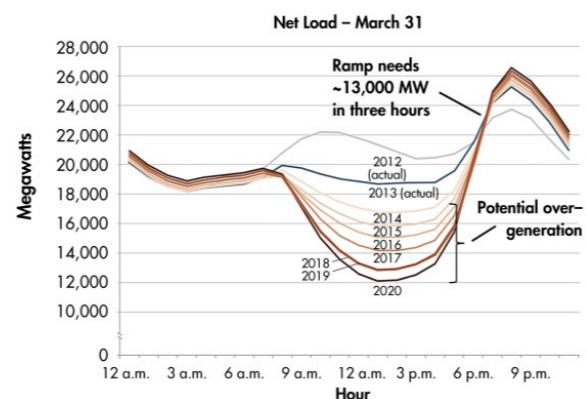

Fig. A.1.2: Low Net-Load shifts from night-time to mid-day due solar-power [11]

A.2 PV- and BESS Price Projections

A.2.1 PV-systems

Many researches show [8], [10], [12]–[16] that price of PV systems did decrease significantly last years. The levelized cost of energy already reached grid parity for Dutch households at the end of 2010.
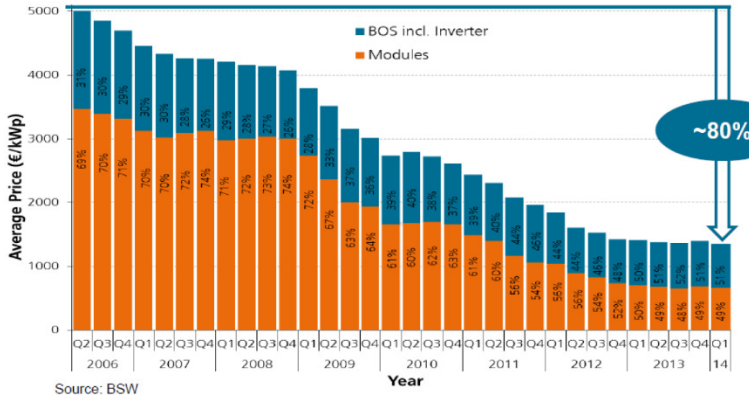

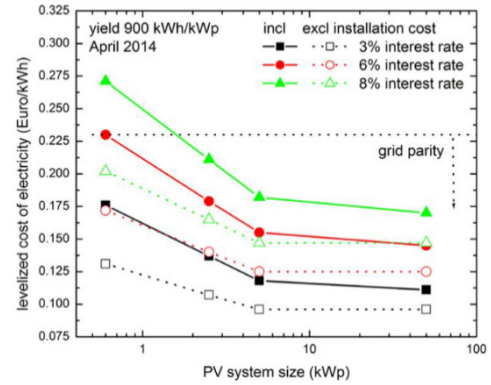Fig. A.2.1: Recent price reduction of PV rooftop system (Germany) [12]   Fig. A.2.2: Dutch: PV generation costs 2014

In the future the price of German solar power will reach values of 4-6ct in 2025 and 2-4 ct/kWh in 2050. It leads into a higher renewable share, and even lower energy costs than fossil powered plants. The mentioned growth will affect the effectiveness of the grid on all levels [17]. This future problem is partly why this research has been established.

A.2.2 BESS

'Energy storage applications in the power system aim to deliver short-term power for power quality, voltage support and frequency support and to supply energy over a longer period for renewable generation smoothing, electrical energy time shifting and end user energy management [18]'.

Integration of electrical storage at buildings is at the moment not economical beneficial, but it is expected that this will rapidly change in the future [19]–[21], [16].

Fig. A.2.3: Blended battery price projections [16]   Fig.A.2.4: IEA Rough cost projections for li-ion EES [15]

Using an ESS is a new-method (for this sector) for servicing the electrical grid during grid-support activities from the demand-side; it is more occasionally applied for maximizing self-consumption of local produced renewable energy and as a back-up service. Integration of ESSs for DSM in the building sector is currently

not a closed business case due battery costs and lack of price incentives of the utility, but it is expected that this will rapidly change in the future. ESSs could become economical feasible in the near future due scaled production and high R&D investments. These projections are often described in research papers [19], [20], in a market review of the Deutsche bank (2015) [16], and in influential news journals, as the BBC [21]. Here [21] is stated that storage would become a booming business and it estimates that 'rather than extra billing consumers to invest in the infrastructure there would be looking at significantly lower investment costs if smart grids and energy storage were fully adopted'.

The Deutsche Bank [16] gives a price indication based on the following assumption: that the incremental cost of storage will decrease from ~14ct/kWh today (2015) to ~2ct/kWh within the next 5 years. It states that when overall system cost decrease is considered, includes PV + components + ESS, it would be a clear financial choice to invest in ESS in mature solar markets in the future. The storage could be integrated to prevent peak demand based charges. Same price drop of PV-systems is going to happen with ESS, due mass adaption and R&D investments. Dependent on the rate of mass production and R&D investments, the expectation is that the Life Cycle Costs (LCC) of decentralized storage systems based on Li-ion technology will decrease to values of 5 to 10ct/kWh in 10 to 20 years [19].

Benefits and applications with PV and ESS according the Deutsche Bank [19]:

- Grid instability by current growth of renewables due intermittent spikes/or through in power generation and voltage. In case of California 2020, where 33% of energy is achieved by renewables. **Batteries** could shave the peak demand at moments that nighttime falls.
- Less suffering of increasing electricity prices, less dependency

- Shift towards Distributed Generation(DG)
- Back-up power during grid outages
- Cutting peak-demand charges, now and in the future
- Providing peak capacity to the grid
- Providing frequency and voltage regulation and improving relationship between DG producer and utility with Smart-Grid implementation

B Smart – Grid: Demand Side Management

B.1 Smart-Grid

The smart-grid is a new concept for power system operation control and (trade) market design, taken active customers and different types of generation sources into account. It provides two-way communication and power flow. The traditional consumers are transitioning into prosumers due the on-site renewable power generators as PV-power. Where traditionally the power flows from top to bottom, now it is becoming bi-directional. Figure B.1.1. show a representation of this new multi directional energy and data flow.
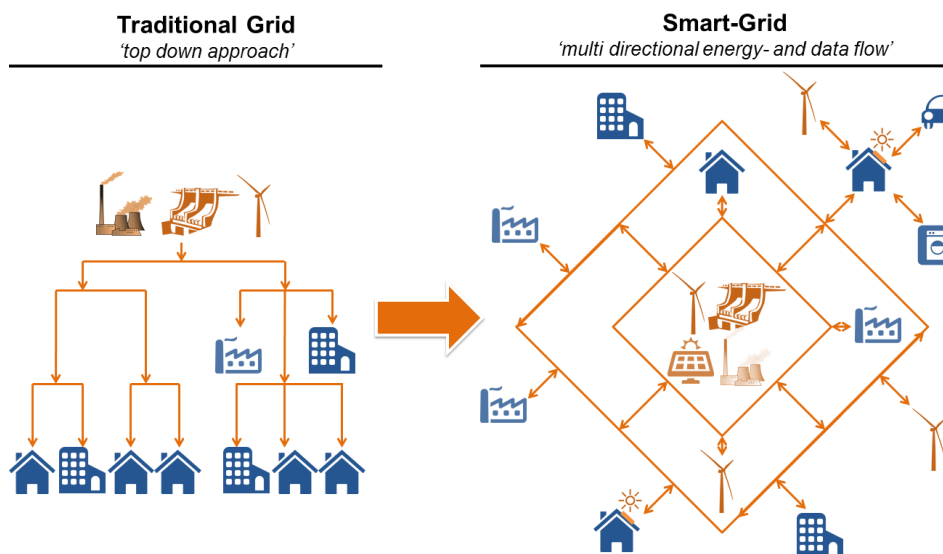

Fig. B.1.1: From a traditional grid towards a smart-grid (self-made)

Next figure show the evolutionary process of the electricity grids, where the right part is the future grid. Where the focus in this research is on the commercial customer.
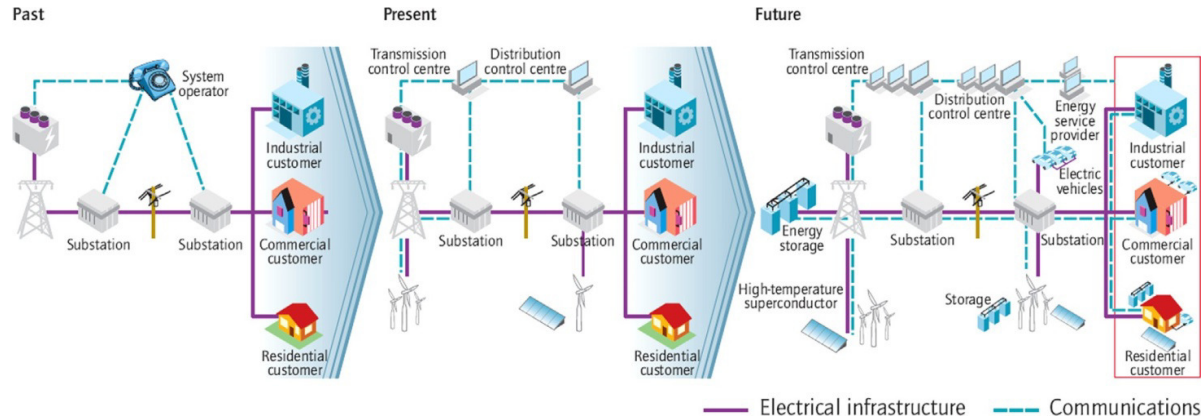

Fig. B.1.2: The evolutionary process of smart grids [18]

In the present situation: demand drives generation, while in the future: generation drives demand.

Controlling these power flows can be achieved *direct* through power flow, but also *indirect* through real time pricing [22]. For both of these control methods *forecasting* is from great importance to define a strategy based on the price, available active loads and production (as wind and solar). Each of these control types can be compiled in a sub aggregator that communicates to a central aggregator connected to the Transmission System Operators (TSOs) and Distributed System Operators (DSOs). Together with other active grid participants, you can form a virtual power plant (VPP), and with this avoid the use of conventional fossil-fuelled reserve power plants. A commercial building, where the focus is on in this research, can in the future be operated as a Distributed Energy Resource (DER) with a dynamic pricing system (indirect control[22]) where forecasting will become important (load and prices). An energy balance in the grid is established with a combination of DERs, dispatchable power plants, storage systems and interconnections.

Currently Dutch commercial buildings are already charged on their highest monthly peak demand (kW), for residential buildings this tariff system does not exist (yet). In the future this peak load (increase or reduction) could be managed real time with price incentives from the utility (DSOs and/or central aggregators − VPP) which would make it more beneficial to shave these peaks. Large scale DSM services aims to achieve a stable and reliable local and national e-grid in a more environmental friendly, energy- and cost efficient way for grid operators.

The next figure shows the new utility balancing equation corresponding to our changing renewable society. All energy in the grid must be 'balanced' at 50 Hz, a higher demand than supply than the frequency will be lower f < 50 Hz, when there is more energy supply than demand than the frequency rises, f > 50 Hz.
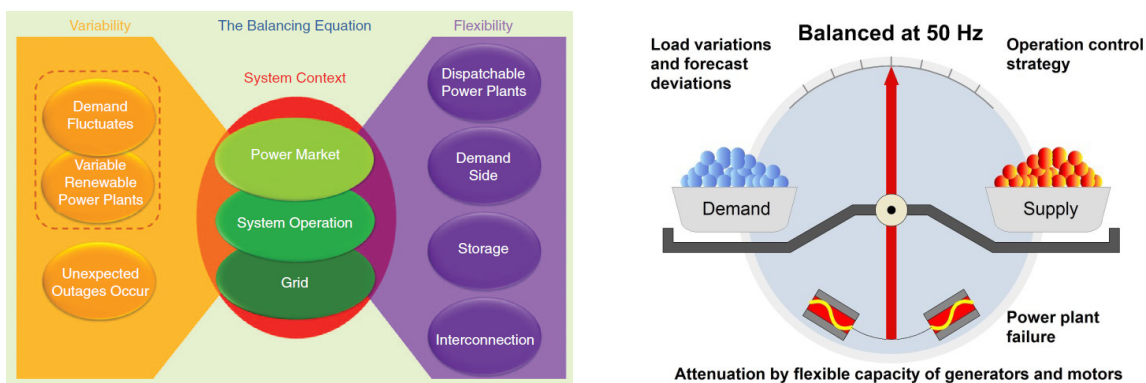
Fig. B.1.3: The balancing equation: [Hannele Holttinen et al. 2013] and [23]

B.2   DSM & DR

Demand Side Management (DSM) means to modify a load profile. Demands response; is to temporarily reduce or increase the energy demand by incentives. There is found that commercial buildings [19] have the highest potential for DSM, but it is also expected that these buildings are charged more for peaks, now and in the future, than residential buildings. For residential buildings this system does not exist yet, but for Dutch commercial buildings there is already a system where a peak demand is charged. In the future this can be dynamic with price incentives from the utility side which would make it more beneficial. At the same time, more (cost) efficient for the grid operators to stabilize the national- and local grid by the demand side.

B.2.1   Peak shaving, Load shifting & Valley filling

Demand side management strategies often written in literature are; peak clipping, load shifting & valley filling. For example commercial building operational flexibility: by dynamic usage of one or a combination of a few building processes, for example with:

- Chiller, fans and/or humidifier
- Curtailment of PV-power production
- Electrical energy storage
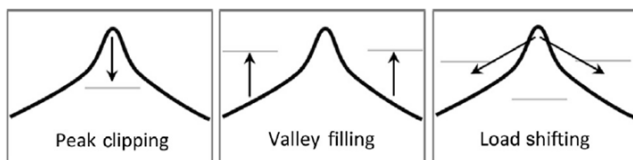
Fig.B.2.1: Demand-side management [19]
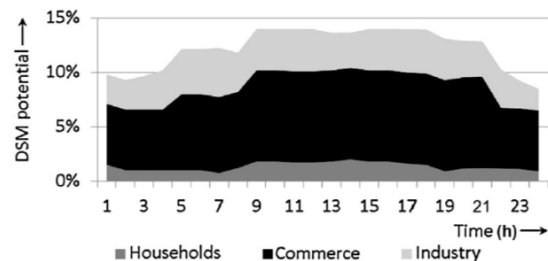
Fig. B.2.2: Potential of load shifting in relation to total hourly for different economic sectors [19]

An example of load shifting with an office building is to shift the cooling load, delay or pre-cool the building to change the load profile as desired. Using the comfort boundaries to change the load pattern over time.

Virtual power plant (VPP). One building is not enough to service the grid, but together with more buildings a virtual power plant can be formed. A central aggregrator could provide incentives to their smart-buildings, storage and RES-E and provide an aggregated energy shift, shave etc. See figure B.2.3.

Rather than upgrading the electrical power transmission/distribution network including reserve capacity (power plants), largely increase capacity of international power connections, or reimburse for curtailment methods another new approach (Smart-Grid) is from interest.
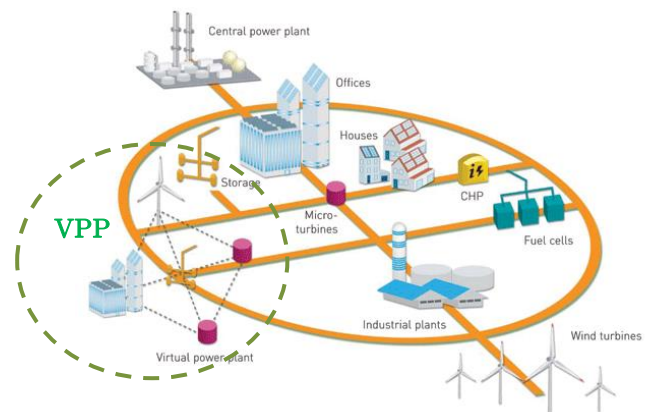

Fig. B.2.3 Virtual power plant [23]

Another fact which already occurs in Germany is that the intermittent RES-E production variations throughout the day are affecting the current open market prices in 2013 significantly [17].

The need for a mechanism to maintain this in the future is required. Rather than upgrading the electrical power transmission/distribution network including reserve capacity (power plants), largely increase capacity of international power connections, or reimburse for curtailment methods another new approach (Smart-Grid) is from interest.

B.2.2   Potential DSM strategies

In table B.2.1 load shaving and valley filling strategies are given, than grid-interaction and trade strategies and as last some other DSM and DR strategies are presented.

Table B.2.1: Potential strategies with case building loads, PV Production & battery storage

	Demand Side management − (Peak-) load shaving and valley filling
1.	**Daily peak shaving** of building load to various thresholds and battery capacities
2.	**Daily peak shaving** of building load to various thresholds, battery capacities and **active use** of building loads
3.	**Short** term **peak shaving** as a result of occasional spikes in building load
4.	**Constant load profile** shaving during work schedule and outside work schedule
5.	**Discharge** the battery during **grid high demand** period at the start of a working day and/or the end of a working day when people return home **as grid service (Providing Peak Capacity → valley filling)**

	Trade & Utility support scenarios
6.	Optimal operation strategies for battery **charge/discharge** and **energy export** to the **grid** for cases of **surplus generation** (negative net-load) in a grid connect PV (g-PV) & battery electrical storage system (BESS) (weekends & workday late afternoon/evening)
7.	Direct **exchange** and trade of electrical energy units to neighbour buildings (car workshop, dwellings etc.)
8.	**Trade** at the **wholesale market** and use **few days differences** (it is **expected** that [26] the difference will be around the **0.05 to 0.06 €/kWh** for a few hours by 2030 with various battery- capacities and price
9.	**Trade** at the **balance market**, some moments price rise to about **600 mWh/euro** [26] (volume is only very limited, e-storage will face competition quickly with other flexible energy sources)
10.	Operate in the **control and reserve power** market with **battery storage** (better perspective than spot-market, only obstacle lies in the regulations of the unbalance market [26]) **Frequency regulation**
11.	Operate in the **control and reserve power** market with **battery storage & active loads** (better perspective than spot-market, only obstacle lies in the regulations of the unbalance market[26]) **Frequency regulation**
12.	**Optimal charging & discharging strategies** under various **tariff** structures (e.g. **night tariff** structure → with variable- battery cycle prices and night tariffs)

	Other Demand Response / DSM strategies
13.	**Active** us of loads (DR or DSM): **fans**, **chiller**, **humidifier**, **plug-loads** (e.g. laptop battery), and **lightning** for **peak shaving, valley filling or load shifting** to stay below a certain contracted power threshold of the grid and/or to balance the intermittent behavior (spikes) of the PV-production
14.	**Active** use of loads: **fans**, **chiller**, **humidifier**, **plug-loads** (e.g. laptop battery), and **lightning** for **peak shaving, valley filling or load shifting** with **price incentives** from the grid side
15.	**Emotional arguments,** the wiling to improve the local, national and international energy management, **for better efficiency** and **easier** implementation of **intermittent RES-E.**

B.3   Price of electricity

2015 use tariff is as following, ex. vat:

Transportation services:

Variable transportation price is:	€ 0.00083 per kWh
Contracted power costs:	€22.21 kW
Actual peak power flow month:	€1.44kW per month

Energy supplier:

Energy tariff peak:	€ 0.0763 per kWh
Energy tariff off-peak:	€ 0.0441 per kWh
Energy tax Zone 1: $0 − 10.000$kWh	€ 0.1232 per kWh
Energy tax Zone 2: $10.000 − 50.000$kWh	€ 0.0515 per kWh
Energy tax Zone 3: $50.000 − 10.000.000$ kWh	€ 0.0115 per kWh
Storage sustainable energy zone 3:	€ 0.00070 per kWh

Case building in Zone 1, 2 and 3:

Zone 3 Price per kWh $= 0.00981 + 0.0885 =$	€ 0.09751 per kWh (peak hours)
Zone 3 Price per kWh $= 0.00981 + 0.0441 =$	€ 0.06301 per kWh (off peak hours)

Production tariff is as following:

Production Energy tariff peak:	€ 0.03044 per kWh
Production Energy tariff off-peak:	€ 0.0193 per kWh
Transport tariff:	Not charged during production (surplus)
Peak hours:	$08:00 − 23:00$
Off-peak hours:	$23:00 − 08:00$ & Weekends

Table B.3.1: Transportation cost categories [Enexis, 2015]

2.1 Tarieven transportdiensten (gecontracteerd transportvermogen t/m 1.500 kW)

Transportcategorie op basis van het gecontracteerd transportvermogen	Vastrecht transport-dienst €/jaar	Gecontrac-teerd vermogen €/kW/jaar	Maximaal vermogen €/kW/ maand	Blind-verbruik €/kVArh	kWh normaal verbruik €/kWh	kWh laag verbruik €/kWh
LS (contract vermogen t/m 50 kW)	€ 18,00	€ 5,30	-	€ 0,0067	€ 0,0320	€ 0,0168
MS/LS (contract vermogen meer dan 50 kW t/m 125 kW)	€ 441,00	€ 22,21	€ 1,44	€ 0,0067	€ 0,0083	€ 0,0083
MS-D (contract vermogen meer dan 125 kW t/m 1500 kW)	€ 441,00	€ 14,39	€ 1,44	€ 0,0067	€ 0,0083	€ 0,0083

C Design

C.1 Case building

The office building of Kropman B.V. located in Breda was chosen a case building for this master thesis and overall PhD research (SG-BEMS).

C.1.1 HVAC

Table C.1.1: Kropman Breda HVAC – system

Heating	Cooling	Ventilation & pumps	Humidification
Gas fired HR-boiler Heat is supplied through a heating coil in the AHU and two radiator groups (north-east & south-west)	Electric compression chiller Cold is supplied through: 3 air-to-water after coolers (1 per group)	Central AHU, with heat recovery wheel One supply- and exhaust fan. 3 ventilation groups (north, south and drawing room) Exhaust fans restrooms	Electrical steam humidifier Supplied in AHU
Remeha: Gas 210 ECO PRO High efficiency boiler Low NO$_x$	Carrier 30RBS-060 Max E$_{power}$ 27.8kW Released T$_e$: 18 °C Switched off T$_e$: 16 °C Two cooling stages 500L buffer tank	Holland heating AHU Operates according the building operation schedule (table 3.1.1) Night ventilation: 23:00 – 06:00 T$_e$: 10 °C and Ti: 22 °C Delta T is more than 2°C Pumps PI(D) controlled	VAPAC VP30 Operates when the outdoor temperature is below the 4 °C (before 15°C) and vapour mixing ratio is below the 6.0 g/kg (since November 2015 – before 8.0 g/kg)

C.2 Design method: Kesselring-S diagram
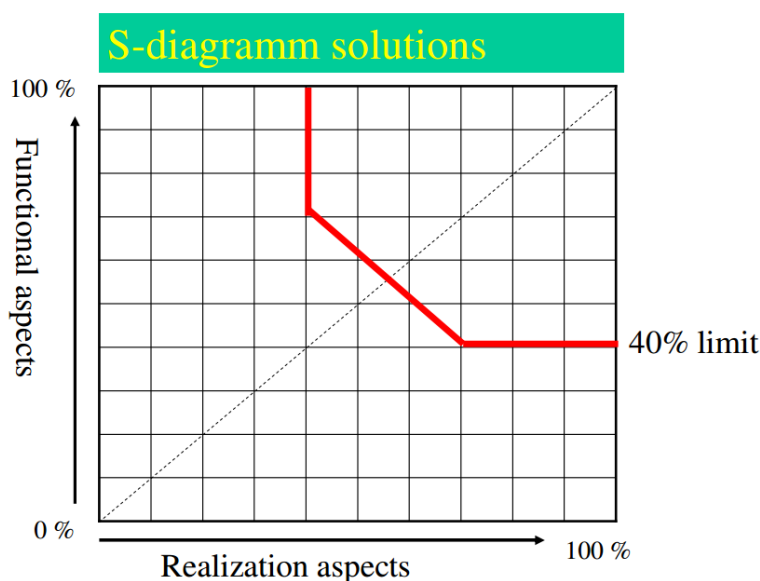
Fig: C.2.1: Functional and realization aspects in Kesselring-S diagram [27]

C.2.1 Assessment criteria: hybrid system variants

Functionality aspects:

Energetic performance Battery part
Is the efficiency of charging and discharging the battery using the internal or external configured charge-controllers and power of the AC-grid. Higher efficiency results in a better score.

Energetic performance PV part
Is the efficiency of the DC to AC conversion system, which includes maximum power point tracker(s) (panel-level in cases with an optimizer) and a DC/AC inverter.

Power – Grid support activity

Includes the available power flexibility for grid support using connected batteries. For example a single-phase all-in-one market ready bidirectional-inverter, has a peak capacity of 5kW (*Power-router) and cases of active PV-production, battery grid support is limited (scores worse). High power capacity is required in relation to comfort-based load clipping as described in the research requirements chapter 2.

Energy – Grid support activity

Includes available battery technologies in relation with inverter/charge-controllers maximum possible battery capacity and configurable technologies for energy-support.

Self-consumption PV

This score includes the efficiency and ability of self-consumption of PV-production surpluses or negative net-loads. One of the research requirements is optimize self-consumption of on-site produced renewable energy.

Control

The Insiteview Building Management System will be used for controlling the system. Therefore, the system must be capable of communicating over Modbus. Higher scores can be given when control system is not manufacture limited and future adaptions can be made.

Monitoring

Since it is a research facility, monitoring is from great importance. Higher scores are given when most variables are measured: for example, PV-panel I-V curves.

Realization aspects:

Investment costs

Only includes estimated investment costs and no life-cycle costs

Flexibility

Flexibility to adapt the system in the future, for research or commercially. For example changing a few PV-panel technologies for PV-cell tests (without compromising on the total efficiency) or another battery chemistry.

Safety & Construction

PV-systems in a string operate at a high voltage. Systems with safe voltages scores higher (for example PV-system with optimizers; safety voltage of 1VDC per panel/optimizer)

C.2.2 Assessment criteria: battery technologies

Functionality scores:

Energy density
Wh/kg and Wh/l

Power density
W/kg and W/l

Cycle efficiency

Battery chemistries lose energy (exothermic and endothermic process) during charging and discharging. For different chemistries, cycle efficiencies are compared. Higher cycle efficiency gives a better the score.

Life cycle (cycles)

The number of cycles. A higher number of cycles usually provides a longer life cycle time.

Charge rate / power capacity

Possible charge and discharge rates are dependent on the battery chemistry. LEAD-AGM technology could provide more power than LEAD-GEL with the same energy capacity.

Non-operation loss

When the battery is not used, it loses some of its energy, a lower loss implies to a higher score.

Charge control / response
There are situation that current rates direction of the current are changed shortly after each. The battery should facilitate that.

Realization scores:

Investment costs
Initial costs of battery technology

Sustainability & Recycling
Sustainability and availability of battery materials and ability to recycle the battery.

(fire-) Safety
Required ventilation, explosive danger and flammability.

Commercial business benefit
Commercial collaborates whom participating in the project, special relation, and provides continuous support have a higher realization score.

C.3 Background information design solutions

C.3.1 PV-technologies

To convert the solar-energy into an electric current different types of solar cells are available [28]:

Crystalline Silicon:
Is the most applied solar cell material in the solar industry. There are two types available; monocrystalline cells and polycrystalline. First cell is cut from single crystals of high purity electronics grade silicon. Second, easier to manufacture and therefore cheaper cell, is made with a cut from a block of crystals or less pure, so called solar grade silicon. Monocrystalline cells can reach an efficiency of 25% at its best, where polycrystalline typically is about 16% efficient and lower due the impurities.

Poly-Crystalline Solar Cell   Mono-Crystalline Solar Cell
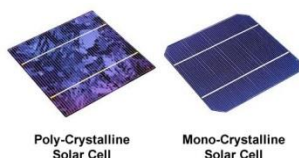
Amorphous Silicon
Appears like a solid but has no regular crystal lattice structure, for example glass. It is often used in electronic calculators etc. Typical cell efficiencies range from 5% to 10%. Manufacturing yield is still a problem and the cells suffer from degradation when exposed to the sun.

Thin Film Silicon
Made by depositing the active PV material, as amorphous silicon (or other semiconductor) onto a glass or other substrate together with the necessary current collecting contact. Efficiencies of 11% to 14% can be reached with this cell type. The construction is fairly easy and less costly than earlier examples. There are also flexible cells on polymer substrates made by Copper Indium Gallium Selenide as active material reaching efficiencies of 10%.

Organic PV
Uses organic semi-conductors in the construction of PV cells. Manufacturing requires way less energy than with crystalline semi-conductors. The material can be printed on a flexible films, low costs and high volume. Conversion efficiency is about 12% maximum. Relative new material, R&D started in 2001 (Best research cell-efficiencies, appendix D)

Multi-Layer cells
The highest conversion efficiencies are currently reached by using multiple layers of differing semiconductor materials optimizes for different wavelength, in a single device. Currently the highest found efficiency is about 45% for a three junction cell.

Exotic materials
Developed to provide particular characteristics to optimize solar cells for specific applications. For example; using Gallium Arsenide to capture high energy photons (ultra violet radiation), high temperature operation, which is used in the military and aerospace sector. Materials can be 100 times as expensive as crystalline solutions. Others can be used for low energy photons as (Indium Nitiride).

Electrochemical
Dye Sensitised Solar Cells (DSSC), relative new, uses Titanium dioxide with a liquid electrolyte. Efficiencies ranging between the 7% and 10%.

C.3.2 Conversion system solution 1, 2 and 3

Table C.3.1: Comparison of PV-system solutions [14]

	Type	*Max. DC power*	*Price excl. vat (Jan. 2014)*	*EU efficiency*	*Standard warranty*
Solution 1 String inverter	SMA − STP15000-TL	15340 W	**0.17 − 0.25 €/Wp**	97.8%	5 years
Solution 2 micro-inverters	Enphase − M250	250	**0.61 €/Wp**	96.5%	25 years
Solution 3 String inverter with optimizers	SolarEdge − SE15k Optimizers	17600 W 300 W	0.10 − 0.12 €/Wp 0.11 €/Wp **Total 0.21 €/Wp**	97.7% inverter 99.1% optimizer	12 years 25 years (optimizers)

[1]A panel with integrated optimizer costs €210.74 (J&M solar) and without €176,86 = € 33.88 for an optimizer

When only the conversion system is taken into account the the first solution may be the cheapest. However, when taking life cycle costs into account than the 3rd solution might be a better solution due the panel level optimization (higher yield during complete lifepsan) and longer warranty. The second PV-system solution require more labour costs, because each optimizer is installed on-site seperatly. More information about the design solutions is provided after the system variant assessment (next page).

C.3.3 Inverter [29]

For each inverter, DC/DC or central AC/DC an operating voltage window exists. It is recommended that the MPPT voltage window matches with the normal operation window of the PV-panels in a string. A normal PV panel generates around the 30VDC. When the PV-string operational voltage is outside the MPPT-window, the inverter or optimizer might nog operate or the solar power might be greatly reduced. In an abnormal sized situation where the panel voltage exceeds the maximum allowed value this could damage the inverter. Care must be taken on module temperature: during sunny periods (cells become warm) PV-module voltage reduces and shall never fall below the minimum operating voltage of the inverter. For calculations a maximum effective temperature of 70°C shall be used. At the other hand the open circuit voltage of a PV-panel, during a cold period

Fig.C.3.1: inverter price as a function of the required DC input power [14] *Increasing the inverter capapcity directly relates into lower PV-capacity costs*

should always be below the maximum allowable voltage of the inverter. Assuming that the maximum allowable voltage of the inverter is 600V, and the Voc at 10C° is $37.73 + (37.73*(15*0.33))/100 = 39.6$ V_{oc}, which implies a string maximum of 600 / 39.6 = 15 panels.

C.3.4 BESS-technologies

In this paragraph battery technologies are evaluated, in figure C.3.2 as distinction is made between different storage mediums.
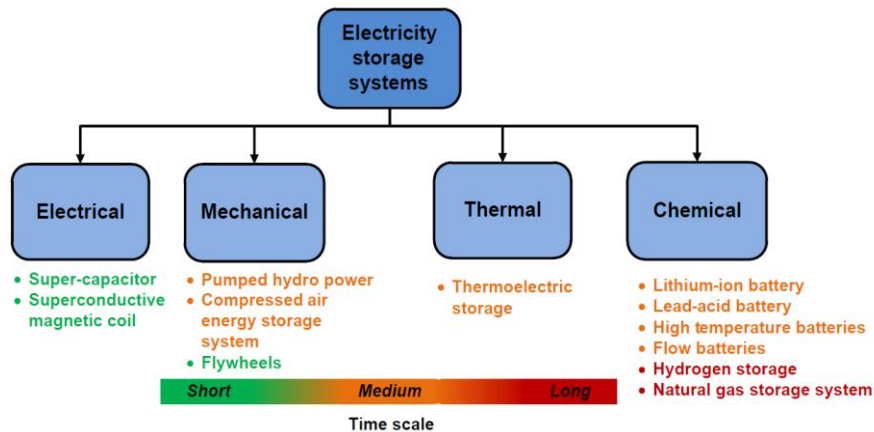
Fig. C.3.2: Electrical storage systems [19]

In this thesis the focus is on chemical energy storage, since this storage technology is can be implemented in a decentralized ESS. The definition already explains the working principle of a chemical battery, namely through a chemical reaction. Each battery chemistry has its own advantages and drawbacks and therefore there is no ideal battery for each purpose. The following simple cell can be used as indication for the chemical reaction and electrical current flow for a battery cell.
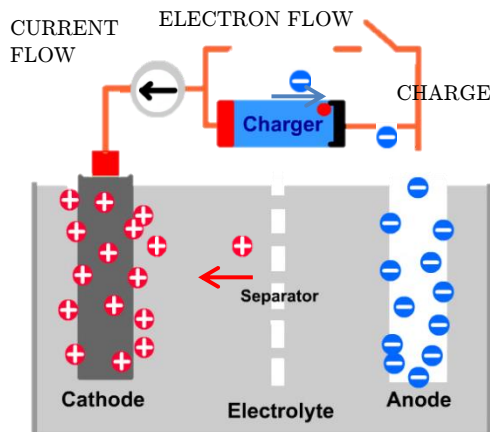
Fig. C.3.3: Simple battery chemistry, charging process (almost full) modified from: [30]
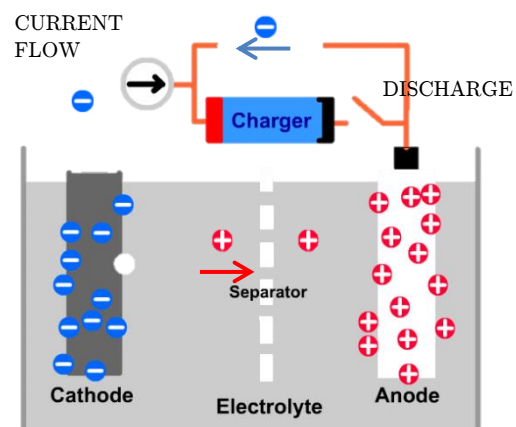
Fig. C.3.4: Simple battery chemistry, discharging process (almost empty) modified from: [30]

Each energy cell consist of at least 3 and often 4 components [30]:

1. The anode: The anode is the negative pole of an energy cell, it gives up electrons to the external circuit and is oxidized during discharge. Discharge: Electrons flow from negative to positive pole and current flows from positive to negative pole. Charge: the opposite. Common used materials in order of relative electrode potentials: Lithium, Zinc, Nickel, Lead, Hydrogen.
2. The Cathode: The cathode is the positive pole of an energy cell, is the oxidizing electrode. It accepts the electrons from the anode. *The cathodic process is the reduction of the oxidizing agent (oxide) to leave the metal.* Common used materials in order of relative electrode potentials: Iron-Phosphate (often used; with Lithium as anode), metallic oxide, sulfide oxide, oxygen.
3. The electrolyte: it transfers the ions between the anode and cathode, it is a non-conductor of electrons to prevent self-discharge of the cell.
4. The separator: electrically isolated the positive and negative electrodes

C.3.5 Design variants

Table C.3.2: System performance design considerations

	System 1: Hybrid all-in-one [1]	System 2: PV-modules connected to Charge controller and separate Bi-Inv [2]	System 3: two independently operating systems; one for ES and one for PV [3]
1 / 3Phase system	Single phase 3 phase → 3 inverters	Single phase 3 phase → 3 inverters	1 or 3 Phase
Nominal power	3,7 – 5,0 kW	2.3 – 6.8 kW: Modular up to 100kW	'Unlimited '-> industrial solution
Nominal voltage	24VDC (lead) / 48VDC (Li-ion)	48VDC (Lead/Li-ion/ custom)	600VDC (programmable PLC)
Charge-controller (CC)	≈ 4,0 – 5,5 kW DC/DC	2,4 – 5,0 kW 97,5 – 98,1% DC/DC	23 kVA AC/DC
Bi-directional inverter		92 – 95,8%	98%
System efficiency surplus of renewable energy → P'PV→Batt→AC	**93%**	**90 – 93,9%**	**93,2%** (=0,97*0,98*0,98) η *DC/AC PV = 97%*
System efficiency grid service (peak shaving)	**93%**	**95.8% (bi-inv)* 98% (CC)= 93.9**	**98%** *with transformer for AC voltage reduction =* **93.1%** *(chapter 3)*
Description:	Ideal for optimizing self-consumption. Algorithms programmable. Single phase solution, developed for household sector. Limited battery types (li-ion / lead) possible and only low (≤48VDC) voltages.	Ideal for optimizing self-consumption and some pre-programmed SG commands. Suitable for lead and li-ion batteries, but also custom programmed. Only in single phase configuration, for 3 phase, there are 3 bi-inverters required.	Operate independently → PV performs at maximum efficiency/capacity, and battery can still be used for peak shaving (for example). Similar efficiency for self-consumption. 100% programmable and monitoring possibilities No direct DC charging of PV-production surplus.

1. Power-router
2. Schneider-XW series / Outback solar / Selectronic / SMA Sunny Island
3. SolarEdge PV-system / KEB F5 bi-directional inverter

The XW (+) inverter can operate with flooded, AGM, GEL, LiON and custom batteries at a nominal voltage of 48 VDC. The grid-tie system only converts DC PV-power to AC. The hybrid inverter/chargers can operate bi-directional, it can invert the power from the charge controllers (PV-arrays)/ battery (DC-side) to AC, but it can also charge the batteries with AC(to DC) power from the grid. DC-power from the PV arrays is DC/DC regulated to a nominal charge voltage and therefore directly be used to charge the batteries directly at moments of a surplus in PV-power.

Table C.3.3: Battery offers

		euro
Intercel **24 2V OPzV lead-acid batteries**	24 x 12 OPzV (~1500Ah) Rack with interconnectors	€ 11.952 € 349
	Total:	€ 12.301
	24 x 16 OPzV (~2187 Ah) Rack with interconnectors	€ 19.332 € 349
	Total:	€ 19.681
Eu.Exide Sonnenschein A 600 GEL batteries (GNB) 3000+ cycles at 60% of DoD (C10) Completely recyclable	24 x A600 solar GEL **2613 Ah** (C120) (assumed a battery capacity of 52.5 kWh discharged in 4.5 hour with a rate of 16.5 kW) 1688 kg/m² total weight 3840 kg Rack with interconnector *Optional mounting* *Required ventilation capacity according EN 50272-2* *19.44 m3/h cross section of inlet/outlet 544.32cm² (23.3 x 23.3cm)*	€ 17.495 € 447 € 1.434
	Total 2613Ah:	€ 17.942 6.69 €/Ah
	24 x A600 solar GEL **1959 Ah** (C120) (assuming a battery capacity of 32 kWh and discharged in 22hours with a rate of 3.7 kW) **C10 = 1593Ah = 40 kWh** @ DoD **0.7** (**46kWh** @ DoD **0.8**) / charg eff. 0.8 / temp corr. 0.97 1791 kg/m² total weight 2760 kg Rack with interconnectors *Optional mounting* *Required ventilation capacity according EN 50272-2* *14.58 m3/h cross section of inlet/outlet 408.3cm² (20.2 x 20.2cm)*	€ 12.457 € 248 € 1.434
	Total 1959Ah (C120):	€ 12.705 6.49 €/Ah
	24 x A600 solar GEL **1413 Ah** (C120) (assuming a battery capacity of 32 kWh and discharged in 14hours with a rate of 3.7 kW) 1254 kg/m² total weight 1920 kg Rack with interconnectors *Optional mounting* *Required ventilation capacity according EN 50272-2* *10.9 m3/h cross section of inlet/outlet305.1cm² (17 x 17cm)*	€ 9.840 € 248 € 990
	Total 1413Ah:	€ 10.088 7.14 €/Ah
Li-ion **Sonnenbatterie ECO** **5000 + cycles at 80% DoD**	30 kWh usable includes inverter	€ 35.000 to € 38.000
NaS **Aquion Energy** 100% DoD possible 3000+ cycles (5.000+ is demonstrated) Non-toxic and inflammable	2 Aquion Energy M100-L082 (612 Ah/C20) 27.8 kWh = 55.6 kWh (C20) 41.4 kWh (C8) Max current = 144A	€ 22.150
Nilar - NiMH	1.2 kWh (10Ah − 120VDC)	Confidential

D PV + BESS model

D.1 Complete model overview
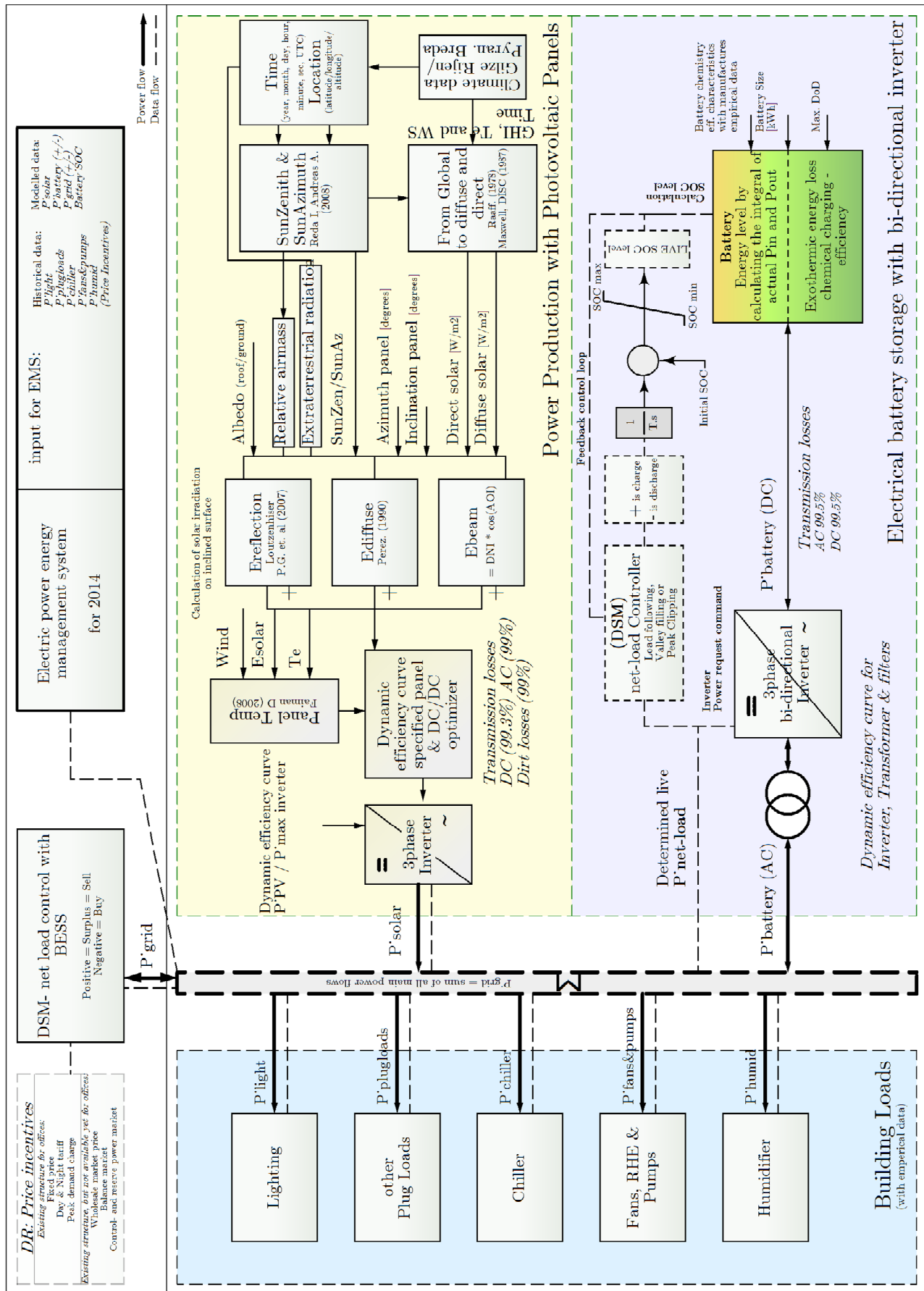
D.2 Photovoltaic-generation model

To historically simulate the behaviour of a Photovoltaic-facility a simulation model is made. The theory and literature behind this model is explained in this paragraph.

D.2.1 Renewable source – Sun

PV-panels use the sun as source of energy. The insolation level on a plane of array is dependent on several factors:

1. Solar irradiation on specific **location** and moment (time)
2. Orientation, inclination and shading
3. Reflections

Insolation values are usually measured with a pyranometer, in the Netherlands the Dutch Meteorological weather institute (KNMI) measure the global horizontal irradiance (GHI) at all weather stations. The GHI is the total radiation on a horizontal surface and contains a diffuse and direct radiation component:

(D.1)

$$E_{GHI} = E_{diffuse} + E_{direct} \quad [\frac{W}{m^2}]$$

Where:

E_{GHI} = Global horizontal irradiance [kWh/m^2]

Meteorological weather station located in 'de Bilt' is the major station of the Netherlands; this station is representative for the Dutch climate. Figure D.2.2 show the hours of sun throughout the year for a horizontal surface, two southern inclination angles in the Netherlands. A southern oriented inclination of 36° provides the highest yearly solar energy. The GHI in the Bilt is 983 kWh/m^2 per year on average (1981 − 2010) and for the case building nearest station slightly more 1013 kWh/m^2 (Gilze − Rijen - Latitude: 51.56° Longitude: 4.933°). In the Netherlands a large fraction of the GHI is diffuse (due relatively cloudy weather), instead of the Sahara, where almost all horizontal insolation is direct (fig D.2.1).
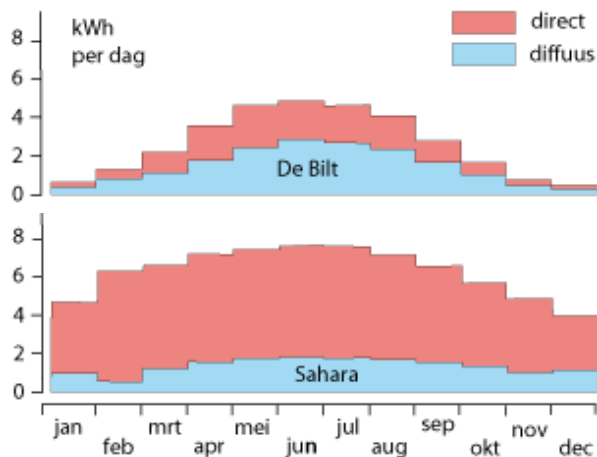
Fig. D.2.1 de Bilt direct and diffuse horizontal radiation [31]
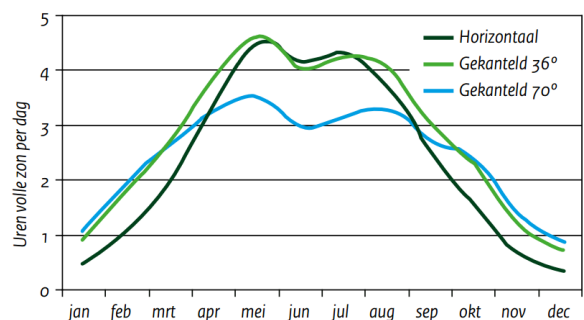
Fig. D.2.2 PV- yield [2]

D.2.2 Irradiance on a Plan of array (E_{POA})

Hourly measurements of Dutch KNMI weather stations can be downloaded from their website, for the solar model wind speed, outdoor temperature and GHI are required. Care must be taken when using this data, since the time series are not adjusted for daylight savings and time zones (Coordinated Universal Time or UTC = 0). The irradiation on an inclined plane is different compared to horizontal placed plane, this is caused by the fact that the angle of incidence of the direct beam (sun) is more perpendicular to the sun in Northern Latitudes. Therefore a solar model must simulate the angle of incidence of a plane of array as input for the irradiance model.

First some definitions for the sun position are given in figure D.2.3 and 2.2.10, <u>altitude</u> is often called <u>elevation</u> angle. Azimuth angle is measured clockwise from north. Zenith angle is measured from vertical. The elevation is measured from horizontal.
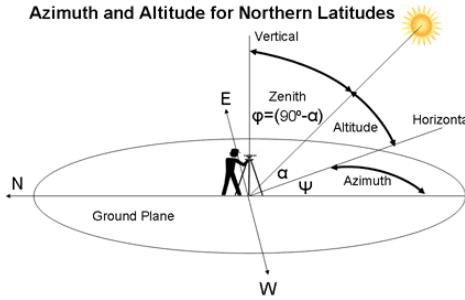
Fig.D.2.3: Sun position [28]
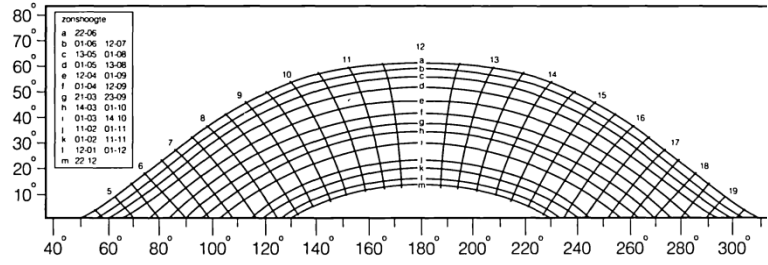
Fig.D.2.4: Sun elevation / altitude throughout the year

To find the irradiance on a POA, the incidence angle due the sun's position for a specific time and location must be calculated and modelled.

Dynamic Sun Zenith & Sun Azimuth model [32]
This model simulates the exact track of the sun for a given moment throughout a year. According the article the best uncertainty achieved in most other articles is greater than ±0.01/ in calculating the solar zenith and azimuth angles. For some, the algorithm is only valid for a limited number of years. This algorithm is able to calculate the solar zenith and azimuth angles in the period from the year -2000 to 6000, with uncertainties of ±0.0003. The model requires date, time, location (latitude/longitude), site pressure, outdoor temperature and UTC-offset as input values. For a detailed description of the modelling steps see the literature [32].

Relative Air Mass
The air mass characterizes the effect of a clear atmosphere on the sunlight and is equal to the relative length of the direct irradiation in the atmosphere. On the equator, an AM of 1.0 is possible; in this case the relative length is shorter and therefore higher insolation values can be expected. AM 1.5 is used as test condition (STC) on a clear day with total irradiance of 1000 W/m².

(D.2)
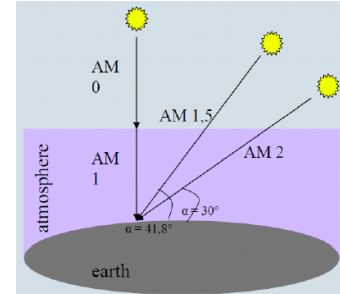
Fig. D.2.5: Air Mass

$$AM = \frac{1}{\sin(\theta_{elev})} \; or \; \frac{1}{\cos\theta_{zen}}$$

This parameter is required as input for the calculation of the irradiation on a specific inclined surface.

Extra-terrestrial irradiation
Another required parameter to calculate the irradiation on an inclined surface is the extra-terrestrial irradiation. This is the radiation value at the edge of the earth's atmosphere: yearly average 1367 W/m2.

(D.3)

$$df = \frac{2\pi * day \, of \, year}{365} \; [-]$$

(D.4)

$$R_{sun \, earth} = 1.00011 + 0.034221 * \cos(Df) + 0.00128 * \sin(Df) + 0.000719 * \cos(2 * Df) + 0.000077 * \sin(2 * Df)$$

(D.5)

$$E_{extrater} = 1367 * R_{sun \, earth} \quad [\frac{W}{m^2}]$$

Where:

Df = day factor

E_{extra} = Extraterrestrial irradiation

$R_{sun\,earth}$ = the orbit factor of the earth sun

D.2.3   Irradiation on a specific inclined surface

First step is to separate the hourly meteorological data of GHI into a direct and diffuse component. In Hambase [33] a model called: Raaf [34] is applied, however literature [35] reveals that DISC [36] (Direct Insolation Simulation Code) is the best model (with lowest BIAS error). It has the smallest Mean Bias Error (MBE: 25 W/m^2) and Root Mean Squared Error (RMSE: 85 W/m^2) under all conditions. Both estimation methods are evaluated [34] [36] (Direct Insolation Simulation Code).
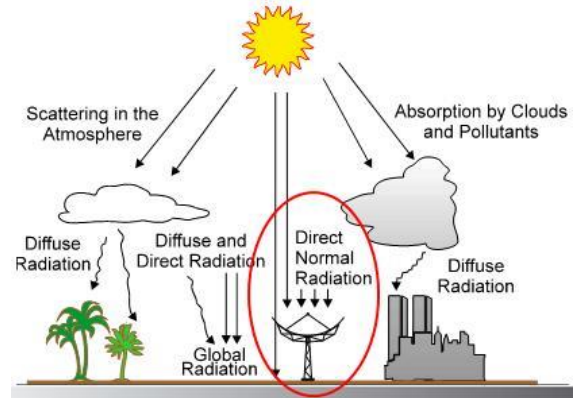
Fig. D.2.6: Direct Normal Irradiance   *www.soda-is.com*

The DISC model [36] uses <u>hourly</u> measured GHI, sun zenith angle, day of year, and average site atmospheric pressure to separate the GHI in direct and diffuse irradiation. It uses the empirical relationships between the direct normal transmittance (K_n), global horizontal transmittance (K_t) and direct clearness indices to estimate the direct beam component (DNI). First it determines K_t as the ratio of measured GHI to the extra-terrestrial radiation, E_{extra}, (is the radiation on the edge of the earth's atmosphere without dissipation through the air, on average 1367 W/m^2 , varies between 1321 W/m^2 and 1414 W/m^2 due earth's elliptical orbit). Then it separates it in two bins, $K_t > 0.6$ and $K_t \leq 0.6$, after this the model estimates the direct normal transmittance (K_n) as a function of Air mass (AM) and global horizontal transmittance (K_t) Than the DNI can be calculated as following:

(D.6)

$$DNI = K_n * E_{extra} \quad [\frac{W}{m^2}]$$

The DNI is not for a specific angle corrected, it is used as input for the direct POA model and to calculate the diffuse horizontal irradiance.

Source of modified Matlab function: [37]

The **direct horizontal irradiance** can be calculated as following:

(D.7)

$$DHI = DNI * cos(\theta_{zen}) \quad [\frac{W}{m^2}]$$

Where:

$\theta_{zen} = Sun\ Zenith\ angle\ [°]$

The Raaf [34] **model** is applied in the building performance model: Hambase [33], it uses hourly KNMI meteorological data, for the calculation of the DNI from the GHI on a horizontal plane for a certain geographical location. Horizontal diffuse irradiation is calculated based on the relation; GHI = $E_{diffuse}$ + E_{direct}. The extra-terrestrial radiation (E_{extra}) is calculated for each KNMI measurement day. Than the ratio (G_{ratio}) of the measured GHI and the E_{extra} is calculated to find an estimation of the direct beam on a horizontal surface according the following formulas;

(D.8)

$$G_{ratio} = \frac{GHI}{E_{extra}} \ [-]$$

$$If\ G_{ratio} \geq than\ 0.8\ than\ E_{direct} = 0.86 * GHI$$

$$If\ G_{ratio} \geq than\ 0.35\ and\ <\ 0.8\ than\ E_{direct} = GHI * ((1.66 * G_{ratio}) - 0.47)$$

$$If\ G_{ratio} \geq\ than\ 0.22\ and\ <\ 0.35\ than\ E_{direct}\ =\ 6.4\ *\ (G_{ratio} - 0.22)^2$$

$$If\ G_{ratio} = <\ than\ 0.22\ than\ E_{direct}\ =\ 0$$

$$E_{diffuse}\ =\ GHI - E_{direct}\ [\frac{W}{m^2}]$$

Where:

        G_{ratio} = Ratio [-]
        GHI = Hourly Global Horizontal Irradiance [W/m^2]
        E_{extra} = Extraterrestrial Irradiation [W/m^2]
        $E_{diffuse}$ = Diffuse Horizontal Irradiance [W/m^2]
        E_{direct} = Direct Horizontal Irradiance [W/m^2]

Diffuse horizontal irradiance:
The diffuse horizontal irradiance can be calculated as following:

(D.9)

$$DHI\ =\ GHI - (DNI * \cos(\theta_{zen}))\quad [\frac{W}{m^2}]$$

Irradiance on POA / fixed PV-panel
From this point the irradiance on a specific **POA** can be estimated. It is the sum of the diffuse, direct and reflection irradiation.

(D.10)

$$\boldsymbol{E_{POA}} = E_{diffuse} + E_{direct} + E_{reflected}$$

Where:

        E_{POA} = Radiation on an inclined surface [W/m^2]
        $E_{diffuse}$ = Diffuse radiation on an inclined surface [W/m^2]
        E_{direct} = Direct radiation on an inclined surface [W/m^2]
        $E_{reflected}$ = Reflected radiation on an inclined surface [W/m^2]

Diffuse radiation on specified POA
To determine the POA diffuse component, $E_{diffuse}$, on a specific oriented/tilted surface the Perez et.al (1990) model [38] is used. It uses the array inclination and azimuth angle, diffuse horizontal irradiance, direct normal irradiance (without angle conversion), E_{extra}, Sun zenith angle, Sun Azimuth angle and the relative air mass as input values. This sky-diffuse model is only for the diffuse component and not for the DNI and ground reflected irradiance.

(D.11)

$$E_{diffuse} = DHI * (1 - F1) * \frac{(1 + \cos(\theta tilt_{array}))}{2} + F1\left(\frac{a}{b}\right) + F2\sin(\theta tilt_{array})$$

Where:
F1 and F2 = complex empirically fitted functions [38]
DHI = Diffuse horizontal Irradiance [W/m^2]
$\theta tilt_{array}$ = Array tilt angle from the horizontal [°]

    $a\ =\ max(0, cos(AOI))$

    $b\ =\ max(cos(85°), cos(\theta_{zen})$
AOI = Angle of Incidence (see DNI model)

Source of modified Matlab function: [37]

Direct normal irradiation on specified POA
The second component is the direct radiation on an inclined surface, E_{direct}. It is the cosines of the angle of incidence, AOI, (between panel and incoming sun rays) times the calculated direct irradiation as calculated with the DISC model [36].

(D.12)

$$E_{beam} = DNI * \cos(AOI)$$

$$AOI = [\cos(\theta_{zen})\cos(\theta tilt_{array}) + \sin(\theta_{zen})\sin(\theta tilt_{array})\cos(\theta_{azi} - \theta azi_{array})]$$

Where:

θ_{zen} = Solar Zenith Angle calculated with: [32]

$\theta tilt_{array}$ = array/panel tilt angle

θ_{azi} = Solar Azimuth Angle [32]

θazi_{array} = array/panel azimuth (north = 0, east = 90, south = 180, west = 270)

Ground reflection

(D.13)

Ground reflection

$$= GHI * Albedo * \left(1 - cosd(\theta tilt_{array})\right)$$
$$* 0.5 \quad \left[\frac{W}{m^2}\right]$$

Where:

GHI = Global horizontal irradiation [W/m²]

Albedo = a specific value for reflectance of surrounding materials (see fig 2.2.5) [-]

$\theta tilt_{array}$ = array/panel tilt angle

In the Netherlands a roof typically have an albedo value of around 0.2 [34].
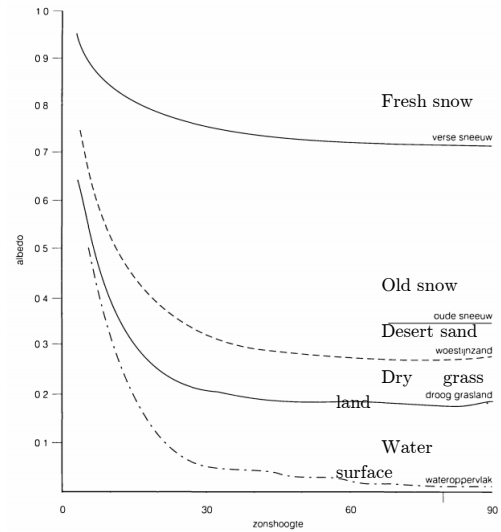
Fig. D.2.7: Typical albedo values in the Netherlands [34]

Panel Temperature estimation

The temperature of a PV-module is an important factor for estimating the conversion efficiency of the incoming irradiance on a plane or array and electrical power output. The E_{POA} is calculated according equation 2.10 and the other two required parameters: Wind Speed and outdoor temperature are (historically) measured. The module temperature can be estimated based on constant heat transfer principles according a research [39]. In this research a simple method is proposed with a maximum uncertainty of ffi2 °C. In the same research is stated that this only represents a maximum error for the estimation of the panel efficiency of 1%, since the efficiency coefficient each degree up or down is 0.5 [%/°C]. The module temperature can be simulated with the following equation:

(D.14)

$$T_{module} = T_e + \left(\frac{E_{POA}}{(U_0 + (U_1 * WS))}\right)$$

Where:

U_0 = constant heat transfer component = 25 [W/m²*K] *

U_0 = convective heat transfer component = 6.84 [W/m²*K] *

* = based on fitted experimental data of 7 crystalline silicon modules

Dynamic panel efficiency

The panel efficiency can be calculated as function of the module temperature (equation 2.14). See table 2.2.4 for these manufacture characteristics. In the model this linear relationship is used to calculate the conversion efficiency of the panel.

(D.15)

$$\eta_{panel} = \eta_{panel_{STC}} + ((T_{module} - T_{STC}) * C_{temppanel} \, [\%]$$

$$P_{PV} = E_{POA} * \eta_{panel} \, [W]$$

Where:

$\eta_{panel_{STC}}$ = Panel efficiency at STC according manufactures datasheet

T_{STC} = Panel temperature at STC normally 25°C

$C_{temppanel}$ = Temperature correction coefficient according manufactures datasheet [%/°C]

P_{PV} = is the DC produced electrical power [W]

Inverter

In this thesis a system with DC/DC optimizers and a central DC/AC inverter is evaluated. In the model the dynamic efficiency can be simplified by fitting the manufactures efficiency curve. The efficiency is calculated based on the function of DC input power divided by the nominal inverter power.

D.3 BESS – model

Electrical circuit from inverter to batteries
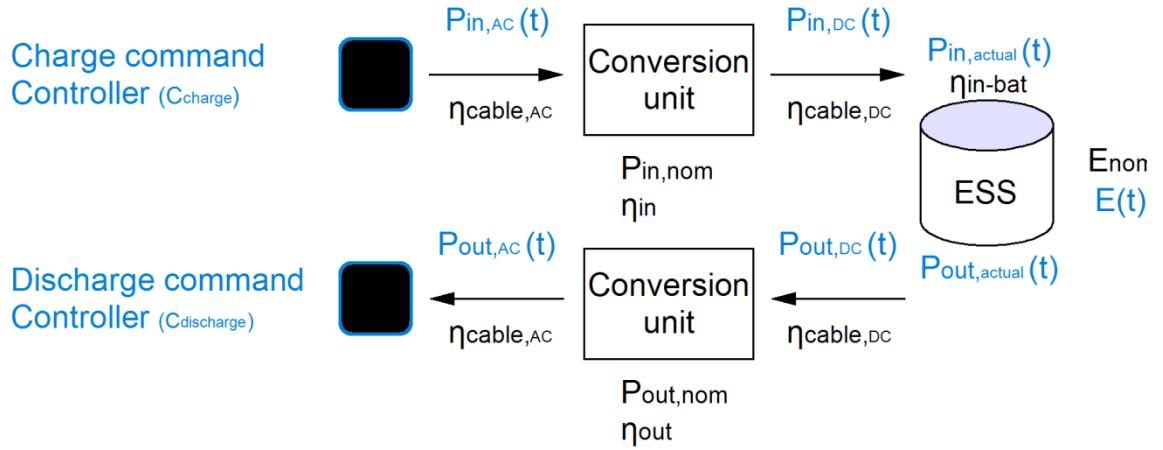
Fig. 2.3.7: Battery Electrical circuit model; modified from [40]

Where:

$P_{in,AC}(t)$ = Positive Power Request [kW] for **charging** at time t (sec)

$P_{in,DC}(t)$ = DC Power after conversion unit [kW] for **charging** at time t (sec)

$P_{in,nom}$ = Nominal power conversion unit [kW]

$P_{in,actual}(t)$ = Actual charged power in battery [kW] at time t (sec)

$P_{out,AC}(t)$ = Negative Power Request [kW] for **discharging** at time t (sec)

$P_{out,DC}(t)$ = DC Power after conversion unit [kW] for **discharging** at time t (sec)

$P_{out,nom}$ = Nominal power conversion unit [kW]

$P_{in,actual}(t)$ = Actual discharged power, battery [kW] at time t (sec)

$\eta_{cable,AC}$ = Efficiency of conversion unit during charging [%]

$\eta_{cable,DC}$ = Efficiency of conversion unit during charging [%]

η_{in} = Efficiency of conversion unit during charging [%]

η_{out} = Efficiency of conversion unit during discharging [%]

η_{in-bat} = Efficiency of internal chemical reaction due exothermic charging process [%]

E_{nom} = Nominal battery capacity [kWh]

$E(t)$ = Storage charging level (energy level) [kWh] at time t (sec)

These acronyms are used in the next equations for simulating the battery storage system.

Charge cycle

The battery charge is controlled with a positive power request; the actual power request for the conversion system is multiplied with the AC cable efficiency:

(D.16)

$$P_{in,AC}(t) = C_{charge}(t) * \eta_{cable,AC} \ [kW]$$

Where:

$\eta_{cable,AC}$ = Fixed at 99.5%

C_{charge} = AC charge command [kW]

The conversion efficiency is a function of the positive power request. This efficiency function can be derived from manufactures data of inverter, transformer and filter. It is the ratio of the AC power input and nominal power.

(D.17)

$$\eta_{in}(t) = f\left(\frac{P_{in,AC}(t)}{P_{in,nom}}\right) \ [-]$$

After the efficiency is determined, the DC charge power can be calculated by the following equation:

(D.18)

$$P_{in,dc}(t) = \eta_{in} * P_{in,AC}(t) * \eta_{cable-DC}$$

This model is developed as representation of a Nilar NiMH battery: according the manufacture there can be assumed that during charging energy is lost, due the exothermic reaction inside the battery. This loss depends on the State of Charge (battery energy level) and charging rate. During the discharging process, energy losses due the endothermic chemical reaction are negligible.

(D.19)

$$\eta_{in-bat}(t) = f(SOC(t)) \ [-]$$

Where:

SOC(t) = State of Charge interval [%]

(D.20)

$$SOC(t) = \frac{E(t)}{E_{nom}} \ [-]$$

As last the actual charged power loaded in the battery can be calculated according the following equation:

(D.21)

$$P_{in,actual}(t) = \eta_{in-bat}(t) * P_{in,dc}(t) \ [kW]$$

Discharge cycle

The model uses an inverse modeling technique (find nearest value) to determine the required output power, $P_{out,actual}(t)$, based on an AC discharge power request ($C_{discharge}$). Discharging in the battery model is achieved through a negative value.

First the basic efficiency relations/calculations are given. The DC output power is determined as following:

(D.22)

$$P_{out,DC}(t) = \eta_{cable,DC} * P_{out,actual}(t) \ [kW]$$

The battery charge is controlled with a positive power request; the actual power request for the conversion system is multiplied with the AC cable efficiency:

(D.23)

$$P_{out,AC}(t) = \eta_{out} * P_{out,DC}(t) \ [kW]$$

The conversion efficiency is a function of the negative power request. This efficiency function can be estimated with manufactures efficiency/power loss information of inverter, transformer and filters.

(D.24)

$$\eta_{out}(t) = f\left(\frac{P_{out,DC}(t)}{P_{out,nom}}\right) \quad [-]$$

After these relations are known, the $P_{out,actual}(t)$ can be estimated by making a function which uses equal sized matrices in Matlab.

(D.25)

$$N = length(\eta_{out}(t)) \, [-]$$

N = number of rows in conversion efficiency function matrix

Define $P_{out,actual}(t)$ power steps with same length as efficiency function $\eta_{out}(t)$. From 0 to $P_{out,nom}$.

(D.26)

$$P_{out,actual} = 0:\left(\frac{P_{out,nom}}{N}\right):P_{out,nom}$$

Than multiply these DC steps with the total efficiency for the whole matrix length (N) to generate a matrix with the resulting $C_{discharge}$.

(D.27)

$$C_{discharge1} = P_{out,actual} * \eta_{out} * \eta_{cable,DC} * \eta_{cable,AC}$$

From this point a function can be made which searches for the nearest requested value $C_{discharge1}$ and corresponding matrix row number. With this row number the required DC-power, $P_{out,actual}$, can be estimated accurately.

(D.28)

$$find\,(row\,no.) = \min(abs(C_{discharge1} - C_{discharge})$$
$$P_{out,actual} = C_{discharge1}(row\,no.)$$

Where:

    $C_{discharge}$ = AC requested value

    $C_{discharge1}$ = AC matrix to find nearest row number (N)

Battery Energy level / SOC
The charging level of a battery can also be expressed as State Of Charge (eq. 2.x), each battery has its SOC range where the battery can operate within. Typically between a SOC of 100% and 20%. This storage level can be expressed as a function of energy level at (t-1) minus storage input and output energy during (t-1) until t (modified from: [40])

(D.29)

$$E(t) = E_{initial} + \int_{t-1}^{t} P_{in,actual}(t)dt + \int_{t-1}^{t} P_{out,actual}(t)dt$$

Where:

    $P_{out,actual}$ = negative (discharge)

    $E_{initial}$ = Initial battery Energy Level = $E(t-1)$

E PV-orientation and yield evaluation

E.1 Panel lay-out

Distance between panels:
To avoid shading on panels from other neighbouring southern facing panels a gap between the panels are recommended. In the Netherlands a tilt angle of 15° is often used on flat roofs. The SBR-standard [41] has evaluated panel gaps, to find an optimal yield in relation to the available roof space and expected energy yield. Based on that study distance between panels are determined and shown in figure E.1.1. Another design solution is an East-west configuration → an E-W configuration result in a higher energy yield per square meter roof surface. Another advantage compared to a southern oriented array is a lower peak during midday and a higher yield during the morning and late afternoon.

For facility sizing, it is important to inspect the roof construction first on strength and quality of the (flat) roof edges and bituminous layer. Also the orientation, cabling and location of inverter should be taken into account. For panel mounting there are fixed and dynamic systems in the market; move by angle, move by inclination or complete solar tracking by azimuth and inclination. Advantage of a moving panel is that it tracks the

Fig. E.1.1: Recommended panel distance, south orientation and east-west [self-made]

solar beams. A tracking system is the most beneficial in regions of high direct sun intensity, which is not the case in the Netherlands. It is more costly and requires maintenance.

E.2 Panel yield

In the first table E.1. energy yield for PV-panels facing south (173°) are presented for placement on flat roof.

Table: E.1: Panel orientation study: panels on flat roof at 173° azimuth (~south) and increased inclination angles

Inclin.	Azi.	Energy on square meter surface	Increase	Energy JAP6-260 Wp Poly-panel	Increase	Yearly Yield
0°	0°	1057 kWh	100%	238.1	100%	31694 kWh
5°	173°	1106 kWh	104.6%	254.5 kWh	106.9%	20622 kWh
10°	173°	1149 kWh	108.7%	263.8 kWh	110.8%	22160 kWh
15°	173°	1186 kWh	112.2%	265.5 kWh	111.5%	22302 kWh
20°	173°	1216 kWh	115.0%	271.8 kWh	114.2%	19026 kWh
25°	173°	1238 kWh	117.1%	276.5 kWh	116.1%	15484 kWh
30°	173°	1254 kWh	118.6%	279.8 kWh	117.5%	15669 kWh
35°	173°	1263 kWh	119.4%	287.8 kWh	120.8%	16117 kWh
40°	173°	1264 kWh	119.5%	281.9 kWh	118.4%	11840 (42pan)
45°	173°	1263 kWh	119.4%	280.7 kWh	117.9%	11789 kWh (42pan)

In the second table (E.2), east-west configuration is shown. Where can be seen that the yield is comparable with a horizontal placed panel. The advantage is that the flat roof can be fully covered with PV-panels, since there is no shadow region problem as with southern faced panels).

Table: E.2: Panel orientation study: panels on flat roof at 83 and 263 (~east/west) and at 10° inclination angle

2: Inclination	2: Azimuth	Energy on square meter surface	Increase	Energy Per JAP6-260 Wp Poly-panel	Increase	Yearly Yield
0°	0°	1057 kWh	100%	238.1 kWh	100%	31694 kWh
10°	83°	1028 kWh	97.2%	231.7 kWh	97.1%	15061 kWh
10°	263°	1070 kWh	102.8%	240.5 kWh	100.8	15633 kWh

Table: E.3: Panel orientation study: panels at 83° and 263° azimuth (˜east/west) and fixed vertical inclination angle

3: Inclination	3: Azimuth	Energy on square meter surface	Increase	Energy Per JAP6-260 Wp Poly-panel	Increase	Yearly Yield
0°	0°	1057 kWh	100%	238.1 kWh	100%	31694 kWh
90°	83°	528.4 kWh	50.0%	117.8 kWh	49.5%	8818 kWh
90°	108°	682.9 kWh	64.6%	153.1 kWh	64.3%	1990 kWh
90°	173°	898.7 kWh	85.0%	206.9 kWh	86.9%	19862 kWh
90°	198°	919 kWh	85.0%	206.2 kWh	86.6%	8042 kWh
90°	288°	507.4 kWh	48.0%	112.2 kWh	47.1%	4825 kWh
90°	353°	186.4 kWh	17.6%	39.08 kWh	16.4%	3556 kWh

E.2.1   Load duration curves of PV-capacity design variants (peak demand period)
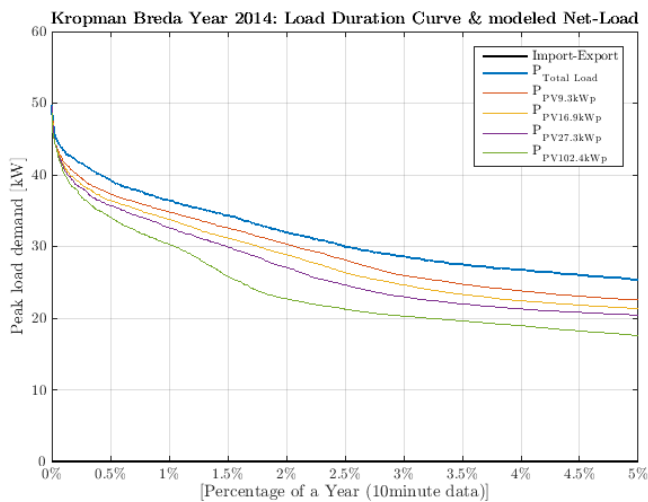
Fig. E.2.1: load duration curve 5% peak demand period
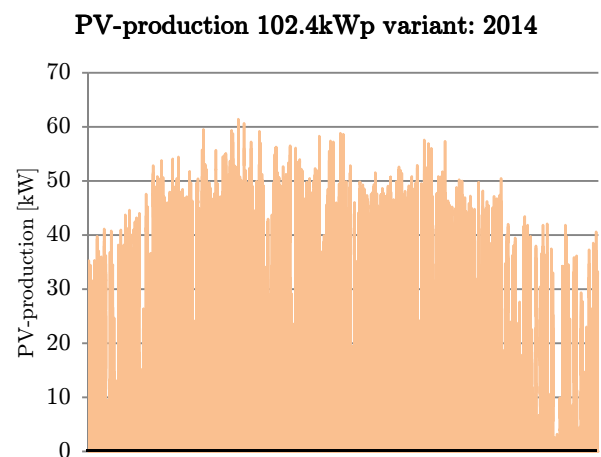
Fig. E.2.2: 2014 simulated PV-production

F Final system design

F.1   One-line-scheme Kropman Breda office
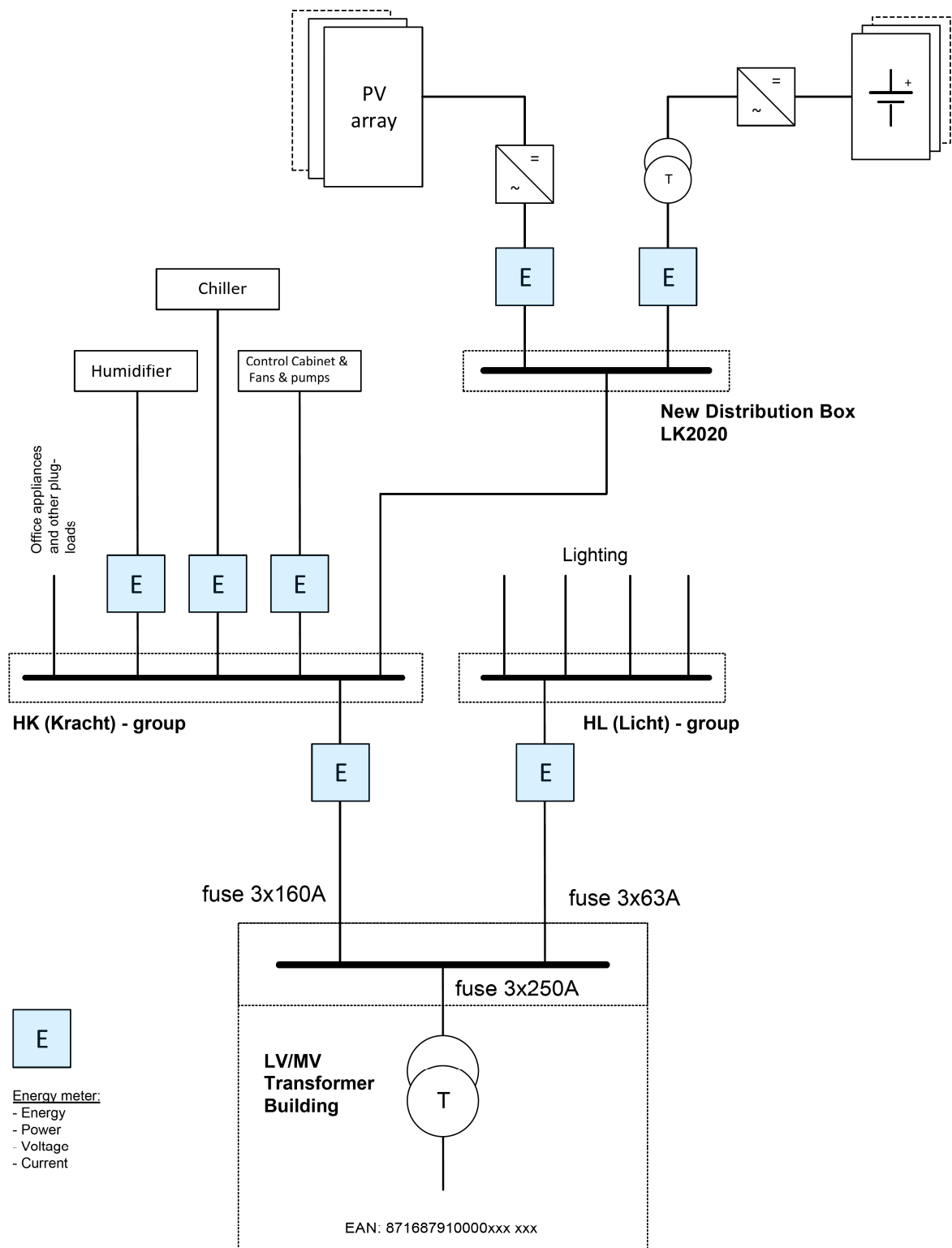
Figure F.1.1: Kropman Breda Office, electrical one line scheme [Modified from drawing W. Verhelst]

F.2 PV-system

F.2.1 Behaviour and performance PV poly-panel

Table F.2.1: Module test characteristics JA Solar - JAP6 260 Wp (these characteristics are used in PV-model)

Description:	Value:	Description:	Value:
Rated maximum Power at STC	260 [W]	Module efficiency	15.90 %
Open Circuit Voltage, Voc	37.73 [V]	Temperature coefficient of Isc	+0.062 %/°C
Maximum Power Voltage, Vmp	[V]	Temperature coefficient of Voc	-0.330 %/°C
Short Circuit Current Isc [A]	8.91 [A]	Temperature coefficient of Pmax	-0.045 %/°C
Maximum Power Current , Imp	8,45 [A]		

The panels have an integrated power-optimizer (P300), with a specific performance curve; the same for the centralized DC/AC inverter (SE15k).
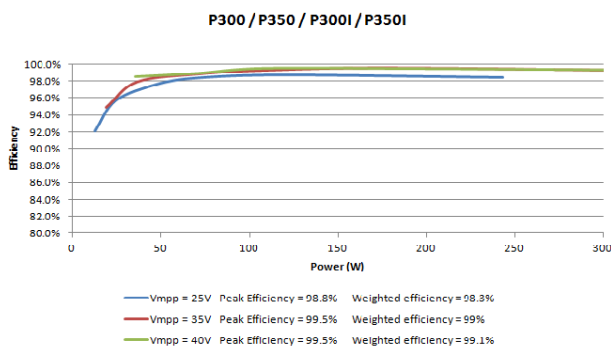
Fig. F.2.2: Efficiency curve SE-P300 DC/DC optimizers
During early morning panel starts to operate around 25 VDC (results) going to 31 VDC, according specs JAP6 panels operate at a maximum voltage power point of 30.63 V_{mp}. In the model the blue curve is used for the 5.5 to 29.7 W region and red curve is used for the rest by fitting the efficiency curve (nearest value)
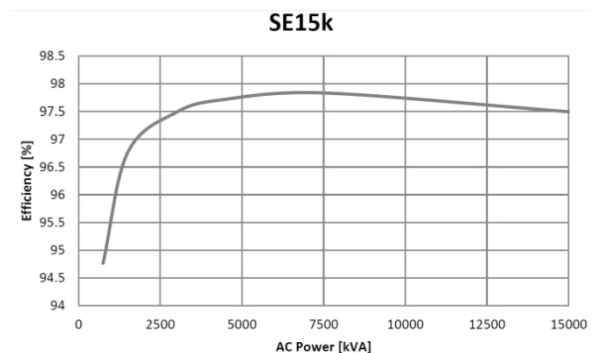
Fig. F.2.3: Efficiency curve of SolarEdge 15 kW inverter
Curves received from Dutch SE distributor (AliusEnergy) According this curve the SE15k inverter starts to operate around an AC power of 300 − 400 W. Efficiency curve is used in PV-model

F.2.2 Impressions

Fig. F.2.4: Installation room: before, and after new PV-inverter (12yrs warranty) and electrical distribution box (LK 2020) for connection of PV-system (32A MCB) and ESS(40A MCB)

Fig. F.2.5: Replacement of existing 6 x25A fuses to 4 x 63 to connect PV+ESS distribution box. Empty group for Electric Car charger. Register installation at Utility (Enexis), new contract: 53kW consumption and 150kW production (transportation only charged for consumption)

Fig. F.2.6: Safety measures and PV-roof accessibility. New safety stair and fall-off protection with safety line.

F.2.7: Temporary storage and vertical transportation. Panel construction, with maximum weight (~300 tiles of 4.5x30x30cm) for optimal safety against high wind gusts. Picture below show the panel integrated optimizer (25yrs warranty).

F.3 BESS

Chosen battery technology from the inside:
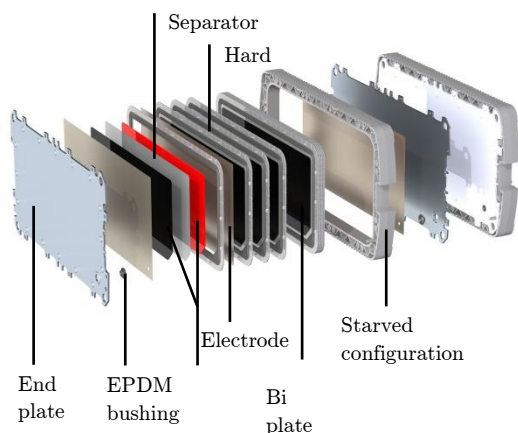
Fig. F.3.1: One module [Nilar international AB]
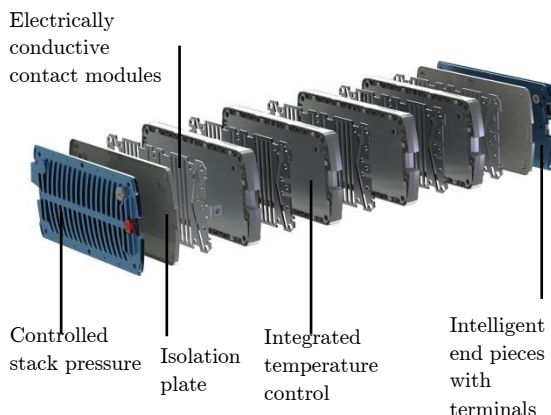
Fig. F.3.2: True bipolar configuration [Nilar international AB]

Battery typical number of cycles in relation with SOC-window:

SOC window	Cycles		
	Typical	**-10%**	**10%**
2%	369 217	332 295	406 139
5%	94 046	84 642	103 451
10%	33 423	30 081	36 765
15%	18 248	16 423	20 073
20%	11 878	10 690	13 066
25%	8 513	7 662	9 365
30%	6 485	5 837	7 134
35%	5 152	4 637	5 668
40%	4 221	3 799	4 643
45%	3 541	3 187	3 895
50%	3 026	2 723	3 328
55%	2 624	2 362	2 887
60%	2 305	2 074	2 535
65%	2 045	1 841	2 250
70%	1 831	1 648	2 014
75%	1 652	1 487	1 817
80%	1 500	1 350	1 650
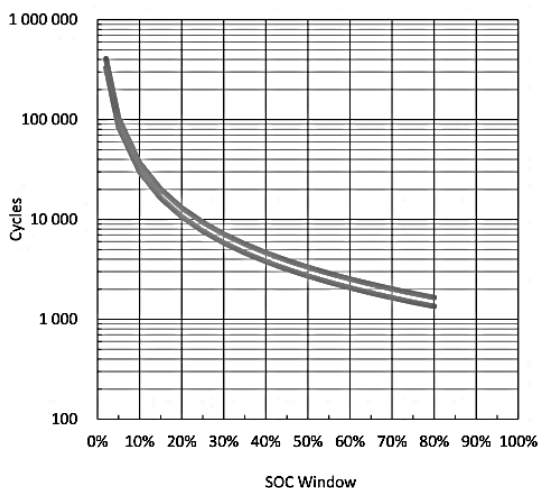
Fig. F.3.3: Typical number of cycles [Nilar international AB]

F.3.1 Design performance BESS

No Load losses: *according KEB-representative (design stage)*
- Inverter = 150W.
- Transformer = 250W.
- Filters approx. = 100W.
- **Total loss = 520W**

Full load losses: *according KEB-representative (design stage)*
- Inverter = 525W.
- Transformer = 800W.
- Filters approx. = 250W.
- **Total loss = 1585W**

F.3.2   Transformer voltage reduction

$3phase\ Grid\ (400VAC) * \sqrt{2} * grid\ flucations\ 1.1 * U_{PID(controller)*}1.05 = 653V =$ to high

$3phase\ Grid\ (300VAC) * \sqrt{2} * grid\ flucations\ 1.1 * U_{PID(controller)} * 1.05 = 490V =$ good
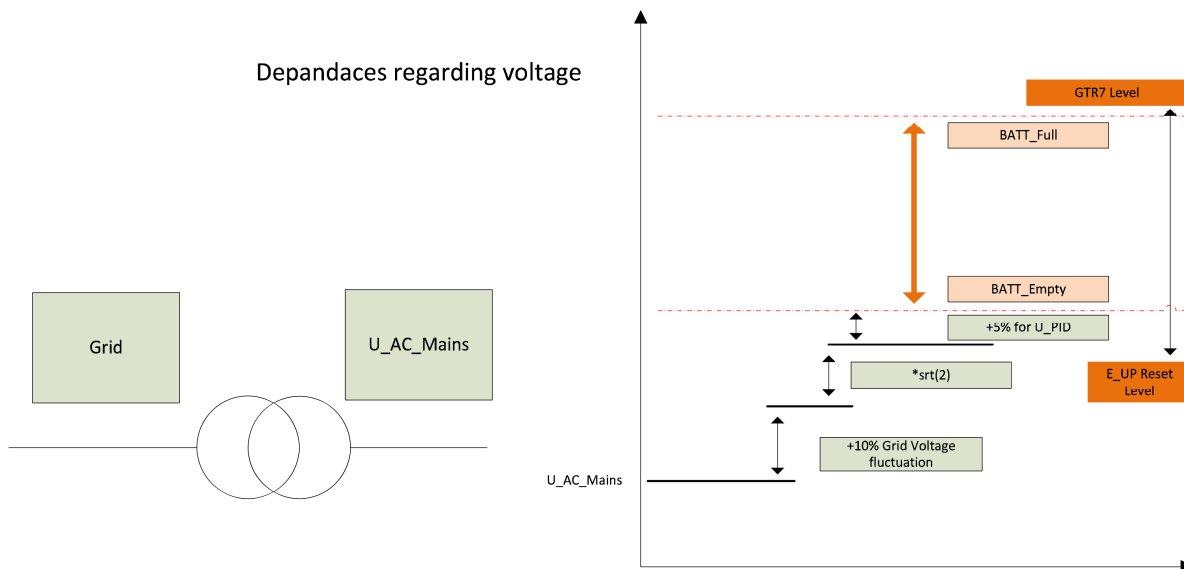
Fig. F.3.4: Voltage reduction in order to match the AC grid voltage to required KEBF5 inverter DC voltage range (500 to 800V).

G Facility Verification

G.1 BESS instrumentation

II. Verification of permanent Schneider Electric energy meter (iEM3155) was checked at primary side of transformer, between decentral distribution box and transformer

III. Secondary side of transformer (KEB-cabinet) was measured, at 3 phase connection between transformer and inverter cabinet

IV. DC-main bus, was measured at BattMS-cabinet

Table G.1.1.: Accuracy of Schneider Electric energy meter measured at point II (PA implies to the PQ-analyzer)

Time	I1$_{iEM}$ [A]	I1$_{PA}$ [A]	Acc.	I3$_{iEM}$ [A]	I$_{PA}$	Acc.	P$_{iEM}$ [W]	P$_{PA}$ [W]	Acc.	S$_{iEM}$ [VA]	S$_{PA}$ [VA]	Acc. charge
2-2-2016 15:10	27.1	27.17	0.3%	27	26.71	-1.1%	-18563	-18486.4	-0.4%	18701	18615.13	0.5%
2-2-2016 15:40	5.4	5.37	-0.6%	5.4	5.36	-0.7%	-3612	-3758.7	3.9%	3617	3656.7	-1.1%
2-2-2016 15:55	23.6	23.52	-0.3%	23.1	23.25	0.6%	16176	16140.8	-0.2%	16268	16232.73	0.2%
2-2-2016 16:00	40.5	40.39	-0.3%	40	39.97	-0.1%	27741	27628.3	-0.4%	27800	27676.12	0.4%

	U1$_{iEM}$ [V]	U$_{PA}$ [V]	Acc.	U2$_{iEM}$ [V]	U$_{PA}$ [V]	Acc.	U3$_{iEM}$ [V]	U$_{PA}$ [V]	Acc.	Q$_{iEM}$ [VAR]	Q$_{PA}$ [VAR]	Acc disch.
2-2-2016 15:10	232	233.4	0.6%	234	234.7	0.3%	234	233.9	0.0%	2276	2172.67	4.8%
2-2-2016 15:40	231	232.2	0.5%	233	233.5	0.2%	232	232.5	0.2%	226	217.63	3.8%
2-2-2016 15:55	230	231	0.4%	232	232.5	0.2%	231	231.3	0.1%	-1728*	837.74*	-306%
2-2-2016 16:00	229	229.9	0.4%	231	231.2	0.1%	229	230	0.4%	-1819	-471.6	-286%

(about 01:20 mm:ss offset) between time PQ-analyser and time Insitehistory, as longest found difference

*Reactive power [Q]: During charging, a large difference is found between measurements of the PQ-analyser and iEM3155-energy meter. Difference is most probably caused by L2; examination of this line is not possible since reactive line power is not registered by the iEM3155 energy-meter. Calculating the

apparent power by $S_{iEM} = \sqrt{Q_{iEM}^2 + P_{iEM}^2}$ equals to the

Table: G.1.2: Line reactive power 15:55[HH:MM]

Q-L1 [VAR]	Q-L2 [VAR]	Q-L3 [VAR]	Q$_{PA}$ [VAR]
639.5	-431.4	629.59	837.74

same value as registered. The PQ-analyzer: registered apparent power (S$_{PA}$ = 16232VA) is higher than determined with Q$_{PA}$ and P$_{PA}$ (S$_{PA}$ = 16161VA). When calculating S$_{PA}$ with the true power value (P$_{PA}$) and reactive power value (Q$_{iEM}$), S = 16232VA which is exactly equal to the registered apparent power (S$_{PA}$). During this measurement, the apparent power of the power analyser is assumed uncertain, possible caused by a wrong placed current clamp or bad PQ-measurement. However further research is required, to see if this happens more often during charging (positive power direction / consumption), since it did not occur during discharging. To summarize, the iEM3155: energy-meter is accurate enough for future research purposes.

Table G.1.3: Measurements AC (KEB-F5 cabinet) – Secondary Side Transformer (from Inverter Cabinet) at point III

	I$_{KEB}$ [A]	I$_{PA}$ [A]	Accuracy	U$_{KEB}$ [A]	U$_{PA}$ [V]	Accuracy	f$_{KEB}$ [Hz]	f$_{PA}$ [Hz]	Accuracy
2-2-2016 16:18 (charge)	5.7	8.28	31.2%	302	304.8	0.9%	49.8	49.98	0.4%
2-2-2016 16:24 (charge)	21.8	22.2	1.8%	320	308.0	-3.9%	49.9	49.97	0.1%
2-2-2016 16:28 (charge)	33.2	35.4	6.3%	326	311.2	-4.8%	50	49.99	0.0%
2-2-2016 16:39 (discharge)	27.1	30.7	11.8%	295	296.1	0.4%	49.9	49.98	0.2%

(about 00:20 mm:ss offset) between time PQ-analyser and time Insitehistory

Current measurements at secondary side transformer are inaccurate and the difference is inconsistent. Measurements of AC voltage is less inaccurate, but still a critical measurement (accurate if ≤ ± 3%, and useful for facility analysis ≤ ± 5%).

Table G.1.4.: Accuracy of DC- main bus measurement (Nilar-BattMS) at point IV

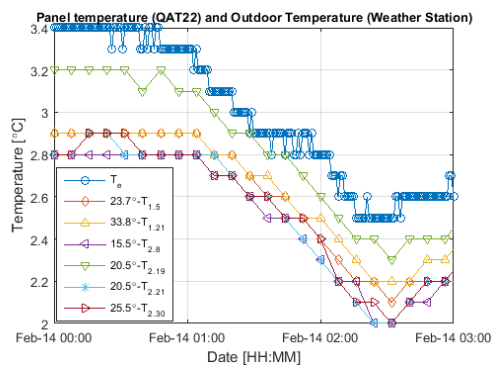|	Measurement	BattMS-measurement (Modbus)	I-Fluke PA [A]	Accuracy
04-02-2016 16:00	I - DC	27.43 A	26.8 A (clamp 1: Fluke) 27.8 A (clamp 2: Fluke) Average = 27.3A	+0.5 %
04-02-2016 16:00	U – DC	630.9 V	629 V	+0.3 %

G.2   Environmental sensors

Fig. G.2.6: Panel temperature sensors
Allowable temperature offset is + or − 0.4℃. Here the maximum offset between 3 hours night-time (cloudy) panel measurements is within +/- 0.4℃ and compared to outdoor measured temperature the offset is 0.6℃. Remember that 1℃ difference only accounts for 0.45% panel efficiency loss. Panel temperature instruments are accurate.
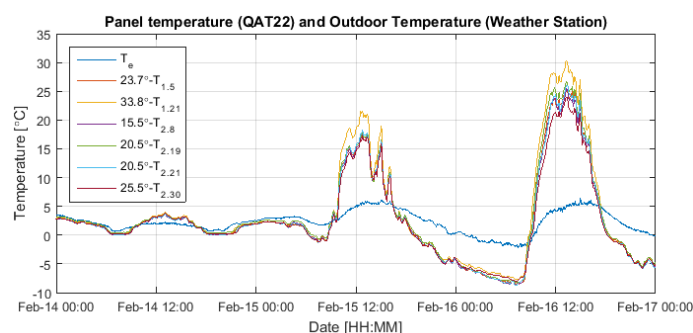
Fig. G.2.7: Panel temperature sensors and outdoor temperature
During an overcast night, outdoor- and panel temperatures are nearly equal (14Feb). During the day, cell temperature increases as result of the incoming solar-radiation. Where the panel mounted at highest inclination angle (33.8°) is warmest at 30.3 °C, and at lowest angle (15.5°) 24 °C. The cell conversion efficiency of incoming E_{POA} to Electricity is about 3% lower than modules at row-15.5°.

G.2.1   Existing outdoor temperature sensors and weather station

Two existing outdoor temperature sensors are attached to the building and were compared to the weather stations temperature measurement. The sensor located at south-west is much influenced by the sun's insolation (see figure G.2.8). On the afternoon 16th of February the difference compared to the weather station was +14.3℃. Even during a cloudy night on february the 14th the temperature difference was +1.9℃. For the sensor located at north-east the difference at the 14th of February (cloudy period) was only between 0.0℃ and 0.2℃. Before, during and after a sunny day (16th) the NE-tempereature measurement lags, which means that during the day the temperature measured at NE is slightly lower (-1℃ to -1.9℃) and during nighttime slightly higher (+0.9℃ to +1.2℃) compared to the weather station (T_e). This lag is most possibly caused by the buildings thermal transmittance.
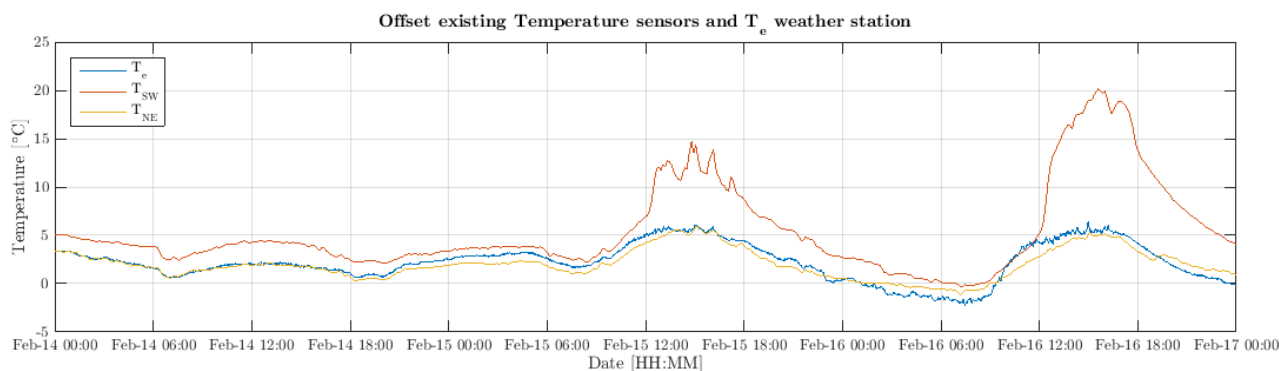
Fig. G.2.8. Difference between existing temperature sensors and outdoor temperature measured at the weather station

G.3 PV-facility
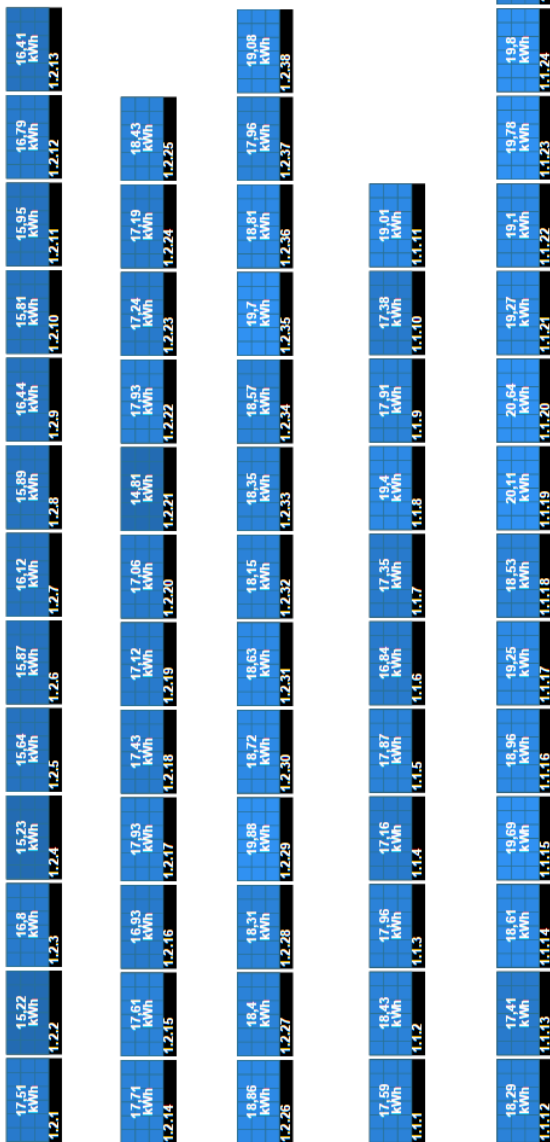
U, I curve row average yielding panels
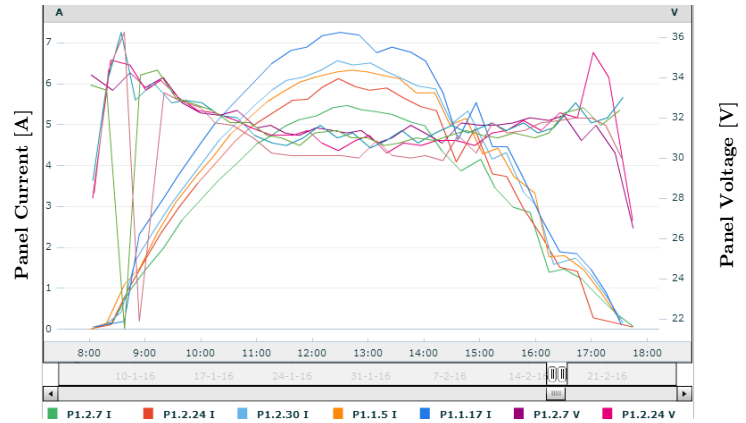
Fig.G.3.2. row average producing PV-panels

Fig.: G3.1: Panel number and total energy yield by panel from January the 8th till February the 25th 2016 [SE]

H PV-Model validation
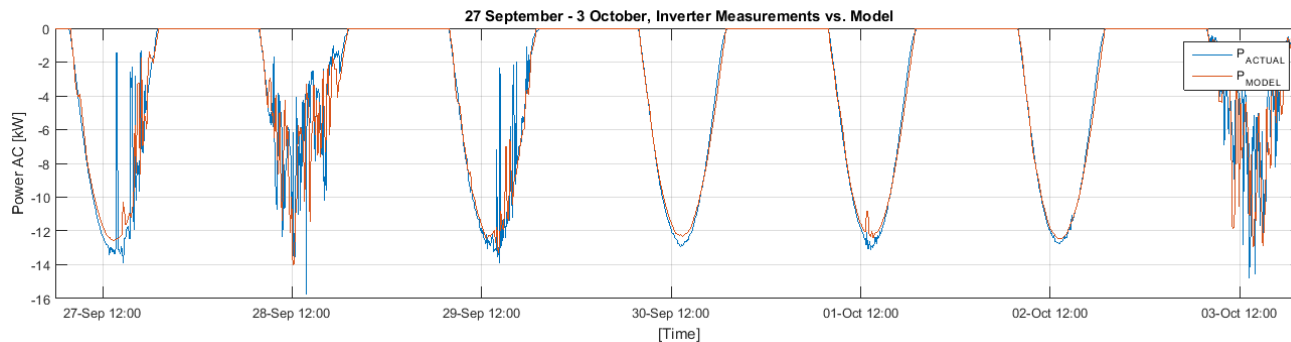
Fig. H.1.1: Weekly PV-production analysis, with 10minute data (KNMI)

Panels are mounted on different inclination angles, and are therefore simulated as separate rows. These modelled results are compared with the measured values in figure 5.2.2.
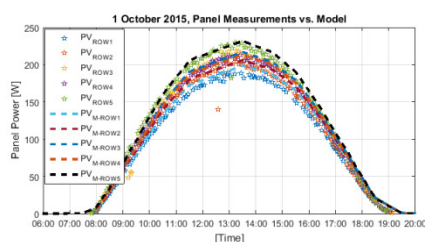
Fig. H.1.2. Comparison panel measurements and modelled row (5x) values
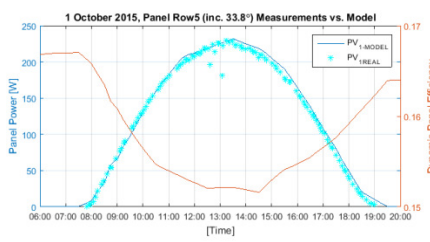
Fig. H.1.3: Measured vs. modelled PV-production (row 5, 33.8°). With on second y-axis the dynamic panel efficiency due the temperature effect
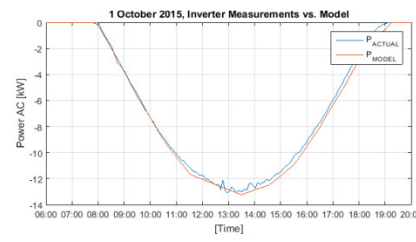
Fig. H.1.4: central AC modelled and measured production with hourly data
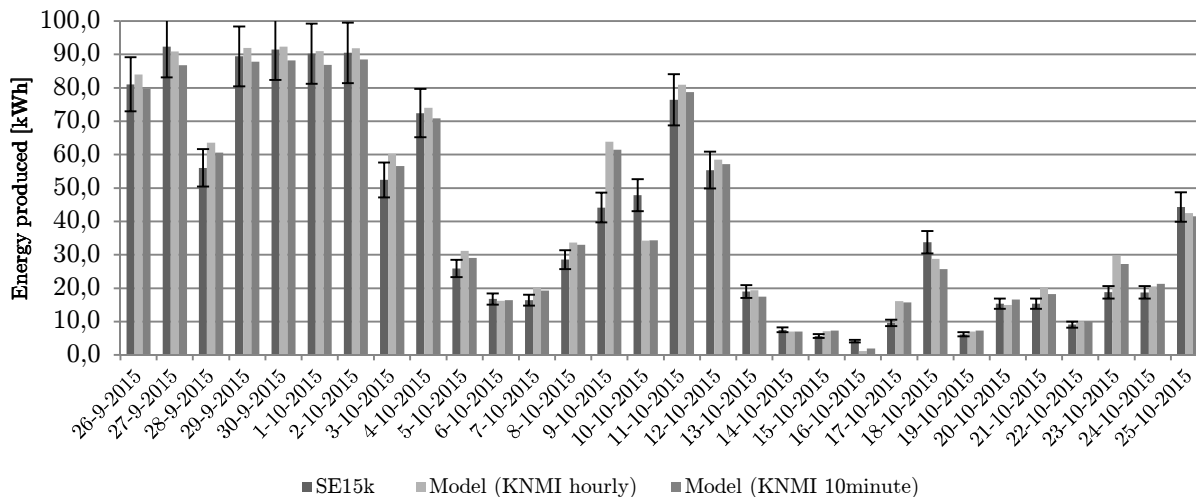
Fig. H.1.6: Daily cumulative energy production, measured (5min data) and modelled with hourly and 10minute climate data

I BESS numerical behaviour

In this appendix numerical behaviour of the BESS-model is presented starting with the conversion efficiency. This curve (figure I.1) is made with the in F.3.1 provided theoretical conversion losses.
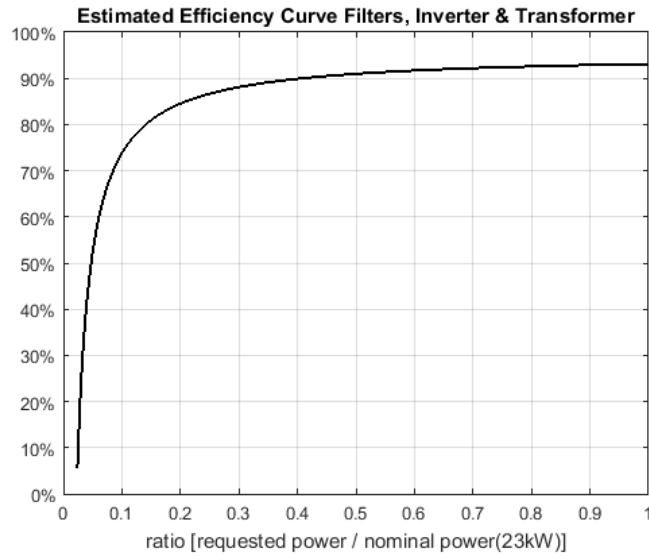
I.1: Modelled efficiency curve for total conversion system of filters, inverter and transformer

Charge and discharge cycles. The black dashed-line corresponds to the AC power request and the blue line is de delivered DC-power. The brown line indicates the Battery State of Charge level (SOC).
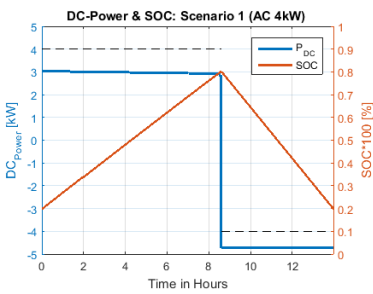
Fig. I.2: Scenario 1 + and − 4kW AC req.
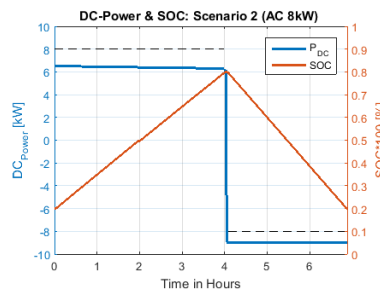
Fig. I.3: Scenario 2 + and − 8kW AC req.
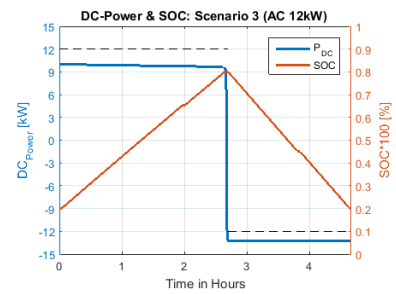
Fig. I.3: Scenario 3 + and − 12kW AC req.
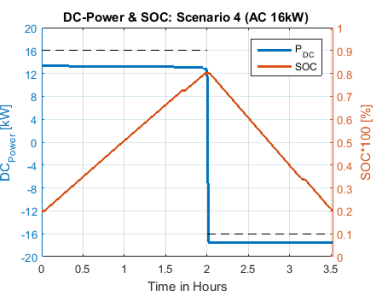
Fig. I.4: Scenario 4 + and − 16kW AC req.
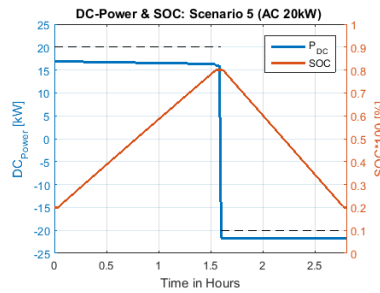
Fig. I.5: Scenario 5 + and − 20kW AC req.
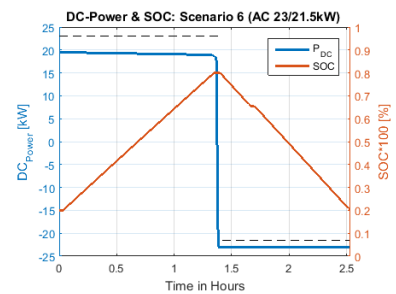
Fig. I.6: Scenario 6 +/- 23/21.5kW AC req.
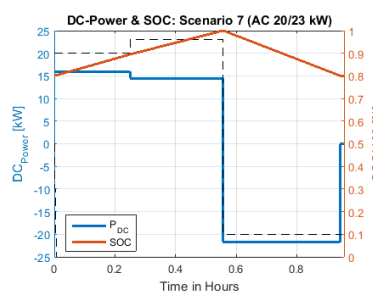
Fig. I.7: Scenario 7 +/- 20/23kW AC req.
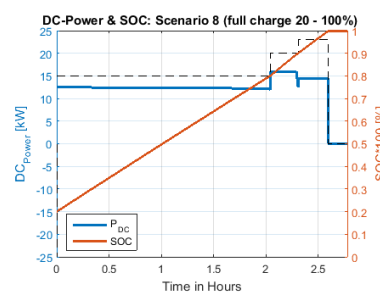
Fig. I.8: Scenario 8: full-charge-procedure

J Calibration report power analyser

Power Quality analyser. Calibration date 03-11-2015

Chauving Arnoux: CA 8335.

| Herleidbaarheid | : | De kalibratie is uitgevoerd met de hieronder vermelde werkstandaarden, die herleidbaar zijn naar de (inter)nationale standaarden. De tijdens de kalibratie optredende meetonzekerheid van de meetopstelling is minimaal een factor 3 beter dan de meetnauwkeurigheid van het gekalibreerde instrument. |
| Meetonzekerheid | : | Een opgegeven onzekerheid is gebaseerd op de standaardonzekerheid, vermenigvuldigd met een dekkingsfactor k = 2, welke overeenkomt met een betrouwbaarheidsinterval van ongeveer 95 %. De standaardonzekerheid is bepaald volgens EA-4/02. |

Kalibratiestandaarden:

Merk	Type	Certificaatnummer	Kalibratiedatum
Fluke	5520A	6212-15-1	15-jan-2015

Spanning AC @ 50 Hz (L1)				
Ingestelde waarde	Aanwijzing	ondergrens	bovengrens	resultaat
100,00 V	100,0 V	99,3 V	100,7 V	pass
200,00 V	200,0 V	198,8 V	201,2 V	pass
300,00 V	300,0 V	298,3 V	301,7 V	pass
400,00 V	400,1 V	397,8 V	402,2 V	pass

Spanning AC @ 50 Hz (L2)				
Ingestelde waarde	Aanwijzing	ondergrens	bovengrens	resultaat
100,00 V	100,0 V	99,3 V	100,7 V	pass
200,00 V	200,0 V	198,8 V	201,2 V	pass
300,00 V	299,9 V	298,3 V	301,7 V	pass
400,00 V	399,9 V	397,8 V	402,2 V	pass

Spanning AC @ 50 Hz (L3)				
Ingestelde waarde	Aanwijzing	ondergrens	bovengrens	resultaat
100,00 V	100,0 V	99,3 V	100,7 V	pass
200,00 V	200,0 V	198,8 V	201,2 V	pass
300,00 V	299,9 V	298,3 V	301,7 V	pass
400,00 V	400,0 V	397,8 V	402,2 V	pass

Stroom AC @ 50 Hz (L1)				
Ingestelde waarde	Aanwijzing	ondergrens	bovengrens	resultaat
5,000 A	4,990 A	4,765 A	5,235 A	pass
25,00 A	24,92 A	24,63 A	25,37 A	pass
50,00 A	49,85 A	49,45 A	50,55 A	pass
75,00 A	74,86 A	74,28 A	75,72 A	pass
100,00 A	99,78 A	99,10 A	100,90 A	pass

Stroom AC @ 50 Hz (L2)				
Ingestelde waarde	Aanwijzing	ondergrens	bovengrens	resultaat
5,000 A	4,990 A	4,765 A	5,235 A	pass
25,00 A	24,91 A	24,63 A	25,37 A	pass
50,00 A	49,86 A	49,45 A	50,55 A	pass
75,00 A	74,85 A	74,28 A	75,72 A	pass
100,00 A	99,78 A	99,10 A	100,90 A	pass

Stroom AC @ 50 Hz (L3)				
Ingestelde waarde	Aanwijzing	ondergrens	bovengrens	resultaat
5,000 A	5,000 A	4,765 A	5,235 A	pass
25,00 A	24,98 A	24,63 A	25,37 A	pass
50,00 A	49,97 A	49,45 A	50,55 A	pass
75,00 A	75,03 A	74,28 A	75,72 A	pass
100,00 A	100,10 A	99,10 A	100,90 A	pass

Stroom AC @ 50 Hz (N)				
Ingestelde waarde	Aanwijzing	ondergrens	bovengrens	resultaat
5,000 A	5,020 A	4,765 A	5,235 A	pass
25,00 A	25,06 A	24,63 A	25,37 A	pass
50,00 A	50,16 A	49,45 A	50,55 A	pass
75,00 A	75,33 A	74,28 A	75,72 A	pass
100,00 A	100,40 A	99,10 A	100,90 A	pass

Met de 5/100 A tangen

K BESS Power Quality

K.1 PQ: Idle and connected state

Table K.1.1: Power quality analysis primary side transformer (building) at standby and BESS connect state

DC request	Active power	PF	DPF	THD (I1)	THD (I2)	THD (I3)	THD(U1)	THD(U2)	THD(U3)
System IDLE 0-request	240W	0.356	0.783	242.6	246.6	136.1	1.4	1.1	1.7
System Active 0-request	990W	0.142	0.15	30.7	29.2	30.8	1.4	1.3	1.7

I_{THD} is very high, but calculating the current TDD for phase 1, it is only 2.1% due the very low current magnitude. U_{THD} value is within limits. PF and DPF not, however the system is only 'active' in a very limited time range, and system idle throughout the day.

K.2 Harmonic distortion during discharging with 0.1C, 0.3C and 0.5C

Fig. K.2.1: Current harmonic distortion of individual harmonics: 0.1C discharging

Fig. K.2.2: Current harmonic distortion of individual harmonics: 0.3C discharging

Harmonic Distortion 1st to 25th harmonic: during discharging
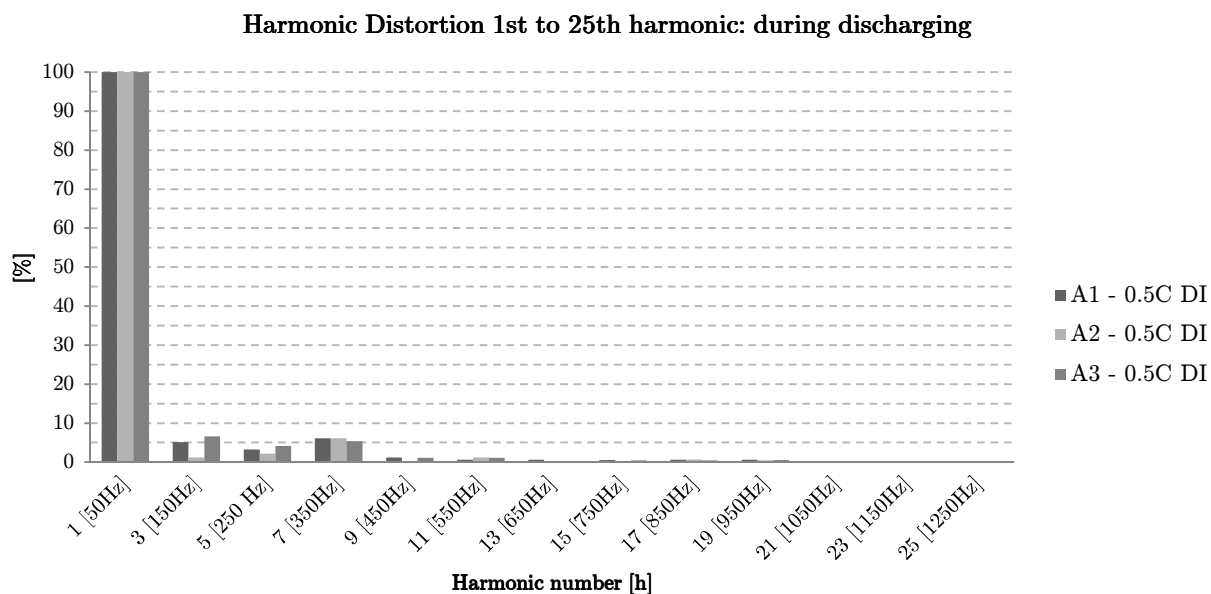
Fig. K.2.3: Current harmonic distortion of individual harmonics: 0.5C discharging

K.3 Harmonic distortion during charging with 0.1C, 0.3C and 0.5C

Harmonic Distortion 1st to 25th harmonic: during charging
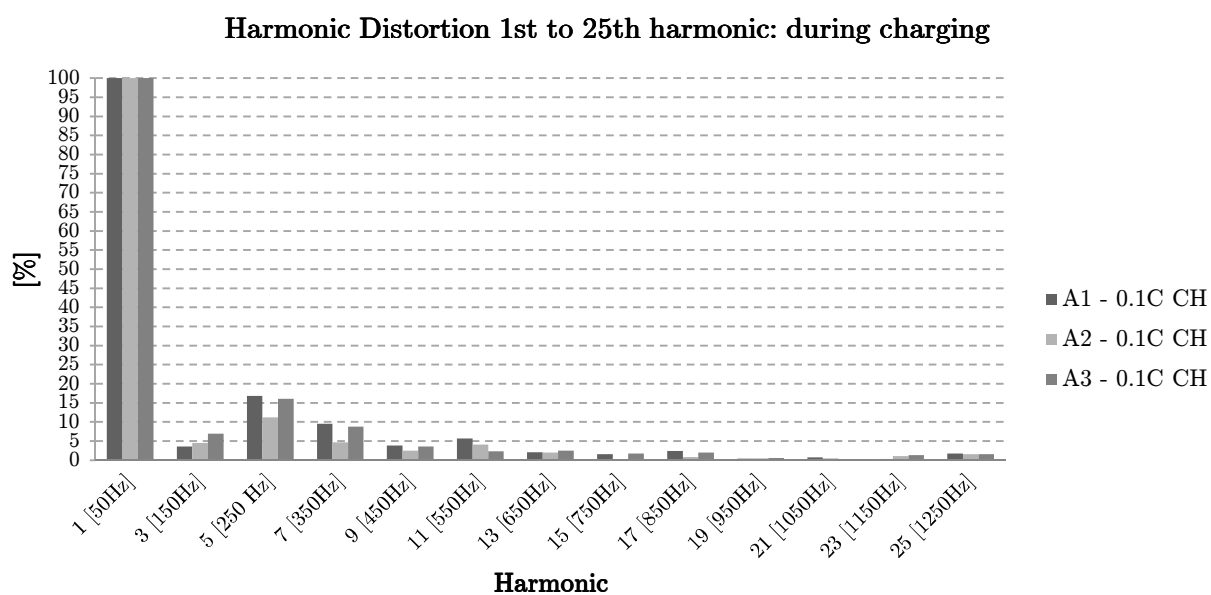
Fig. K.2.4: Current harmonic distortion of individual harmonics: 0.1C charging

Harmonic Distortion 1st to 25th harmonic: during charging
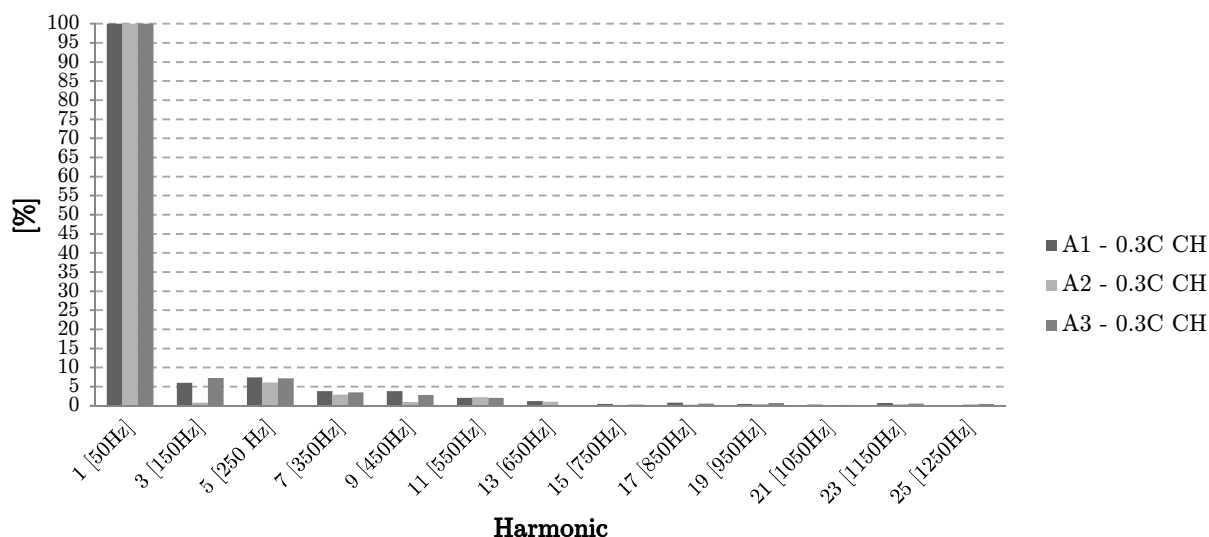
Fig. K.2.5: Current harmonic distortion of individual harmonics: 0.3C charging

Harmonic Distortion 1st to 25th harmonic: during charging
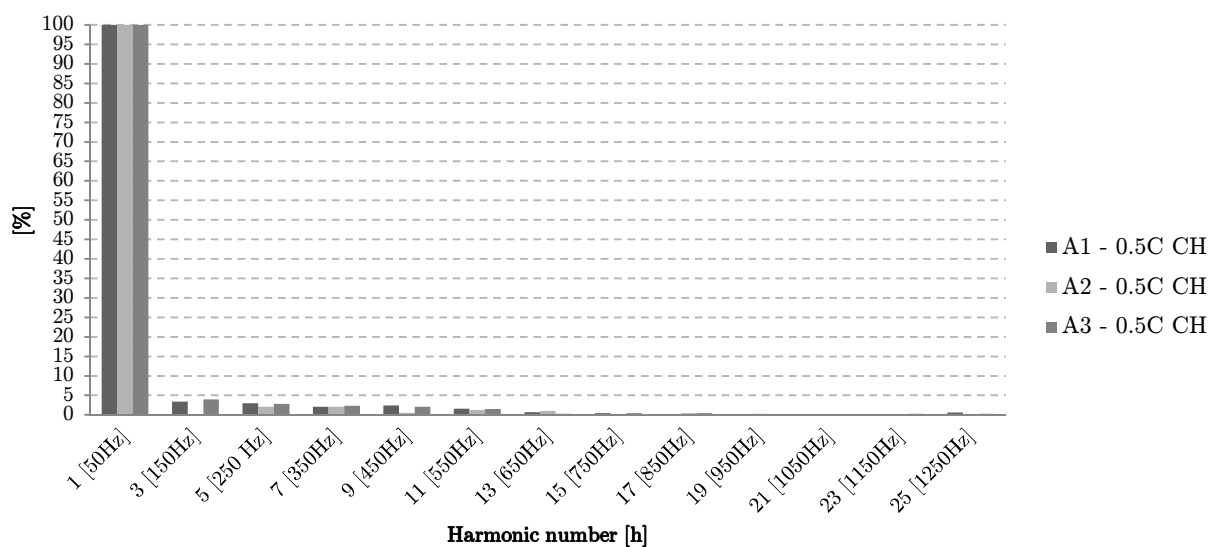
Fig. K.2.6: Current harmonic distortion of individual harmonics: 0.5C charging

L BESS Operational performance day test: an overview

Experiment day 2: Cycle performance analysis, February 3rd 2016
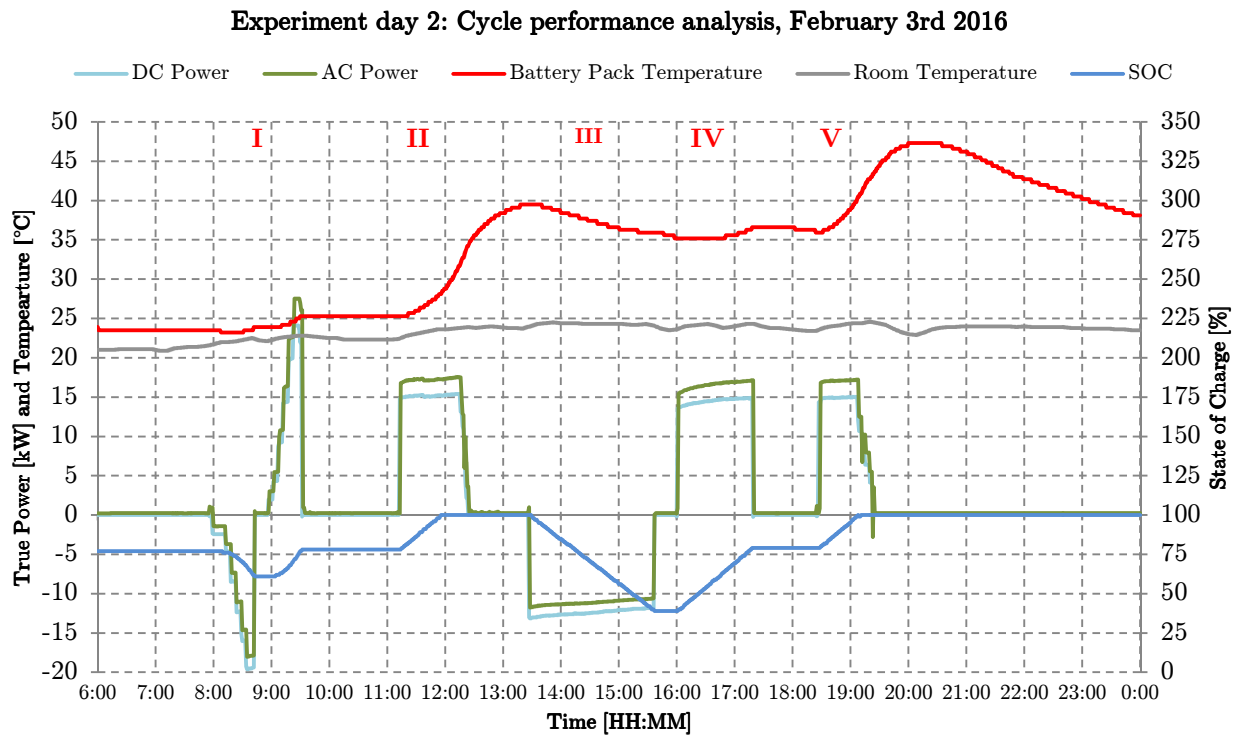
Fig. L.1: Cycle performance analysis

I: Component efficiency experiments

II: Full charge procedure to make sure battery SOC is 100%

III: Discharge from 100% to 39% SOC

IV: Charge from 39% to 79% SOC

V: Full charge procedure from 79% to 100%

M Full charge behaviour BESS

Full charge procedure (Strings are disconnect independently)
Measured secondary side transfomer
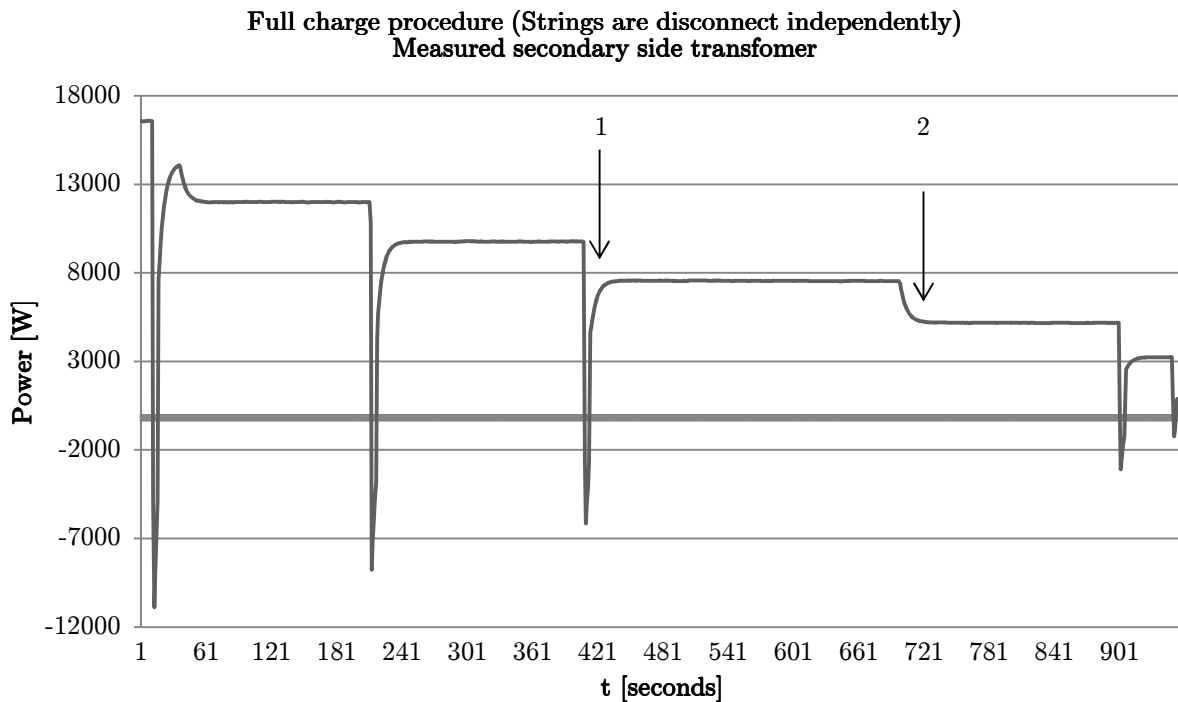
Fig. M1. BESS power behavior during full charge procedure

Charging drops indicated at (1) are caused by a measurements problem or system fault more research is required. Only at point 2, a desired curve is measured.

N Numerical DSM-scenario tests

In this appendix additional figures are provided about the numerical tested DSM-scenarios (chapter 7).

N.1 Smart scenario: increase self-consumption of PV-production surpluses
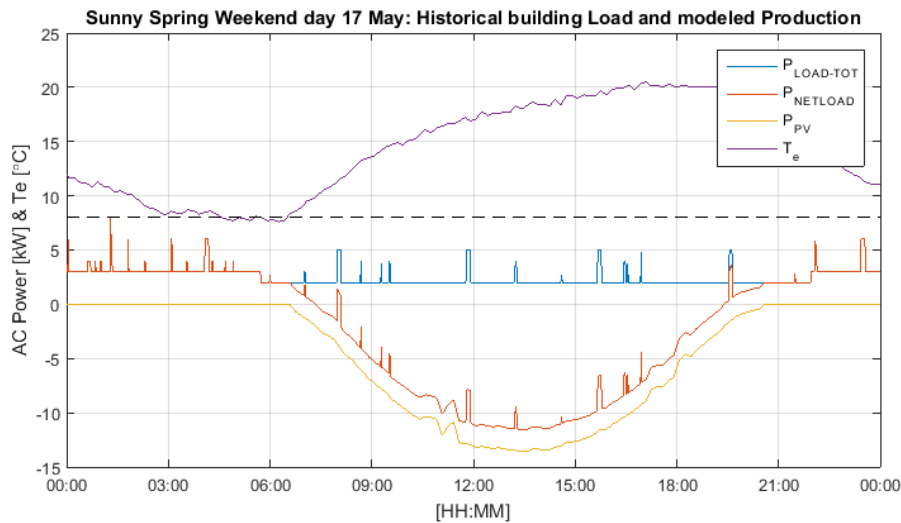
Fig. N.1.1: Historical data of measured load (blue). Yellow line indicates the simulated PV-production for that specific day and the brown line provided the resulting net-load (= Pload − Ppv)
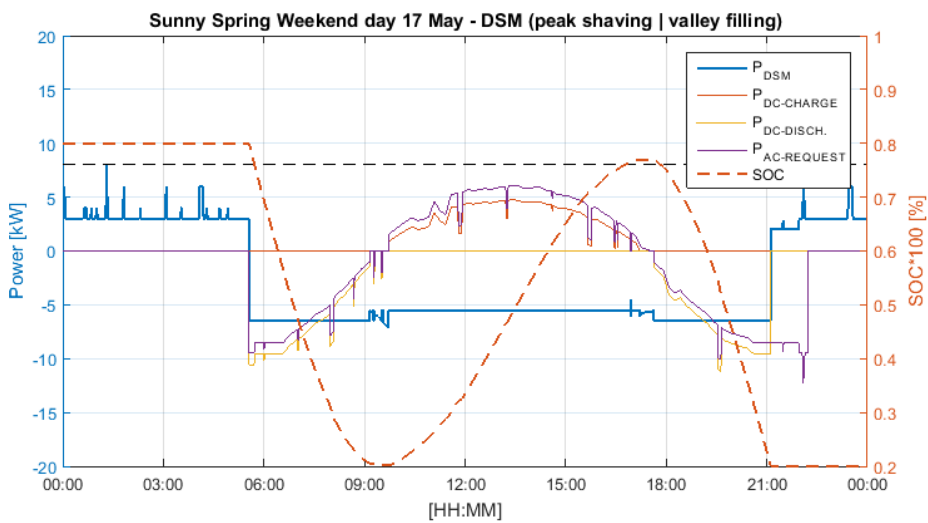
Fig. N.1.2: The blue line represents the new building load curve by requesting an AC-power with the DSM-net-controller model (purple line). The gap between the purple and; yellow (P-DC-discharge) and brown (P-DC-charge) is due to the conversion loss (chemical loss of the battery and transformer+inverter)
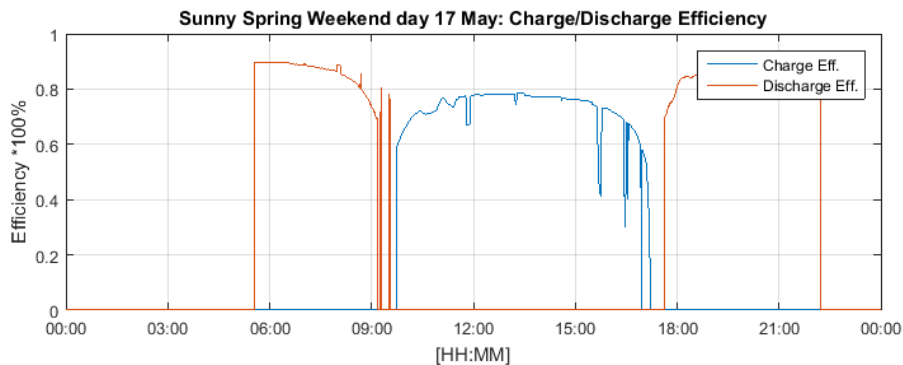
Fig. N.1.3: Total system conversion effeciency which includes all losses (conversion loss due too: transformer, filters, interter and chemical loss in battery)

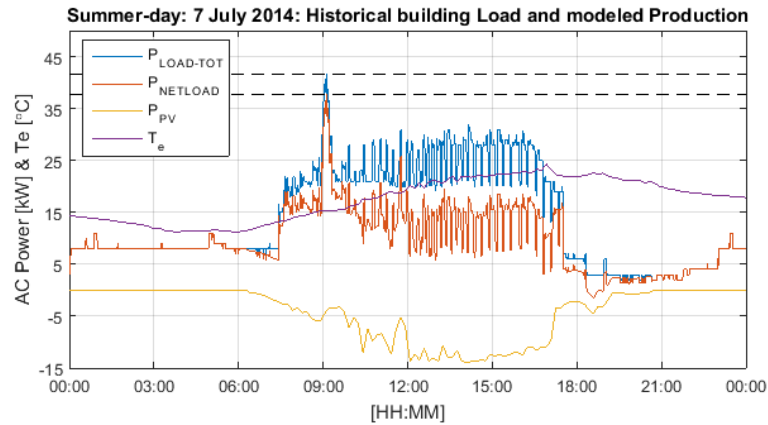## N.2 Smart scenario: Summer period: electrical chiller

Fig. N.2.1: Summer-day operations (max temp 25°C). At the start of the day chiller started to operate in 2nd stage, continued with an on/off behaviour (blue-line). The yellow-line indicates the simulated PV-production and the brown line the resulting net-load. Due to the PV-production, net-load decrease and an early morning peak occurs.
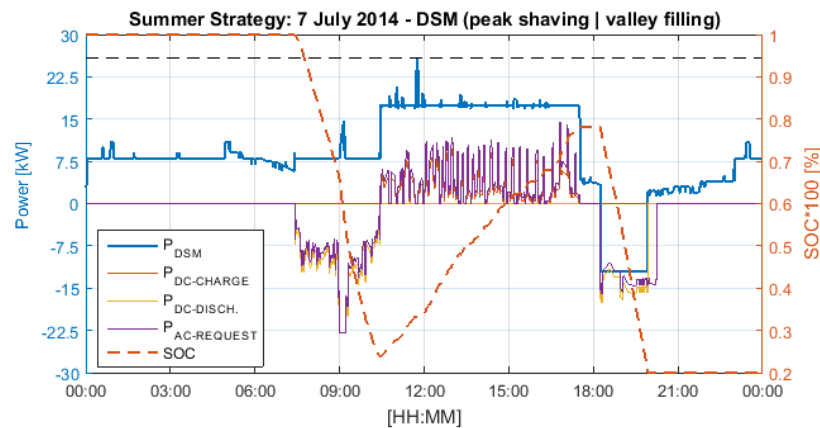

Fig. N.2.2: Summer-day 7th of July: Peak shaving continued with valley filling and ending with a grid-support activity at the end of the day (18:00 − 20:00).
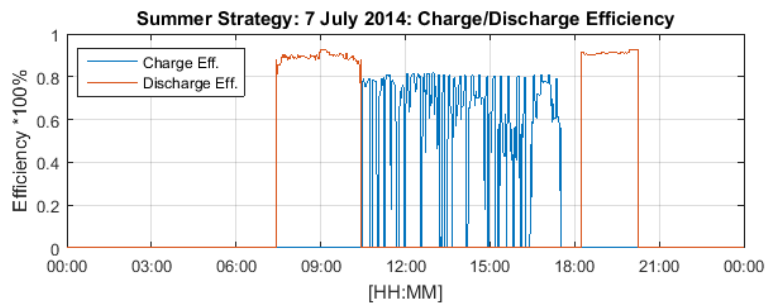
Fig. N.2.3: Charge (blue) and discharge (efficiency) curves. During the middle of the day valley-filling has been set. The BESS is during that period constantly changing the current rates. This effect should be tested in reality.

N.3   Smart scenario: Winter period: electrical steam humidifier

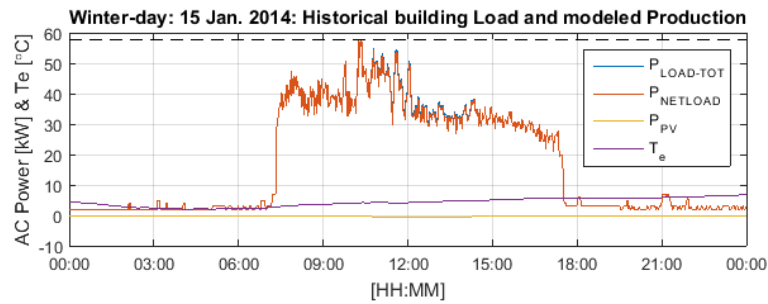### N.3.1   First winter scenario test on the 15th of January.

Fig. N.3.1: 15th of January, humidifier operations: total load, net-load and PV-production curve. Nearly zero PV-power was produced (yellow-line)
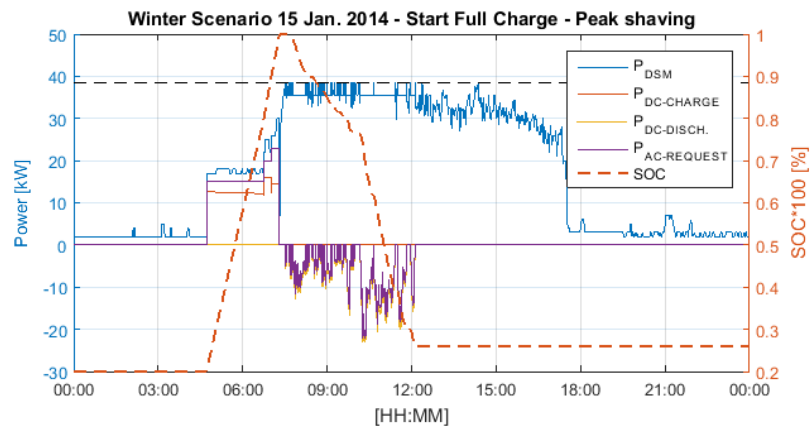

Fig. N.3.2: night-time/early-morning full charge procedure (100% SOC) continued with peak clipping
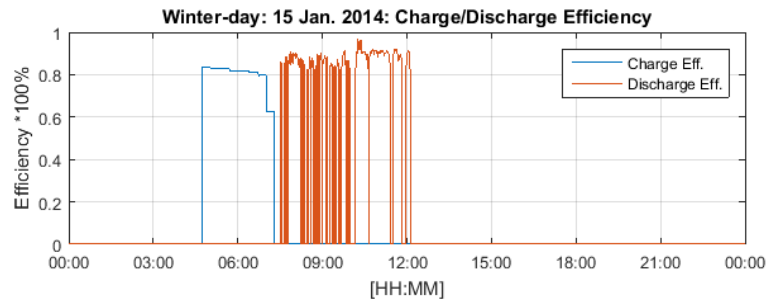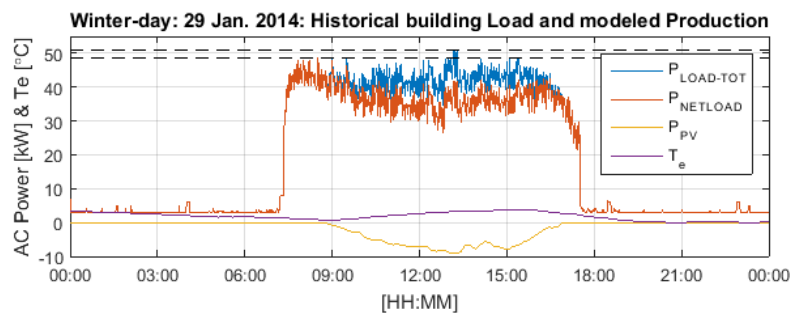

Fig. N.3.3: Charge (blue) and discharge efficiency curves.

N.3.2   Second winter scenario test on the 29th January

N.3.3: 29th of January, humidifier operations: total load, net-load and PV-production curve.
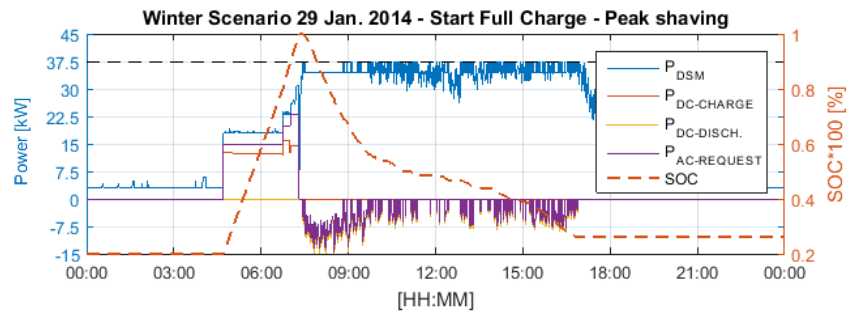
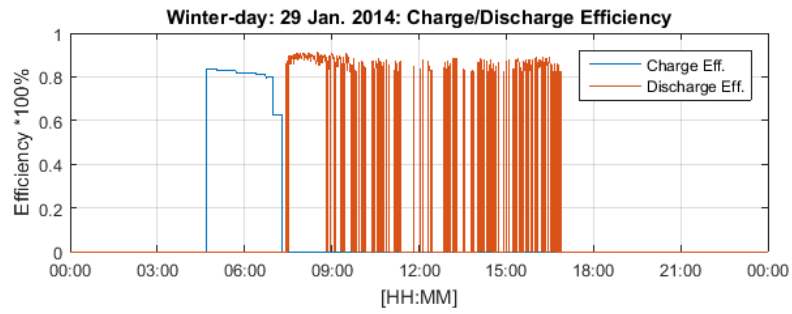Fig. N.3.2: night-time/early-morning full charge procedure (100% SOC) continued with peak clipping

Fig. N.3.3: Charge (blue) and discharge efficiency curves. On/off behaviour shall be tested in practice.

O References

[1]   R. Monroe, "WHAT DOES THIS NUMBER MEAN?," *Nature*, 2015. [Online]. Available: https://scripps.ucsd.edu/programs/keelingcurve/2015/05/12/what-does-this-number-mean/.

[2]   B. Bregman and W. Ligvoet, *Klimaatverandering. Samenvatting van het vijfde IPCC-assessment en een vertaling naar Nederland.* 2015.

[3]   SER, "Energieakkoord voor duurzame groei," *Rep. From http//Www.Energieakkoordser.Nl/*, no. September, pp. 1–146, 2013.

[4]   J. Teyssen, M. Fuchs, M. Hoppe-Kilpper, U. Wagner, and H.-J. Haubrich, "Wind Report 2005," pp. 1–22, 2005.

[5]   G. Knier, "How do Photovoltaics Work? - NASA Science," *NASA*, 2002. [Online]. Available: http://science.nasa.gov/science-news/science-at-nasa/2002/solarcells/.

[6]   PV Resources, "Large Ω Scale Photovoltaic Power Plants," 2016. [Online]. Available: http://www.pvresources.com/en/pvpowerplants/top50pv.php. [Accessed: 12-Jan-2016].

[7]   G. Masson, S. Orlandi, and M. Rekinger, "Global Market Outlook for Photovoltaics 2014-2018," 2013.

[8]   Fraunhofer ISE, "Current and Future Cost of Photovoltaics. Long-term Scenarios for Market Development, System Prices and LCOE of Utility-Scale PV Systems," 2015.

[9]   Planbureau voor de Leefomgeving & DNV GL, "Het potentieel van zonnestroom in de gebouwde omgeving van Nederland," p. 35, 2014.

[10]   W. Sinke, "Zonnestroom : van niche naar impact," 2015.

[11]   D. Howarth and B. Monsen, "Renewable Energy Faces Daytime Curtailment in California," 2014. [Online]. Available: http://www.nawindpower.com/issues/NAW1412/FEAT˙04˙Renewable-Energy-Faces-Daytime-Curtailment-In-California.html. [Accessed: 08-Jul-2015].

[12]   G. Mulder, D. Six, B. Claessens, T. Broes, N. Omar, and J. Van Mierlo, "The dimensioning of PV-battery systems depending on the incentive and selling price conditions," *Appl. Energy*, vol. 111, pp. 1126–1135, 2013.

[13]   IRENA - International Renewable Energy Agency, "Renewable Power Generation Costs," no. November 2012, p. 12, 2012.

[14]   W. van Sark, P. Muizebelt, and J. Cace, "Inventarisatie PV markt Nederland," 2014.

[15]   IEA, "Technology Roadmap," 2013.

[16]   D. Bank, "F . I . T . T . for investors Crossing the Chasm," 2015.

[17]   R. Venekamp, Gerben, J. Kamphuis, M. Laarakkers, and van den Berge, "OS4ES : Increasing awareness of DG-RES and demand response processes by registry enabled services," *PowerTech*, 2015.

[18]   I. Colak, S. Sagiroglu, G. Fulli, M. Yesilbudak, and C.-F. Covrig, "A survey on the critical issues in smart grid technologies," *Renew. Sustain. Energy Rev.*, vol. 54, pp. 396–405, 2016.

[19]   P. T. Moseley and J. Garche, *Electrochemical Energy Storage for Renewable Sources and Grid Balancing Edited by*. Elsevier, 2015.

[20]   R. Dufo-López and J. L. Bernal-Agustín, "Techno-economic analysis of grid-connected battery storage," *Energy Convers. Manag.*, vol. 91, pp. 394–404, 2015.

[21]   R. Anderson, "Energy storage: The key to a smarter power grid," *BBC News*, 2014. [Online]. Available: http://www.bbc.com/news/business-27071303.

[22]   H. Madsen, "Stochastic Modelling of Energy Systems," 2015, no. February, p. 212.

[23]   M. Fürst, "The 50.2 Hz Problem," 2011. [Online]. Available: http://www.vde.com/en/fnn/pages/50-2-hz.aspx. [Accessed: 25-Sep-2015].

[25]   Fraunhofer ISE, "Fraunhofer Institute," 2014, pp. 1–114.

[26]   KEMA Nederland B.V., "Routekaart energieopslag nl 2030," 2015.

[27]   W. Zeiler, P. Savanovic, and E. Quanjel, "Design Decision Support for the Conceptual Phase of the Design Process," *Int. Assoc. Soc. Des. Res.*, pp. 1–15, 2007.

[28]   MPowerUK, "Electricity Generation from Solar Energy, Technology and Economics," 2015. [Online].

Available: http://www.mpoweruk.com/solar˙power.htm#domestic˙pv. [Accessed: 15-Oct-2015].

[29]   IRENA, "Design of Grid-connected PV Systems," 2013.

[30]   MPowerUK, "How Energy Cells Work," *Electropaedia*. [Online]. Available: http://www.mpoweruk.com/chemistries.htm. [Accessed: 18-Jan-2016].

[31]   ISSO, "ISSO-HANDBOEK ZONNE-ENERGIE," p. 472, 2012.

[32]   I. Reda and A. A. Nrel, "Solar Position Algorithm for Solar Radiation Applications (Revised)," *Nrel/Tp-560-34302*, no. January, pp. 1–56, 2003.

[33]   A. W. M. Van Schijndel, "Integrated Heat Air and Moisture Modeling and Simulation," University of Technology Eindhoven, 2007.

[34]   C. a. Velds, *Zonnestraling in Nederland*. 1993.

[35]   D. R. Myers, "Solar radiation modeling and measurements for renewable energy applications: Data and model quality," *Energy*, vol. 30, no. 9 SPEC. ISS., pp. 1517–1531, 2005.

[36]   E. Maxwell, "A quasi-physical model for converting hourly global horizontal to direct normal insolation," *Unknown*. 1987.

[37]   PVPMC, "PVPerformance Modeling Collaborative," 2015. [Online]. Available: https://pvpmc.sandia.gov/.

[38]   R. Perez, P. Ineichen, R. Seals, J. Michalsky, and R. Stewart, "Modeling Daylight Availability and Irradiance Components From Direct and Global Irradiance," *Sol. Energy*, vol. 44, no. 5, pp. 271–289, 1990.

[39]   D. Faiman, "Assesing the Outdoor Operating Temperature of Photovoltaic Modules," *Prog. Photovoltaics Res. Appl.*, vol. 16, no. 4, pp. 307–315, 2008.

[40]   M. Zisler, S. Spann, and M. Tragner, "Modelling of decentralised grid-connected electricity storage," *Symp. Energyinnovation*, vol. 13, pp. 1–11, 2014.

[41]   SBRCURnet, "Plaatsing van pv-panelen op platte daken," 2015. [Online]. Available: http://www.sbrcurnet.nl/producten/infobladen/plaatsing-van-pv-panelen-op-platte-daken. [Accessed: 12-Aug-2015].